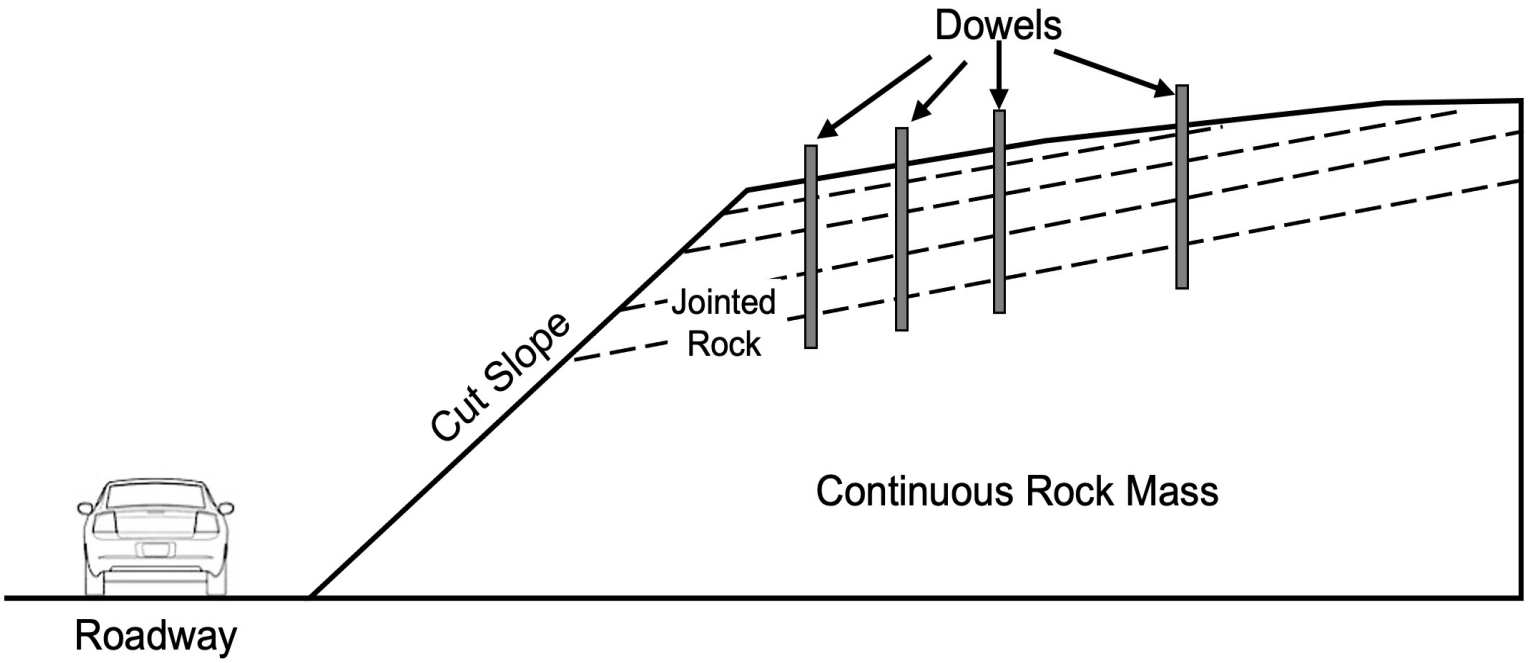

TN TDOT Department of Transportation

U.S. Department of Transportation
Federal Highway Administration

Design Considerations and Limitations of Rock Dowels/ Anchors Loaded in Shear

Research Final Report from University of Tennessee | Angelica M. Palomino and Sarah J. Mobley | May 30, 2022

Sponsored by Tennessee Department of Transportation Long Range Planning Research Office & Federal Highway Administration

THE UNIVERSITY OF TENNESSEE KNOXVILLE

DISCLAIMER

This research was funded through the State Planning and Research (SPR) Program by the Tennessee Department of Transportation and the Federal Highway Administration under ***RES #: 2020-14, Research Project Title: Design Considerations and Limitations of Rock Dowels/Anchors Loaded in Shear.***

Technical Report Documentation Page

1. Report No. RES2020-14	2. Government Accession No.	3. Recipient's Catalog No.
4. Title and Subtitle *Design Considerations and Limitations of Rock Dowels/Anchors Loaded in Shear*		5. Report Date May 30, 2022 6. Performing Organization Code
7. Author(s) Angelica M. Palomino and Sarah J. Mobley		8. Performing Organization Report No.
9. Performing Organization Name and Address University of Tennessee 851 Neyland Drive Knoxville, TN 37996		10. Work Unit No. (TRAIS) 11. Contract or Grant No. RES2020-14
12. Sponsoring Agency Name and Address Tennessee Department of Transportation 505 Deaderick Street, Suite 900 Nashville, TN 37243		13. Type of Report and Period Covered Final Report August 2019 – May 2022 14. Sponsoring Agency Code
15. Supplementary Notes Conducted in cooperation with the U.S. Department of Transportation, Federal Highway Administration.		

16. Abstract

In Tennessee, cut rock slopes with exposed discontinuities are often reinforced with grouted steel anchors installed across the discontinuity to stabilize the system by immobilizing the rock material above the sliding surface. These elements resist shear loading rather than function in tension. Yet, the steel bar may bend in cases where the discontinuity is sufficiently large. The purpose of this study was to investigate the performance of simulated un-tensioned dowel-jointed rock block systems subjected to shear loading and evaluate whether bending likely occurred as well as its contribution to the reduction in dowel capacity. Variables studied were aperture size (joint spacing), dowel diameter, and dowel angle of inclination with respect to the joint normal. Physical experiments were conducted using large concrete blocks to simulate the jointed rock material, steel rebars to simulate the dowels, and tested in a large-scale direct shear apparatus. A numerical model was developed to extend the dowel size and joint thickness. A dowel shear capacity design chart was also developed. The chart identifies the threshold between the pure shear capacity and the reduced capacity due to bending effects as a function of joint thickness and bar size. Conclusions from this study include (1) rebar double bending phenomenon was inferred from strain gage data in the case of a large aperture size, (2) bending starts at an aperture size relative to bar diameter and strength, and reduces the dowel shear capacity by a quantity related to bar size and aperture size, (3) all results from physical and numerical analyses show sufficient agreement with the governing equations for theoretical dowel shear and bending conditions to warrant the conservative use of the developed design chart (4) dowel inclination angle had little influence on ultimate shear resistance, and (5) free and fixed dowel placement show no significant difference in resistance.

17. Key Words **UN-TENSIONED ROCK DOWELS, ROCKFALL, MITIGATION, DOWEL BENDING**	18. Distribution Statement No restriction. This document is available to the public from the sponsoring agency at the website http://www.tn.gov/.

19. Security Classif. (of this report) Unclassified	20. Security Classif. (of this page) Unclassified	21. No. of Pages 107	22. Price

Acknowledgement

The authors thank the Tennessee Department of Transportation (TDOT) for their financial support of this project. We also thank Ann Beaver, Transportation Project Specialist Senior (Materials & Tests Division/Geotechnical Section, TDOT) for her valuable insights and supporting information provided during the completion of this work. We also acknowledge Syed Gulzar for his contributions in completing the experimental testing and developing the numerical model. The authors thank Drs. Eric Drumm and Richard Bennett for their contributions to the research ideas, formulating the scope of work, and the laboratory testing. We also thank Mr. Larry Roberts (Design Technician) and Mr. Andy Baker (Technical Manager) for their contributions to the experimental set-up.

Executive Summary

In Tennessee, cut rock slopes with exposed discontinuities are often reinforced with grouted steel anchors. These elements are installed across the discontinuity to stabilize the system by immobilizing the rock material above the sliding surface (discontinuity). The function of the rock anchors is to resist shear loading rather than tension. However, the steel bar may experience bending in cases where the discontinuity is sufficiently large. The purpose of this study was to investigate the performance of simulated un-tensioned dowel-jointed rock block systems subjected to shear loading and evaluate whether bending likely occurred as well as its contribution to the reduction in dowel capacity. The performance of simulated un-tensioned dowel-jointed rock block systems subjected to shear loading was investigated through physical testing and numerical simulations. The dowelled rock block system response was studied as a function of aperture size (joint spacing), dowel diameter, and dowel angle of inclination with respect to the joint normal. Physical experiments were conducted using large concrete blocks to simulate the jointed rock material and steel rebars to simulate the dowels. A large-scale direct shear apparatus was used to apply shear loading. A numerical model was developed to generate additional results by extending the dowel size and joint thickness. The results from the experimental and numerical studies were used to develop a design chart describing the capacity of a given diameter dowel which identifies the threshold between the pure shear capacity and the reduced capacity due to bending effects as a function of joint thickness.

Key Findings

This study focused on confirming the assumptions used in the design of rock slopes reinforced with grouted steel anchors (un-tensioned dowels) and to determining the joint aperture size where bending instead of shear failure occurs through physical testing and numerical analyses. The key findings from this study are:

- The rebar double bending phenomenon (formation of plastic hinges) was inferred from the strain gage data in the case of a large aperture size (joint spacing of 0.75 inches). However, this observation is limited given most of the collected strain gage data for other test cases was unusable due to physical damage caused by concrete encasement process.
- Bending reduces the dowel shear capacity by a quantity related to bar size and aperture size.
- Bending begins to occur at an aperture size relative to bar diameter and strength.
- Based on the conducted physical tests and numerical analyses results, dowel response is in good agreement with the governing equations for theoretical shear and bending conditions. All data sets show sufficient agreement to warrant the conservative use of the theoretical shear and bending governing equations in the creation of the developed design chart (Figure 4.8.).
- The dowel inclination angle with respect to the joint increases the theoretical capacity of a dowel as it increases the subject cross-sectional area. In this study, dowel inclination angle had little influence on ultimate shear resistance based on the test results used to derive this design chart. This finding is in agreement with results found in the literature (Spang & Egger, 1990).

- Free and fixed dowel placement show no real difference in resistance. In other words, the bonding condition of the rebar in the upper block did not significantly influence the ultimate shear resistance of the rebar, regardless of size or joint opening size.

Key Recommendations

The following recommendations are made based on the findings of this study.

- Un-tensioned dowels may be safely used to mitigate rock masses exhibiting the potential of planar type failures. However, consideration must be given to whether relative rock movement has already taken place, compressive strength of the surrounding rock, number of dowels proposed, extent of discontinuities, etc.
- The design chart should be used as an additional approach to rock stabilization in particularly dangerous areas. Because dowels are more cost effective than tensioned rock anchors, a greater number of slopes can be remediated for the same cost. Furthermore, un-tensioned elements require fewer site visits.
- A survey of the use of rock anchors/dowels in every state should be completed. This would be beneficial in the development of a national standard or guidelines.

Table of Contents

List of Tables

List of Figures

Chapter 1 Introduction

In Tennessee, cut rock slopes with exposed discontinuities are often reinforced with grouted steel anchors. These elements are installed across the discontinuity to stabilize the system by immobilizing the rock material above the sliding surface (discontinuity). The function of the rock anchors is to resist shear loading rather than tension. However, the steel bar may experience bending in cases where the discontinuity is sufficiently large. This study is an investigation into the response of simulated jointed rock systems reinforced with a steel bar (dowel) as a function of discontinuity size, bar insertion angle, and bar size.

1.1 Problem Statement

Rockcut slopes typically result from highway and roadway construction and are commonplace in mountainous regions. However, these cut slopes have the potential to become rockfall sites, causing significant damage, driver inconvenience, and even death (Chau et al., 2003). In Tennessee, almost 2000 rockfall sites are categorized as Moderate to Very High Risk Sites (FHWA 1994), with 1000 of these sites in the High to Very High Risk range according to the Federal Highway Administration (FHWA) Rockfall Hazard Rating System (FHWA, 1993; Mauldon et al., 2007).

The consequences of rockfall can be extensive. The correction measures for landslides, including rockfall, cost many millions of dollars annually across the U.S. (Walkinshaw, 1992). Each year, rockfalls or subsequent debris flows kill 25-50 people in the U.S. (USGS, 2021). Rockfall debris obstructs roadways, delaying or halting traffic for hours to weeks (Hungr et al., 1999). Slope failures have direct and indirect impact on the overall cost of the damage caused. Direct costs include removal of rock debris and the design and installation of a slope stabilizing structure. Indirect costs include property damage, utility interruption, injuries to commuters, and traffic delays (Wyllie & Mah, 1981).

Rockfall sites requiring mitigation are intrinsically difficult and dangerous to access. These sites are typically cut rock faces with steep to near-vertical slopes, and some are at elevations exceeding 100 ft (> 30 m) above the road surface (Mauldon et al., 2007). The hazardous nature of these sites increases the risk of injury or even death to workers at such sites.

Rock anchoring is a common rockfall mitigation technique in Tennessee due to the existing geological formations and site conditions. Rock anchors are steel reinforcement bars placed in a borehole drilled into a discontinuous (jointed) rock mass and grouted in place across the discontinuity. Rock anchors connect and transfer the weight of the unstable rock material above the discontinuity to the stable continuous rock below, “pinning” the rock layers together and preventing rockfall (Wyllie & Norrish 1996; Wyllie 2018). Even a small degree of roughness (as observed in the relatively smooth joints formed in the bedding planes of Tennessee sedimentary rocks) creates asperities in the rock joint which causes dilation or separation of the joint when shearing deformation takes place. For tensioned rock anchors, this dilation increases the anchor tension which then increases the anchor clamping force.

Most existing reinforcement methods consider the effect of post-tensioning the rock bolt or anchor after the grout has set. While this tension force provides additional stability by placing

the rock joint into compression and inducing additional frictional resistance to sliding, the post-tensioning requires additional equipment, time, and cost. Furthermore, the rock anchor installation process requires two site visits for tensioned elements. During the first visit, the steel bar is placed into a drilled hole, and the lower portion of the anchor is grouted. The second visit is for post-tensioning the anchor and grouting the remaining portion of the bar.

One advantage of passive rock dowels is that they can be installed in a single visit as post-tensioning is not required. This single visit approach reduces the risk of worker injury. However, the use of passive rock dowels is not common practice due to a lack of research into the behavioral structural response of the system (Liu and Li, 2017). For many slopes, a satisfactory level of safety can be obtained with un-tensioned (fully grouted) rock anchors, or dowels, relying only on the shear capacity of the anchor. TDOT has successfully utilized this method in the past, but the typical design method based on the pure shear capacity of the dowel fails to consider the effect of rock discontinuity (joint) thickness, which likely introduces bending to the dowel at some threshold opening size. *Understanding the role of joint thickness or bending in the capacity of un-tensioned shear dowels is critical. This understanding could lead to wider application of these less expensive un-tensioned dowels. As a result, a greater number of slopes can be remediated for the same cost.*

1.2 Study Purpose

For un-tensioned dowels, joint (discontinuity) dilation or separation may introduce bending to the dowel, reducing its capacity. Although the un-tensioned dowels are not pre-tensioned, small tensile forces will likely develop in the grouted dowel as the joint begins to dilate. Despite this reduction in capacity, un-tensioned dowels may still be a cost-effective mitigation technique. However, the decreased capacity due to bending must be understood so that it can be compensated for with additional inexpensive un-tensioned dowels. While not applicable to all conditions, un-tensioned dowels could be applied to some sites where rock bolt stabilization is appropriate. The advantage is that un-tensioned dowels can be deployed more quickly and inexpensively since there is no need to revisit the site after the grout has set to perform the post-tensioning operation.

The purpose of this study is to investigate the performance of simulated un-tensioned dowel-jointed rock block systems subjected to shear loading and evaluate whether bending likely occurred as well as its contribution to the reduction in dowel capacity. The results from the experimental and numerical studies were used to develop a design chart for the capacity of a given diameter dowel which identifies the threshold between the pure shear capacity and the reduced capacity due to bending effects as a function of joint thickness.

The overarching research question addressed in this study is:

What is the relationship between the rock joint thickness and reduced dowel shear capacity due to bending?

The objective of this study is to develop a user-friendly design chart for shear capacity that combines the resistance force due to applied shear and bending. The design chart was developed for several typical dowel sizes and strengths over a range of likely joint aperture sizes.

1.3 Methodological Approach

The investigation of the performance of simulated un-tensioned dowel-jointed rock block systems subjected to shear loading was conducted using physical laboratory experiments and numerical simulations. The dowelled rock block system response was studied as a function of aperture size (joint spacing), dowel diameter, and dowel angle of inclination with respect to the joint normal. Physical experiments were conducted using large concrete blocks to simulate the jointed rock material and steel rebars to simulate the dowels. A large-scale direct shear apparatus was used to apply shear loading. A numerical model was developed based on the physical testing set-up to generate additional results by extending the dowel size and joint thickness. The behavior observed in the physical tests was used to calibrate and validate the numerical models of the un-tensioned rock dowel-rock discontinuity system. The results from the experimental and numerical studies were integrated into a design chart for the capacity of dowels with selected diameters, which identifies the threshold between the pure shear capacity and the reduced capacity due to bending effects as a function of joint thickness.

These results of this study will lead to a better understanding of the shear capacity reduction as a function of nominal joint thickness and allow for more widespread use of this cost-efficient method to stabilize rock blocks.

1.4 Report Organization

This report is organized as follows:

- **Introduction.** The Introduction includes the problem statement, study purpose, and methodological approach.
- **Literature Review.** The Literature Review provides contextual information for this report, including discussion on rock slope failure modes, geological impacts on failure mode types, rockfall mitigation techniques, and rock dowel failure modes.
- **Methodology.** The Methodology includes a discussion on the relationship between the selected field conditions and experimental laboratory model, as well as detailed descriptions of the concrete block specimen preparation and test set-up, test equipment, investigated variables, data collection methods and analysis, technical assumptions, and a description of the numerical model developed for this study.
- **Results and Discussion.** The results from the large-scale testing and numerical modeling are presented in this chapter. The dowel shear capacity design chart is also presented in this chapter.
- **Conclusions.** The Conclusions includes the key findings and observations from this study as well as recommendations stemming from the results of this study.
- References
- Supplemental information is provided in the Appendices:
    - Appendix A Specimen Laboratory Test Conditions and Measured Load-Displacement Responses
    - Appendix B Numerical Model Derived Load-Displacement Responses
    - Appendix C Rebar Certified Mill Test Reports
    - Appendix D Dowel Shear Capacity Design Chart

Chapter 2 Literature Review

2.1 Rock Slope Failure Modes

Most rock masses consist of groups of intact blocks with discontinuities between them. Discontinuities may arise from bedding surfaces, joints, foliation, or some other rock fracture. The set of discontinuities within a rock mass is termed the structural fabric. This structural fabric governs the overall rock mass material properties, e.g., strength, and the potential for slope failure (Norrish & Wyllie, 1996).

Rock slopes may fail either due to the rock mass structural fabric or weathering effects. The principal modes of simple structurally controlled rock slope failures along discontinuities are depicted in Figure 2.1. Planar sliding failures (Figure 2.1.a) are those in which a rock block has moved along a single planar surface dipping out of the slope face. The sliding plane strikes parallel or within ±20° of the face of the slope (Wyllie, 2018). For example, planar failures in sedimentary rock occur along the bedding planes. Igneous and metamorphic rock may also be subject to planar failure along joints or foliations (Higgins & Andrew, 2012). Wedge failures (Figure 2.1.b) result when a rock wedge is formed by the intersection of two planar discontinuities – each striking the slope face at some oblique angle – slides along the line of intersection. Wedge failures are more likely to occur in rock masses with angled bedding/foliation and well-defined intersecting joint sets, such as shale, siltstones with small bedding thicknesses, claystones, limestones, and foliated rock (e.g., slate) (Norrish & Wyllie, 1996). Toppling failures occur when blocks or columns of rock material rotate about some fixed base. Toppling is observed in metamorphic and sedimentary rock with distinct bedding or foliation planes and columnar basalts (Norrish & Wyllie, 1996). Circular sliding failures are defined by the circular-like shape of the failure surface. They differ from planar, wedge, and toppling failures in that they are not the result of some structural discontinuity. Circular failures often occur when the particle size is on a scale much smaller than that of the slope, e.g., partially to highly weathered rock or highly fractured rock in which the fractures are closely spaced together (Norrish & Wyllie, 1996; Wyllie, 2018). Planar, wedge, and toppling failure mechanisms are controlled by discontinuities in the rock mass due to geologic features such as joints or bedding planes defining the sliding surfaces (Wyllie, 2018).

Figure 2.1 *Simple Structurally Controlled Rock Slope Failure Modes (after Wyllie, 2018)*

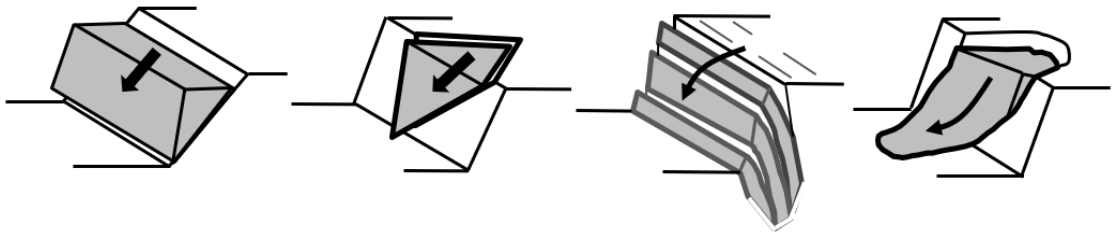

a. Planar Sliding b. Wedge Sliding c. Toppling d. Circular Sliding

Other, non-structurally controlled causes of failure are due to environmentally controlled processes. Differential weathering is the non-uniform weathering of the rock slope due to the presence of adjacent rock materials with different lithologies and weathering rates. The

different erosion rates often lead to at least one structural failure mode, such as toppling. Cobbles and boulders freed from a surrounding finer-grained matrix when the finer material is eroded results in boulder fall. Raveling, the most common type of rockfall failure, is the uniform detachment of smaller rock blocks from the rock formation due to erosion or other non-structural failure mechanisms (i.e., freeze-thaw action, blasting, etc.). Raveling is characterized by the continuous, slow detachment of blocks with no distinct sliding or rotational failure mechanism as would be observed in planar, wedge, toppling, or circular failures (Norrish & Wyllie, 1996; Mauldon et al., 2007; Higgens & Andrew 2012).

2.2 Geological Impacts on Rock Slope Failure Mechanisms

Geology plays a critical role in the potential for rock slope failure due to roadcuts. Potential failure modes are closely linked to differences in lithology in adjacent rock masses and the number of discontinuities (Vandewater et al., 2005). A geologic map of Tennessee with an overlay of the TDOT regions is shown in Figure 2.2. In east Tennessee, sedimentary and metamorphic rock formations – siltstone, sandstone, shale, and slate – are located in the portion of Region I known as the Blue Ridge Province. These rock types are susceptible to planar and wedge type failure modes. (Moore, 1986; Higgens & Andrew 2012).

Figure 2.2 *Geologic Map of Tennessee with Overlay of TDOT Regions (after Tennessee State Government, 2022)*

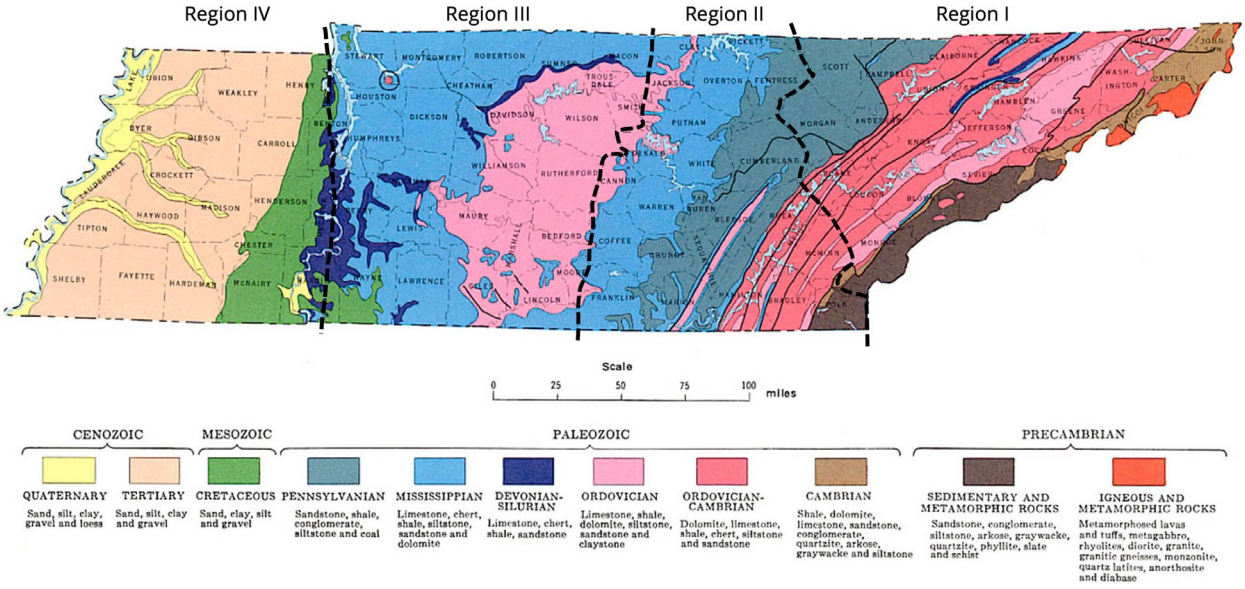

In Tennessee, Mauldon et al. (2007) inventoried potentially hazardous rockcut slopes. The inventory results are summarized in Figure 2.3. The rockcuts were rated as either "A," "B," or "C" according to the Tennessee Rockfall Hazard Rating System (TRHRS), where "A" cuts designate high hazard rockcut slopes with the greatest potential for fallen rock debris to enter a nearby roadway. While planar and wedge failure modes are the least prevalent in Tennessee, almost all of rockcut slopes with these identified potential failure modes exist in Regions 1 and 2 (east Tennessee). Region 1 has many locations in which rock discontinuities are prevalent (Mauldon et al. 2007).

Figure 2.3 *Rock Slope Failure Mode Distribution in Tennessee Average Across the State and By Region (after Mauldon et al., 2007)*

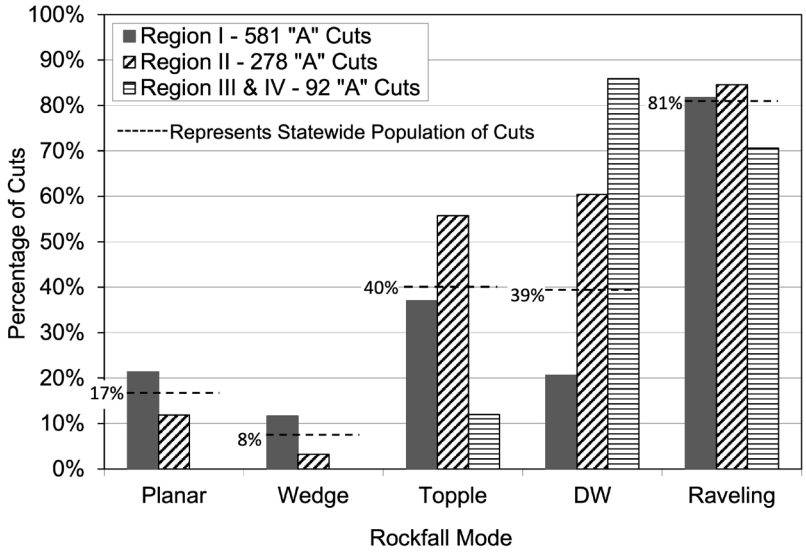

Note. DW indicates differential weathering mode.

2.3 Rockfall Mitigation Techniques

Rockfall mitigation methods are categorized as reinforcement, rock removal, or protection (Wyllie, 2018). Typical methods are listed in Figure 2.4.

While many factors must be considered in selecting a rockfall mitigation approach, the potential rockfall failure mode is a key consideration. Reinforcement type measures are often applied to rock formations exhibiting the potential for planar and wedge failure modes. Tensioned rock anchors or un-tensioned (fully grouted) dowels have been applied to both types. Other considerations include site geology, site access, available equipment, and construction time, among others. In addition to reinforcement, mitigation practices for sites exhibiting the potential for wedge failure include removal of failed wedge material, catchment fences, anchored wire mesh, catchment ditches, and retaining walls (Moore, 1986; Wyllie, 2018).

Figure 2.4 *Common Rock Cut Stabilization and Protection Methods (after Pierson & Vierling, 2012; Wyllie, 2018)*

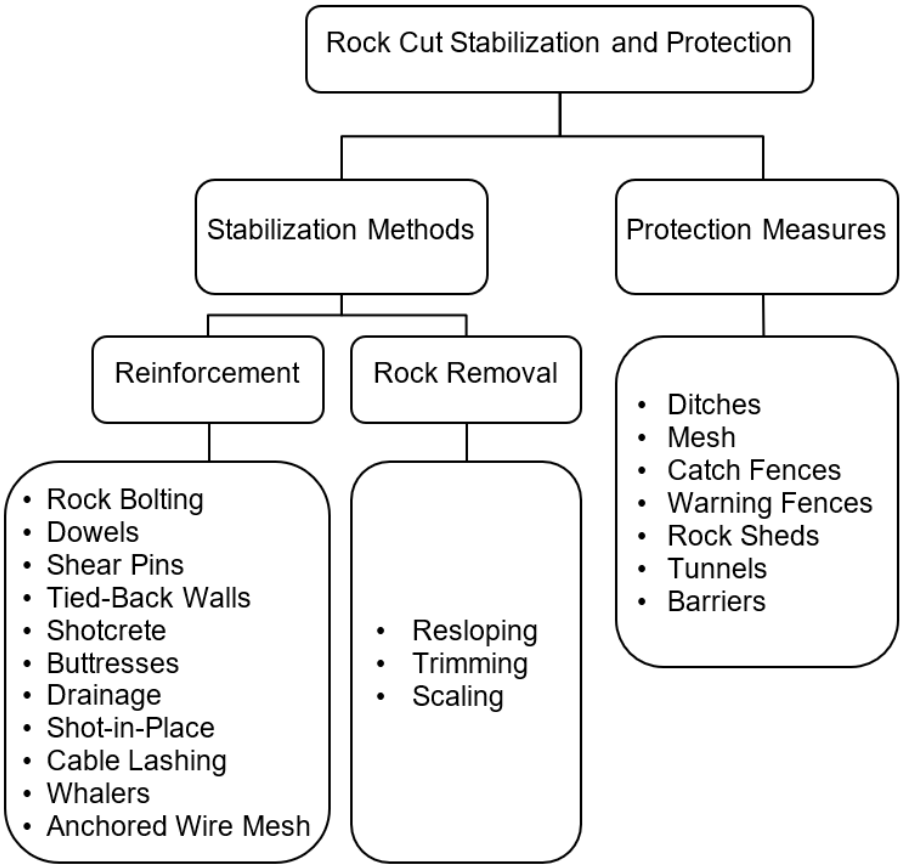

2.4 Rock Dowel Failure Modes

Rock anchors may be either tensioned or un-tensioned. A borehole is drilled prior to placement of the bar element. Tensioned anchors are initially anchored to the competent rock at the distal end, grouted at the distal end, tensioned to some predetermined load, then grouted through the free stressing length after tensioning. Un-tensioned anchors are placed and fully grouted without tensioning. Fully grouted un-tensioned elements are also referred to as dowels (Wyllie, 2018). Dowels offer only passive resistance to shear-induced sliding, and so their performance is most effective when no previous movement has occurred along the rock discontinuity as in newly cut slopes. If movement along the discontinuity occurs, the shear strength of the bar engages. The shear resistance along the discontinuity increases due to the resistance to sliding (bar engagement) and the increase in the normal force between the two sliding surfaces. The grout must also provide a strong contact between the dowel and rock to maximize interlock and minimize relative movement along the sliding surface (Wyllie & Norrish, 1996; Simons et al., 2007; Andrew & Pierson, 2012). Some disadvantages of un-tensioned dowels are the capacity is less than tensioned rock anchors, and the capacity cannot be tested in-situ. The advantages of using un-tensioned dowels are they are typically less expensive to install, and they are a potential option in rock masses with random joint orientations (Wyllie, 2018).

These steel bars act as rigid shear elements pinning the upper rock block(s) to the lower rock block(s). While the shear strength of the steel bar contributes to the overall shear resistance of the system, the steel shear strength at the anchor-discontinuity location should not be relied on. Instead, rock anchors are designed to modify the normal and shear forces along the sliding planes (Wyllie 2018).

The use of rock anchors is not appropriate for circular failures (Figure 2.1.d) and not typically used in toppling failures (Figure 2.1.c). However, rock anchors are widely used in to stabilize planar failures (Figure 2.1.a) and wedge failures (Figure 2.1.b). The forces and resulting stresses in the rock block for the planar and wedge failures are similar, except that the wedge failure develops frictional resistance on two planes. Although un-tensioned rock dowels could be applied to both planar and wedge failure modes, the following discussion will focus on the acting forces and resulting stresses in the context of the planar failure mode.

Spang & Egger (1990) studied the behavior of fully bonded rock bolts, i.e., un-tensioned (fully grouted) rock dowels. They completed approximately 60 laboratory shear strength tests, 10 large-scale field tests, and numerical modeling of direct shear laboratory tests.

Figure 2.5 shows the initial state of a jointed rock mass fitted with an un-tensioned fully grouted dowel assumed by Spang & Egger (1990). The rock mass has a single discontinuity with some nominal opening size. The dowel is fully bonded to the rock through the mortar. The rock mass above the discontinuity tends to move along the sliding surface resulting in relative displacement. If the sliding surface is textured, dilatancy will occur in the vertical direction perpendicular to the sliding motion. The rock material immediately adjacent to the dowel may either be in tension or compression as indicated by the "T" or "C" in Figure 2.5.

Figure 2.5 *Initial State of Dowelled Joint In-Situ (after Spang & Egger, 1990)*

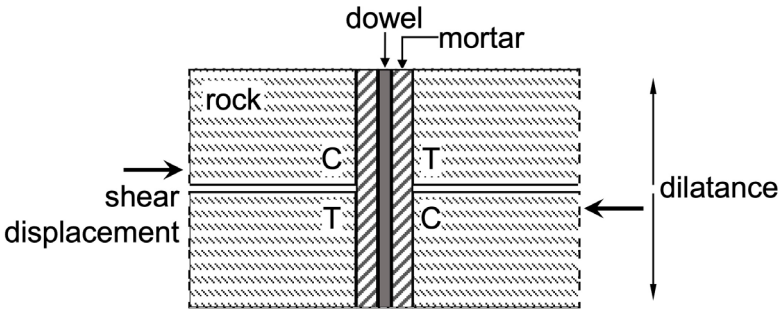

Note. The locations in which the rock material experiences compression or tension are indicated by "C" and "T", respectively.

As shear displacements are induced in an un-tensioned (fully grouted) steel dowel-rock joint system, the response can be described according to three distinct stages: (1) elastic stage, (2) yield stage, and (3) plastic stage (Spang & Egger, 1990).

(1) The elastic stage takes place once the rock blocks overcome cohesive/adhesion forces at the joint and relative sliding starts. The total shear resistance of the system is the summation of the joint shear strength and that of the dowel, and the elastic response is a function of the elastic properties of the dowel, rock, and mortar, i.e., Young's moduli. Stresses on these materials may either be compressive or tension, depending on the

location with respect to the applied shear force and the bolt. (Figure 2.5). However, once the mortar debonds from the steel dowel, the tensile stresses in the mortar and rock become zero.

(2) The yield stage depends on the steel, mortar, and rock yield strengths and takes place when these materials yield strengths are reached due to bending in the steel and compression in the mortar (mortar thickness ~1/2 dowel diameter). The yield stage is observed when a dowel is inserted into a relatively deformable material, i.e., weaker rock, so that shear resistance is mobilized only when the dowel deforms. Yielding typically occurs at relative low shear displacements (can be < 1mm) and low shear forces.

(3) The plastic stage takes place after the yield stage and governs the shear response of the dowel-jointed rock system given that yield occurs at low shear forces. The factors that most influence the dowel's contribution to the total joint shear strength are shear sliding plane friction angle, dowel inclination with respect to the joint normal, dowel diameter, mortar and rock stiffness, dilatancy angle (for rough planar surfaces), steel working capacity and deformability, and mortar thickness.

Spang & Egger (1990) developed the following empirical equations for the maximum shear resistance, T_0, of a dowel-jointed rock system and the corresponding shear displacement, δ_s, normalized with respect to the dowel diameter:

$$T_0 = P_t\left[1.55 + 0.011 \cdot \sigma_c^{1.07} \cdot \sin^2(\theta + i)\right] \cdot \sigma_c^{-0.14} \cdot (0.85 + 0.45 \cdot \tan\phi)$$

$$\delta_s = (15.2 - 55.2 \cdot \sigma_c^{-0.14} + 56.2 \cdot \sigma_c^{-0.28}) \cdot (1 - \tan\theta \cdot (70/\sigma_c)^{0.125} \cdot (\cos\theta)^{-0.5})$$

where P_t is the maximum tensile load of the dowel in kN, θ is the dowel inclination angle with respect to the joint normal, ϕ is the friction angle along the shear plane, i is the dilatancy angle, and σ_c is the compressive strength of the intact rock in MPa. Note that $\delta_s$is dimensionless.

Key findings from Spang & Egger (1990) are:

1. When the angle of inclination is zero (dowel is perpendicular to the joint):
    - only very small shear forces are required to bend the bolt, creating plastic hinges above and below the discontinuity
    - once the plastic hinges form, failure may occur by combined shear and tension near the discontinuity or by bending in one of the hinges; thus, the exact failure location cannot be determined
    - shear resistance cannot take place without bending and yielding of the dowel
2. When the angle of inclination is greater than zero:
    - less bending occurs at small shear forces
    - the ultimate dowel load is first reached near the discontinuity
    - shear resistance is mobilized with no bending in the dowel
    - maximum deformation and plastic deformation are less in inclined dowels than in perpendicular dowels
    - the stiffness of inclined dowels is greater than that of perpendicular dowels
    - shear displacement decreases with increasing angle of inclination up to 30°
3. For varying dowel diameters:

- as dowel diameter increases, the shear displacement at the maximum load increases
- normalized shear force-shear displacement values are not a function of dowel diameter
- as diameter increases, the shear displacements decrease at a given shear force

Three potential failure mechanisms for an un-tensioned rock dowel should be evaluated during the mitigation design for a given rock slope. These mechanisms – pure shear failure, double bending failure, and bearing failure – are similar to those described by Ferrero (1995). Pure shear (Figure 2.6), exists when the rock discontinuity is smooth and planar, producing a very thin nominal joint. This mechanism produces a shear force acting on the cross-sectional area of the rock dowel. Due to the inclination of the rock joint relative to the dowel, this shear force acts on an elliptical shaped area. This failure mechanism and the resulting design methods are straightforward and so were not addressed in this study.

Figure 2.6 *Pure Shear Loading on a Rock Dowel in a Rock Mass with a Single Discontinuity. (a) Elevation View Through a Section of Rock with a Nominally Thin, Smooth Discontinuity. (b) Enlargement of Dowel Section at the Discontinuity Depicting the Shear Force Acting Across an Elliptical Surface Area of the Dowel.*

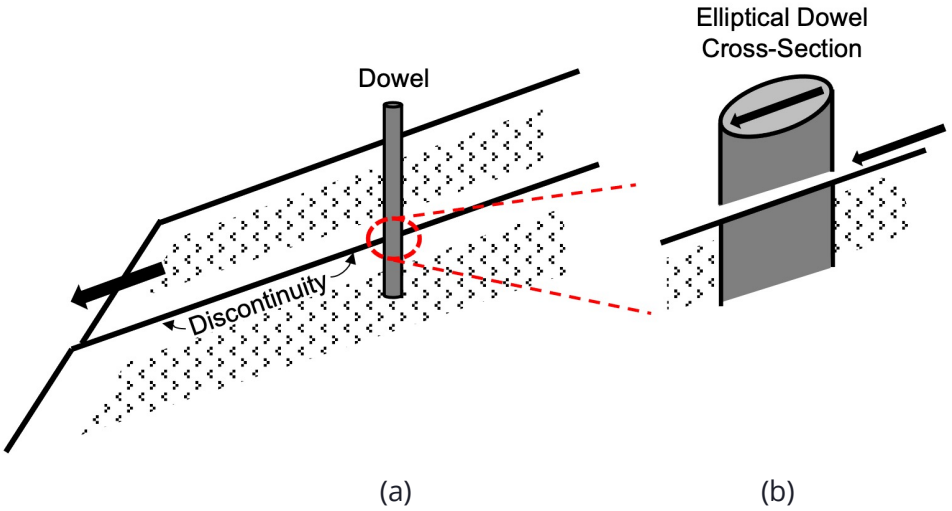

Note. The inclination of the discontinuity relative to the vertical axis of the dowel produces a shear force acting across an elliptical surface area of the dowel. Arrows indicate relative movement of rock block in (a) and direction of shear force in (b).

The double bending failure mechanism exists when there is some larger nominal aperture size or roughness to the rock discontinuity. As shown in Figure 2.7, the resulting aperture produces a separation between the driving and stabilizing forces and thus creates bending moments in the rock dowel. Due to the clamping effects provided by the grout and rock surrounding the dowel on both sides of the discontinuity, a double or reverse bending in the dowel develops. The magnitude of this bending moment is proportional to the nominal size or roughness of the aperture/joint.

Figure 2.7 *Double Bending Loading on a Rock Dowel in a Rock Mass with a Single Discontinuity. (a) Elevation View Through a Section of Rock with a Discontinuity Characterized by a Nominally Large Aperture Size. (b) Enlargement of the Dowel Subjected to Bending Forces in Opposite Directions due to the Spacing Between the Two Rock Blocks.*

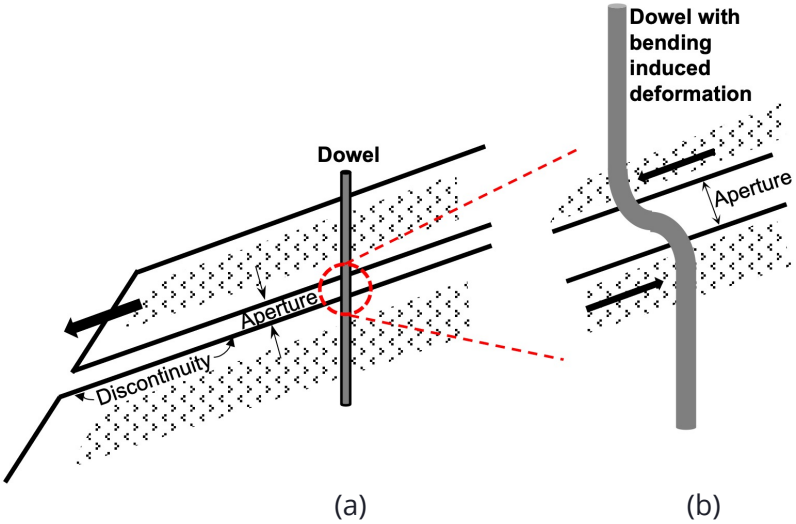

Note. Arrows depict relative movement direction in (a) and the direction of the shearing forces acting on the dowel in (b).

The third potential failure mechanism for un-tensioned rock dowels is the bearing failure of the rock and/or grout surrounding the dowel. This failure mechanism can occur in combination with either the pure shear or double bending mechanisms (Ferrero, 1995). Figure 2.8 shows the bearing failure mechanism in combination with the double bending mechanism. The forces acting on the rock block impose high bearing stresses on the rock and grout in the regions adjacent to the discontinuity. The high bearing stresses may cause crushing of the rock and/or grout material in these regions. The case of the double bending mechanism is assumed to impose more severe stresses than the pure shear case. However, this double bending failure mechanism is not well understood, and there is a need to incorporate this mechanism into current design methods.

Figure 2.8 *Bearing Failure of the Rock or Grout Adjacent to the Dowel with Bending Induced Deformation*

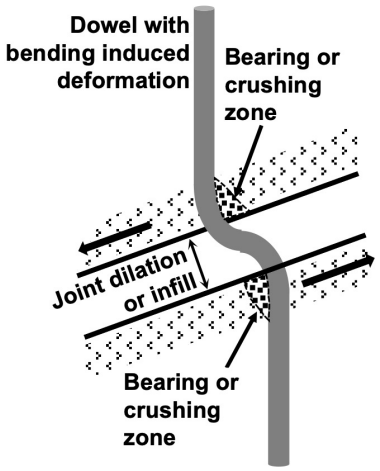

Note. Arrows depict relative movement direction of the rock block above and below the joint.

Chapter 3 Methodology

This study focused on the reinforcement of a rock cut slope with a planar-type failure mode (joint) using un-tensioned dowels. As shown in Figure 3.1, rock slope failures were simulated through large scale direct shear tests of concrete specimens pinned together with a steel rebar. In the selected field condition (Figure 3.1.a), a joint separates a rock block from the remaining rock mass. Dowels are inserted at some angle of inclination relative to the joint normal. The dowelled joint-rock system counters the tendency of the rock block to slide along the joint surface, i.e., the shear force due to the rock block. The laboratory model (Figure 3.1.b) consisted of two concrete blocks representing the upper (movable) rock block and lower (fixed) rock mass. A steel rebar was cast within the rock blocks simulating the dowel. Spacer bars placed between the two concrete blocks maintained a constant aperture size during testing. During the large-scale direct shear tests, one concrete block was fixed in place while the other concrete block was subjected to an applied shear force. This simulated the relative movement of the rock block to the fixed rock mass. A normal force (not shown) was also applied to the concrete block system to simulate the overburden. The materials used, specimen preparation, test equipment and set-up, variables investigated, and data collection and analysis are described in detail in the following sections.

Figure 3.1 *Field Condition of Dowelled Jointed Rock Mass and Corresponding Laboratory Model Direct Shear Test*

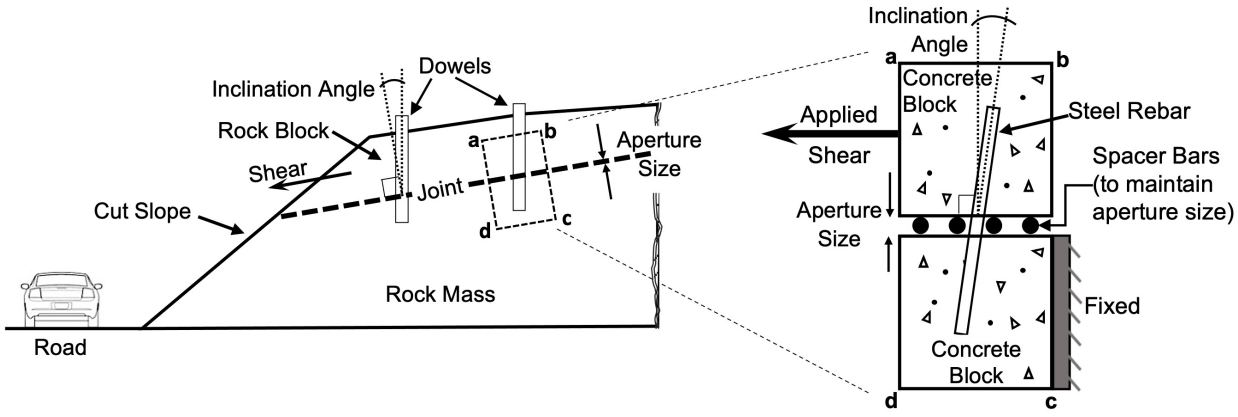

a. Field Condition b. Laboratory Model

Note. Dowelled jointed rock section **abcd** is modeled in the laboratory with two concrete blocks pinned together with a steel rebar.

3.1 Materials

Laboratory tests were conducted on simulated dowelled-jointed rock systems consisting of concrete blocks and steel rebars.

The concrete for this study was designed to have unconfined compressive strength representative of moderately hard rock. Moderately hard rock unconfined compressive strength ranges from 50 to 100 MPa (~ 7250 to 14500 psi; Deer & Miller, 1966). A minimum strength of 10,000 psi (70 MPa) was selected for this study to compensate for any uncertainties in strength gained of concrete mixed manually in the laboratory while still ensuring that the strength would be greater than the minimum value in the moderately hard rock strength range.

The strength of each specimen was determined using the measured unconfined compressive strength of concrete cylinders simultaneously cast using the same concrete mix as the given specimen. Three cylinders were each subjected to unconfined compressive strength testing following ASTM C39 (MC-500PR Gilson Company Inc) between 7 and 14 days (7, 10, 14 days) after casting to track the increase in strength with curing time. The block specimens were tested on the same day the target minimum strength was reached or surpassed based on the cylinder strength measurements. The concrete block strength was taken as the average strength of the 3 cylinders tested when the minimum strength was reached/surpassed.

The concrete consisted of coarse aggregate (# 57), fine aggregate, Type I Portland cement, tap water, and a high-range water reducer (ViscoCrete 2100, Sika Group). The coarse and fine aggregate were obtained from a local supplier (Buzzi Unicem). The grain size distribution curves for the coarse and fine aggregate are shown in Figure 3.2. A concrete volume of 10 cubic feet (ft^3; 0.283 m^3) was mixed for each specimen to accommodate both the block specimen and the unconfined compressive strength test cylinders. The concrete mix design is shown in Table 3.1. Cement, fine aggregate, and coarse aggregate were mixed in the proportions of 1:1.19:1.91 by weight.

Figure 3.2 *Grain Size Distributions for Coarse and Fine Aggregate Used in This Study*

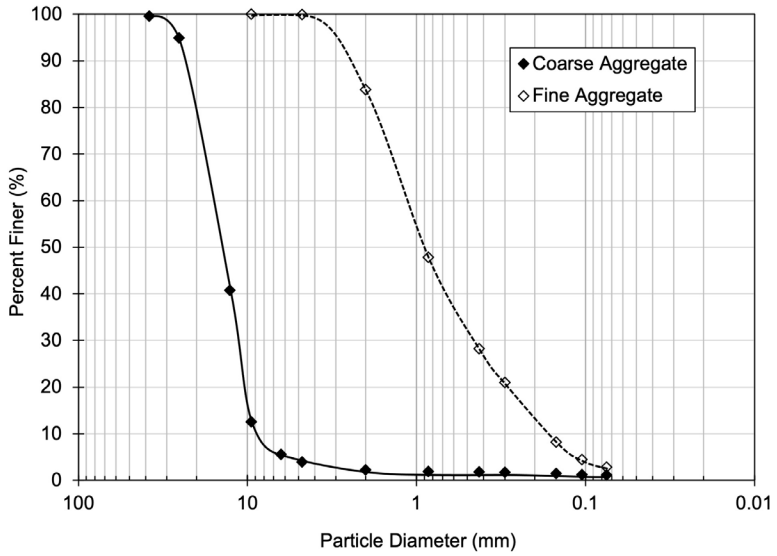

Table 3.1 *Concrete Mix Design for Simulated Dowelled-Jointed Rock Systems Subject to Large Scale Direct Shear Testing*

Material	Quantity Per 10 ft^3-Volume Batch of Concrete
Coarse Aggregate	667 lb (303 kg)
Fine Aggregate	416 lb (189 kg)
High-Range Water Reducer	600 mL
Water:Cement Ratio	0.29-0.31

Note. 10 ft^3 is approximately equal to 0.283 m^3.

The dowels were modeled using commercially available rebar. Rebar with three different diameters were selected to investigate the influence of dowel diameter on the rebar-concrete block system response. Grade 60 rebar with diameters ½ inch (1.27 cm; #4 rebar), 5/8 inch (1.59 cm; #5 rebar), and ¾ inch (1.91 cm; #6 rebar) conforming to ASTM A615-20 were obtained from Southern Rebar & Supplies, Inc. (Knoxville, TN). The yield strengths for the ½" (#4), 5/8" (#5), and ¾" (#6) diameter rebars were 86.4 ksi (692 MPa), 84.5 ksi (583 MPa), 81.8 ksi (564 MPa), respectively (average values based on data provided by the manufacturer, see Appendix C). The ultimate tensile strengths for the ½", 5/8", and ¾" rebars were 103.6 ksi (714 MPa), 101.2 ksi (697 MPa), and 99.4 ksi (685 MPa), respectively (average values based on data provided by the manufacturer, see Appendix C).

Rebar strain response during loading was measured using strain gages. The selected strain gages were obtained from Micro-Measurements (model #C4A-06-125SL-39P) and had a measurement range of ±3%. The stain gages were placed at specific locations along the length of the rebar to capture regions of large strain (near the aperture) and low strain (away from the aperture). Eight strain gages were applied at the following locations with respect to the aperture centerline as shown in Figure 3.3: -10 inches (-25.4 cm), -6 inches (-15.24 cm), -3 inches (-7.62 cm), -1 inch (-2.54 cm), 0 inches (0 cm), 1 inch (2.54 cm), 3 inches (7.62 cm), and 10 inches (25.4 cm). Each strain gage was assigned the notation of SG#, and the strain gages were numbered sequentially along the rebar length. The negative and positive signs indicate that the strain gages were applied at rebar locations within the bottom and top concrete blocks, respectively. For example, SG1 was fixed at 10" (25.4 cm) from the centerline of the aperture into the bottom concrete block (-10" (-25.4 cm)). Heat-shrink tubes made from cross-linked polyolefin were used to protect the strain gages from the surrounding concrete during the placement and curing process. All the strain gages were placed on the predicted tension side of the rebar during the shear test.

Figure 3.3 *Cross-Sectional View of Instrumented Rebar with 8 Strain Gages. Strain Gage Locations are Shown as Distance from the Aperture Centerline in Inches*

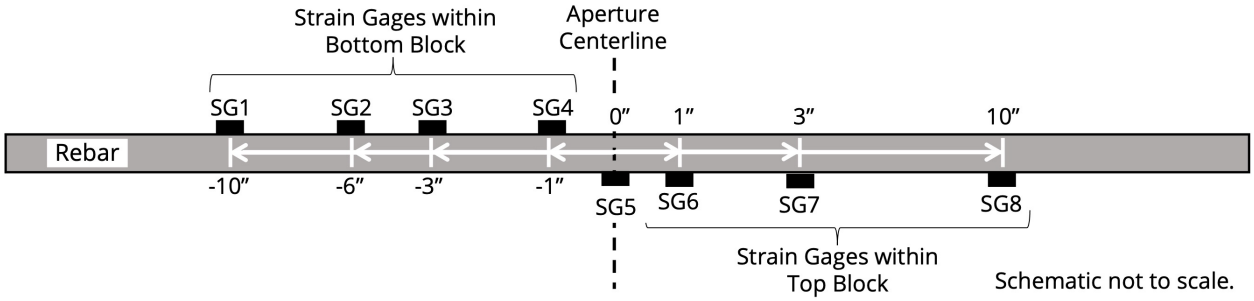

Note. SG# indicates the strain gage number assigned to the location on the rebar.

3.2 Concrete Block Specimen Preparation

Each specimen consisted of two concrete blocks – a top concrete block and a bottom concrete block – and an instrumented rebar. Wooden molds used to form the top and bottom blocks of each specimen were constructed from hardwood red oak plywood (Figure 3.4).

Figure 3.4 *Wooden Mold with Instrumented Rebar and Steel Spacer Plates*

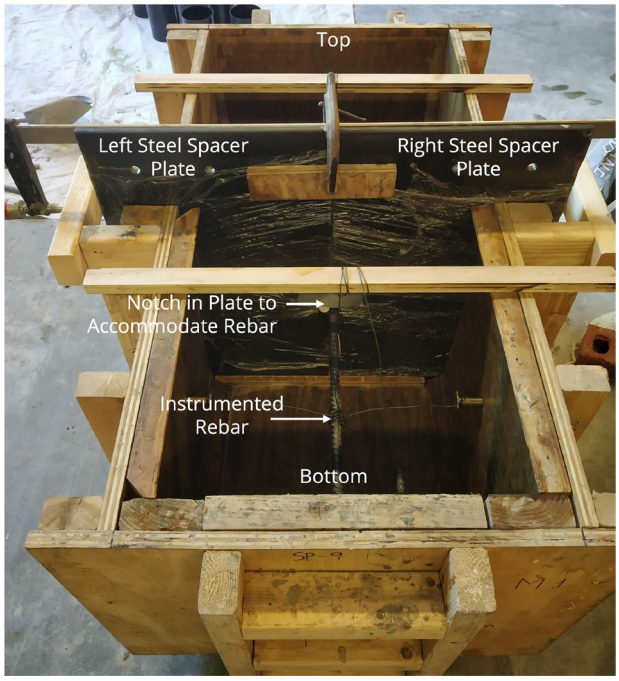

The molds were designed to include and maintain a selected aperture (joint) size, s, between the top and bottom blocks and fix the instrumented rebar in place during the concrete pouring and curing processes. An instrumented rebar was placed in the mold such that it would be at the geometric center of the abutting surfaces of the two concrete blocks at a predetermined inclination angle, θ, with respect to the simulated joint normal. Note that for rebars with diameters >0.5", one end of the rebar was bent into a hook shape (hooked end placed into the bottom concrete block) prior to placement in the mold to allow for appropriate development length inside the concrete specimen during testing. The aperture size was fixed using some combination of one or more steel plates with thickness 0.25" (0.098 cm), 0.5" (0.197 cm), and 0.75" (0.295 cm). The steel plates separated the top and bottom concrete blocks during the curing process. Small notches were machined into the steel plates to accommodate the portion of the instrumented rebar within the aperture. The concrete was mixed in a 3-ft^3 rotating drum concrete mixer (Gilson), and so several batches were required for each specimen and corresponding test cylinders. Care was taken to slowly pour and tamp the concrete into the wooden molds to minimize disturbance to the instrumented rebar. The filled molds were then covered in damp jute to maintain a humid environment during the curing period. The specimens were allowed to cure undisturbed until the target concrete unconfined compressive strength was reached, typically 10 to 14 days.

A schematic of a typical concrete block specimen is shown in Figure 3.5. The bottom block dimensions were 19"x19"x20" (48.3cm x 48.3cm x 50.8cm). For each aperture spacing test condition, the top block was constructed to accommodate the thickness of the steel spacer plate(s), i.e., the aperture thickness. Thus, the dimensions of the top block were 19"x19"x(21"-s") (48.3cm x 48.3cm x (53.3cm – s in cm), where s is the aperture size. Note that the depth of both concrete blocks, 19" (48.3cm), are not shown in Figure 3.5. The steel spacer plates were

removed prior to testing and replaced with smooth spacer bars with diameter equal to the aperture size.

Figure 3.5 *Schematic of Concrete Block Specimen with Instrumented Rebar*

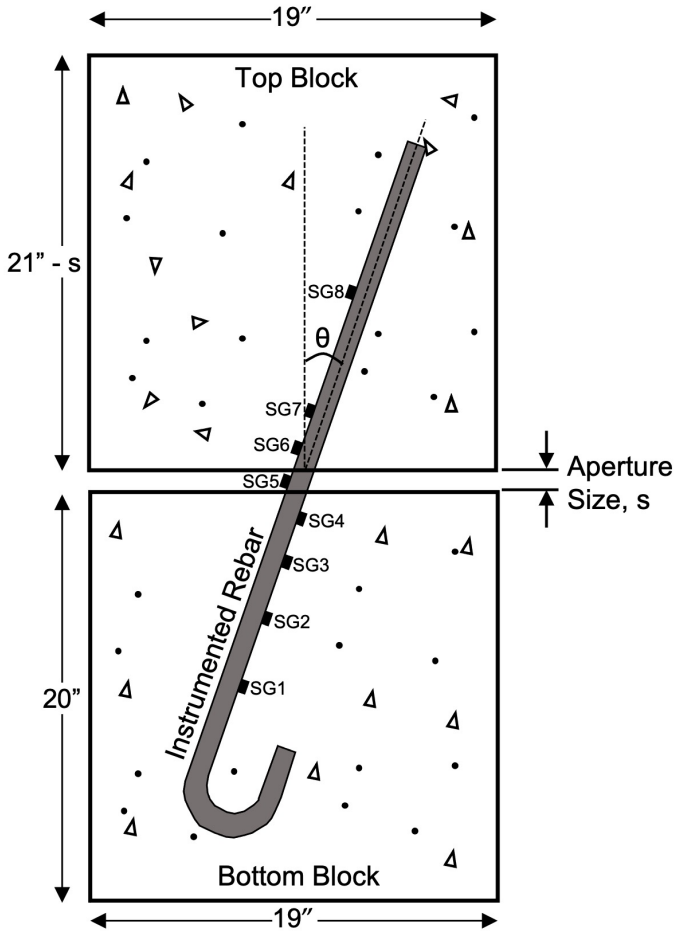

Note. The depth of each concrete block is 19 inches (not shown). θ indicates the rebar inclination angle with respect to the simulated joint normal. Schematic is not drawn to scale.

3.3 Test Equipment and Set-Up

The simulated dowelled-jointed rock specimens were tested in a large-scale direct shear apparatus. A schematic and digital image of the direct shear test system fitted in a large-scale steel frame are shown in Figure 3.6 and Figure 3.7, respectively. The direct shear system consists of two compartments – an upper shear box and a lower shear box – and a horizontal actuator. The system is housed in a large steel reaction frame. The upper shear box is rigidly connected to the steel frame to restrict the relative horizontal movement of the top concrete block. The lower box is allowed to move unrestricted in the horizontal direction. A hydraulically operated horizontal actuator (MTS, Model No. 244.22) with maximum capacity of 22 kips (100 kN) is attached on one end to the frame and on the other end to the lower shear box to exert horizontal stress on the specimen. A static dead load acted as the normal force during the testing process. Since the weight of the top concrete block varied depending on the aperture

thickness, enough static load was added to reach the required normal load for each test. The combined weight of the dead load and upper concrete block was held constant at 800 lb (3.56 kN) for all tests. This normal force simulates the weight of the rock material above the joint in the field. The aperture spacing was maintained during testing using smooth spacer bars with a diameter equal to the thickness of the aperture. During the direct shear testing, the upper box remained fixed, and the lower shear box assembly was subjected to a constant horizontal displacement rate of 1mm/min during loading. Load was applied until either the specimen showed signs of failure or the equipment reached capacity at 22 kips.

Figure 3.6 *Schematic of Direct Shear Test System*

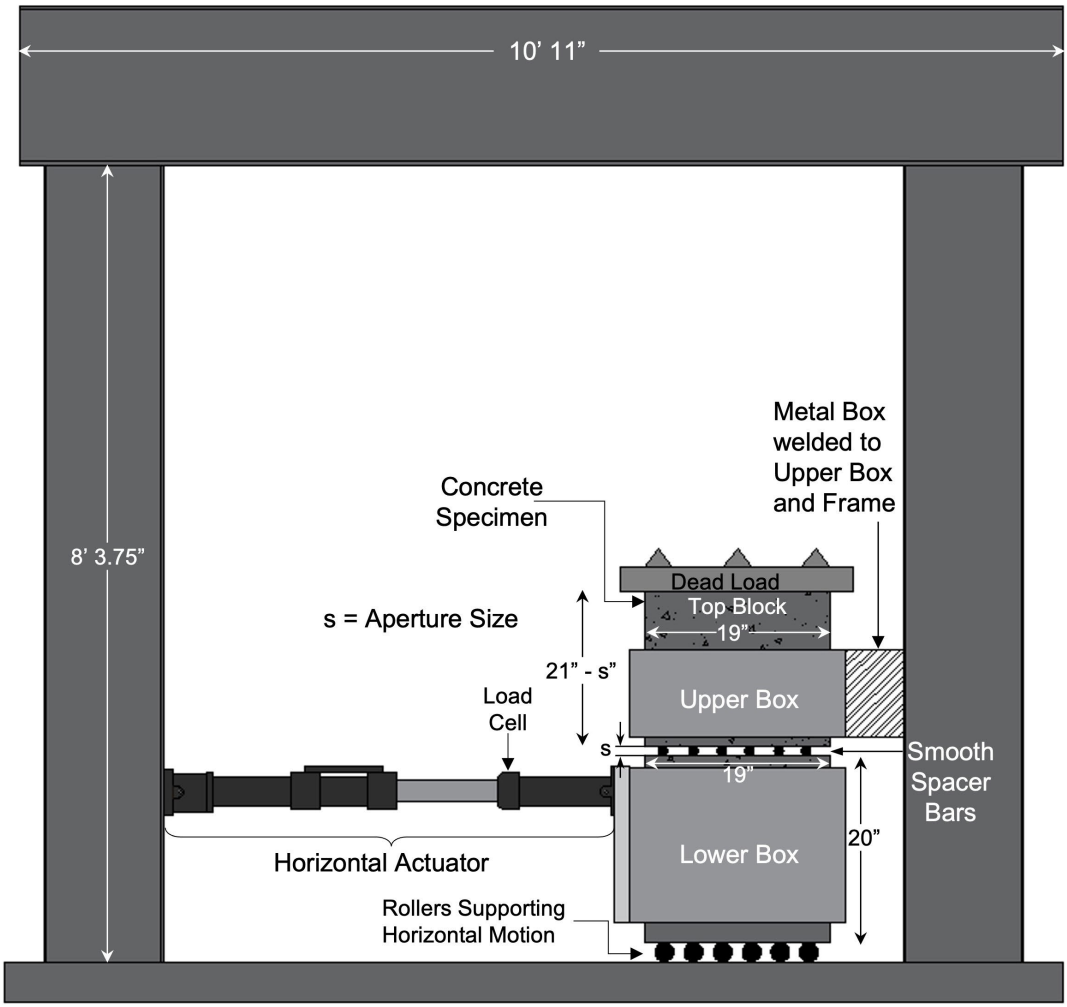

Note. Dimensions are given in English units, feet and inches. Schematic is not drawn to scale.

Figure 3.7 *Image of Direct Shear Test System*

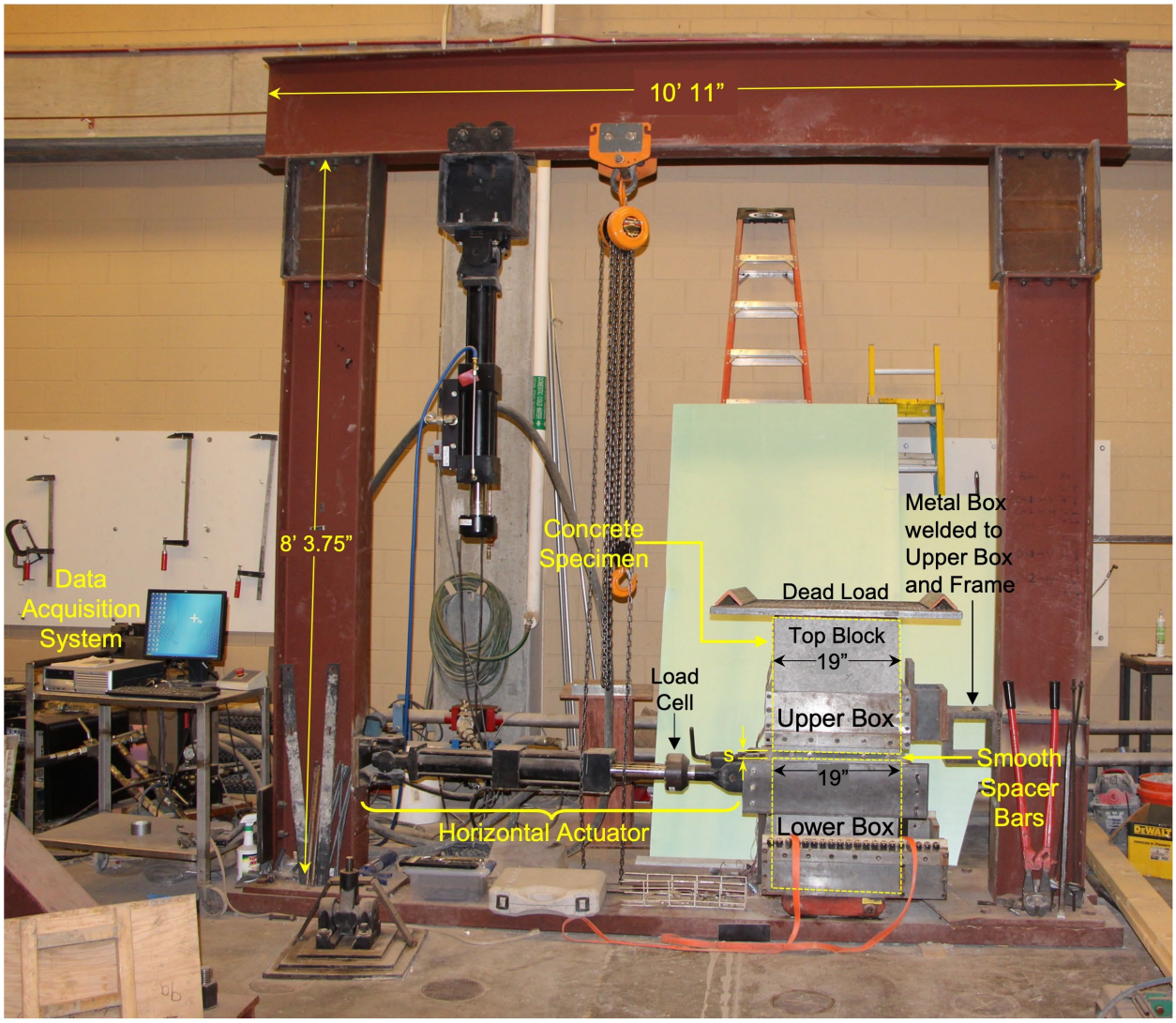

3.4 Investigated Variables

Based on the literature review, this study included the investigation of the influence of selected variables on the response of simulated dowelled-jointed rock systems subjected to shear loading. The variables included in this study are dowel (rebar) diameter, aperture (joint) size, dowel (rebar) angle of inclination with respect to the joint normal, and the dowel-rock (rebar-concrete block) bonding condition. The values selected for each variable are listed in Table 3.2.

Table 3.2 *Selected Variables and Their Values for Laboratory Direct Shear Test Conditions*

Variable	Selected Values
Rebar Diameter (bar #)	1/2" (1.27cm; #4) 5/8" (1.59cm; #5) 3/4" (1.91cm; #6)
Aperture Size	0.25" (0.64cm) 0.50" (1.27cm) 0.75" (1.91cm)
Inclination Angle	0°, 15°, 30°
Rebar-Concrete Block Bonding Condition	Top Block: unbonded (free/un-grouted) or fully bonded (fixed/grouted) Bottom Block: all cases fully bonded (fixed)

Based on the selected variables and variable values, 14 cases were tested. These 14 cases were tested in a randomly selected order to minimize the effect of operator experience from the beginning to the end of the test sequence. A subset of these 14 cases were then duplicated to ensure repeatability. Eight cases were randomly selected from the original combinations of variables/variable values for duplicate tests (again tested in a randomized order). Thus, a total of 29 laboratory tests were completed for this study. The sample IDs and variable descriptions for the 29 laboratory tests are listed in Table 3.3

In the unbonded condition, the portion of the rebar above the aperture was free to move along the rebar length to ensure that a pure bending load is applied to the rebar. As the aperture thickness increases, so does the moment acting on the rebar. The unbonded condition was accomplished by wrapping the upper portion of the rebar in a Teflon sheet prior to pouring the concrete in the mold. A select number of test cases were repeated in which the upper portion of the rebar was grouted so that tension developed as the aperture deforms, and mixed bending/tensile forces were introduced to the dowel. In practice, the full length of the dowel is grouted in place, which can induce tensile forces in the dowel as the joint slides or if the joint were to dilate. A packer or grout sleeve is used to keep the grout out of the joint in the field.

Table 3.3 *Sample ID and Variable Description for All Samples Tested*

Sample ID	Rebar Diameter (in)	Joint Aperture (in)	Angle (°)	Fixed/Free
1	0.5	0.25	15	Free
2	0.5	0.5	15	Free
2a	0.5	0.5	15	Free
3	0.75	0.75	15	Free
4	0.625	0.75	15	Free
4a	0.625	0.75	15	Free
4b	0.625	0.75	15	Free
5	0.625	0.25	15	Free
5b	0.625	0.25	15	Free
6	0.625	0.5	0	Free
6a	0.625	0.5	0	Free
7	0.75	0.25	15	Free
7a	0.75	0.25	15	Free
7 b	0.75	0.25	15	Free
8	0.625	0.5	15	Free
8a	0.625	0.5	15	Free
9	0.75	0.5	15	Free
9a	0.75	0.5	15	Free
9b	0.75	0.5	15	Free
10	0.625	0.5	30	Free
10a	0.625	0.5	30	Free
10b	0.625	0.5	30	Free
11	0.5	0.75	15	Free
11b	0.5	0.75	15	Free
12	0.625	0.25	15	Fixed
13	0.625	0.5	15	Fixed
13b	0.625	0.5	15	Fixed
14	0.625	0.75	15	Fixed
14b	0.625	0.75	15	Fixed

Note. "a" designates a repeated test, not randomly selected, and "b" designates a randomly selected retest.

For rebars with diameter > ½", one end of the rebar was bent into a hook shape (hooked end placed into the bottom concrete block) prior to placement in the mold to allow for appropriate development length inside the concrete specimen during testing. The rebars with ½" diameter (#4) had a total length of 38" (96.5cm). The rebars with 5/8" diameter (#5) had a total length of 43" (109cm) prior to bending. After bending one end of the bar into a hook shape, the length of the straight portion was 34" (86cm). The rebars with ¾" diameter (#6) had a total length of 43" (109cm) prior to bending. After bending, the length of the straight portion was 32" (81cm).

Note that aperture sizes ranging from <0.1mm-0.5mm are classified as very tight to partly open, 0.5mm-2.5mm are open, 2.5mm-10mm are moderately open, >10mm are wide, 1cm-10cm are very wide, 10cm-100cm are extremely wide, and >1m are cavernous (Higgins & Andrew, 2012).

3.5 Data Collection and Analysis

Measured data for all direct shear tests included applied shear load, lower box horizontal displacement, and strain gage responses. The shear force and resulting horizontal displacement were collected using a FlexTest GT controller (MTS 793 software, version 3.5C 1815). A digital data acquisition system (MM 8000 Application, Version: 1.0.16.0) was used to collect rebar strain response from the attached strain gages throughout the duration of each test. The strain gages were connected to the data acquisition system prior to the start testing.

The raw data was collected and processed for comparative analysis details of which can be found in Chapter 4.

3.6 Technical Assumptions

Several technical assumptions in the research methodology described previously were applied:

1. There is no interaction between dowels, the dowel spacing is sufficient that each dowel can mobilize its full capacity.
2. The role of joint friction in the shear resistance is neglected.
3. The un-tensioned dowel method could be applied to wedge failures as well as planar failures. The focus of this investigation was planar geometry.
4. The role of dowel diameter relative to the joint spacing can be investigated with anchor diameters less than typically deployed in practice, since the governing stress and strain relationships are the same.

3.7 Numerical Model

Physical testing inherently has limitations in terms of the number and values of variables that can be investigated. A numerical model of the physical testing set-up was developed to supplement the experimental results from the direct shear testing and increase the robustness of the developed design chart.

ABAQUS FEA software was used to simulate the large-scale direct shear tests performed in the laboratory. A 3D Finite Element model was adopted for analysis in ABAQUS. The concrete blocks were modelled with dimensions of 20” × 20” × 20” (50.8 cm x 50.8 cm x 50.8cm) with various aperture sizes to simulate the physical testing conditions. Note that the model dimensions are slightly different from those of the actual concrete blocks but have a minimal influence on the results. The rebar was modelled with different diameters and inserted in the virtual concrete blocks at different inclination angles. The material properties of concrete blocks and rebar were held constant for different arrangements of specimen assembly. Material properties used for the concrete were elastic and concrete damaged plasticity (CDP) parameters. Steel elastic and plastic material properties were used for the rebar. Table 3.3 and Table 3.4 list the material properties adopted for the concrete and steel throughout the analyses. Poisson’s ratios of 0.2 and 0.25 were obtained during model calibration for concrete

and steel, respectively. These values are consistent with those found in the literature (Dudziak et al., 2021; Eiriksson et al., 2018).

The CDP model for concrete requires specific parameters to be defined such as dilation angle (Φ), eccentricity (ε), ratio σ_{b0}/σ_{c0}, K_c, and viscosity parameter (μ). These parameters define the response of concrete when subjected to loads that lead to the failure of concrete. The dilation angle (Φ) and eccentricity (ε) in CDP relate to the plastic flow potential as described by the Drucker-Prager hyperbolic function. Eccentricity (ε) defines how the hyperbolic flow potential approaches its asymptote. The ratio σ_{b0}/σ_{c0} and K_c are parameters related to the yield surface. The ratio σ_{b0}/σ_{c0} is the ratio of equibiaxial compressive yield stress to the uniaxial compressive yield stress of concrete. The parameter K_c is defined as the ratio of second stress invariant on the tensile meridian to that on the compressive meridian. The ABAQUS default values of ε, σ_{b0}/σ_{c0} and K_c were used for the numerical analysis (Kaminski & Kmiecik, 2011; Prado et al., 2021). The viscosity parameter (μ) is used to describe viscous materials. A value of μ (1×10^{-6}) was used to converge the laboratory and model results (Mathern and Yang, 2021).

The modeled system consisted of a rebar inserted between the concrete blocks. Contact interactions were provided for the rebar and concrete blocks. Only free (un-grouted) cases were simulated and analyzed.

Table 3.4 *Material Properties of Concrete and Steel Used in the Numerical Analysis*

Property	Modulus of Elasticity psi (Mpa)	Poisson's Ratio	Density lb/in^3 (kg/m^3)
Concrete	60000 (415)	0.2	0.085 (2353)
Steel	15000000 (103420)	0.25	0.285 (7890)

Table 3.5 *Plasticity Parameters Defined in the Concrete Damage Plasticity (CDP) Model (Mathern & Yang, 2021)*

Categories	Plastic Flow Potential		Yield Surface		Viscosity parameters
Parameters	Φ	ε	σ_{b0}/σ_{c0}	K_c	μ
Values	30◦	0.1	1.16	0.667	1×10^{-6}

The interaction for the rebar and the top block was made using a general surface to surface contact, with a very small coefficient of friction, 1E-05. The low value of coefficient of friction between the top block and the rebar simulated the actual laboratory condition (rebar unbonded to the top block). The interaction for rebar and bottom block was made using the general surface to surface contact with coefficient of friction equal to 0.25. The higher value of coefficient of friction simulated the condition that the rebar was fully bonded in the bottom concrete block. A normal load of 0.3 psi was applied to the top concrete block. The bottom block was subjected to a displacement of approximately 1 inch (2.54 cm) in the x–direction and the top block was restricted for any movement in the x-direction.

The selection of element type and mesh density played a critical role in obtaining accurate results. Hexahedral elements were adopted for the generation of mesh in the model with global size of 1.5 inch to obtain the finer mesh (Figure 3.8). To improve the quality of the model mesh, partitioning of the cells was carried out to generate more edges for developing mesh seeds. An eight-node linear brick element, reduced integration (C3D8R) elements were used to prevent any shear locking effects (Genikomosou & Polak, 2015).

Figure 3.8 *Meshing for a Typical Specimen in ABAQUS*

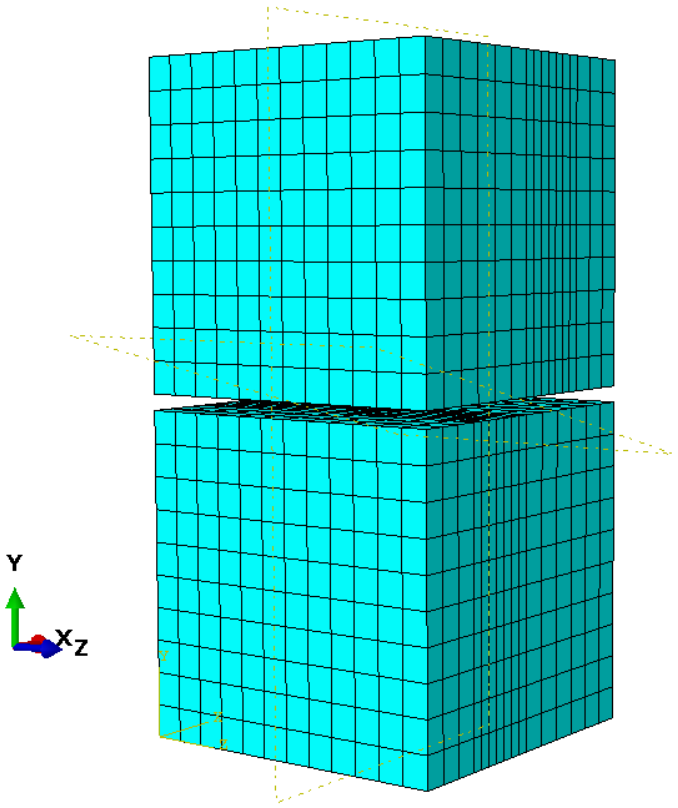

The Finite Element Analysis of the model was carried out in two steps. The first step involved the creation of interaction between the rebar and concrete blocks, creation of boundary conditions, and the application of the normal load. The second step involved the application of displacement on the bottom block. Calibration and validation of the model based on the load-displacement plots were carried out prior to the application of the model for parametric analysis. Calibration of the model was based on the physical testing results (load-displacement response) from selected specimens tested in the laboratory: Specimens 7 and 7b (see Appendix A). For a given load-displacement dataset, several parameters were varied such that the response from the model approached that of the laboratory test (see Figure 3.9). Accuracy of the model results was improved by applying different meshing sizes. Stiffness and yield stress values of both steel and concrete were also varied during the calibration process. The concrete damage plasticity for concrete was calibrated by varying the dilation angle (Genikomosou & Polak, 2015). The peak load value obtained from the load-displacement results for Specimen 7b used for model calibration was 11.52 kips. The calibrated model

resulted in a peak value of 12.37 kips. Validation of the model was carried out by comparing the model results (load-displacement response) with a selected set of laboratory test results not previously used for calibration: Specimens 6a, 8, 9b, and 11 (see Appendix A). The model was considered validated once the physical testing and model results approximated each other. For example, the peak load from the laboratory load-displacement curve for Specimen 8 was 7.21 kips. The corresponding model resulted in the peak value of 7.36 kips. The sample IDs and variable descriptions for the specimens analyzed using numerical modelling are listed in Table 3.6.

Figure 3.9 *Example of a Comparison of Physical Testing Load vs. Displacement to ABAQUS Model Results*

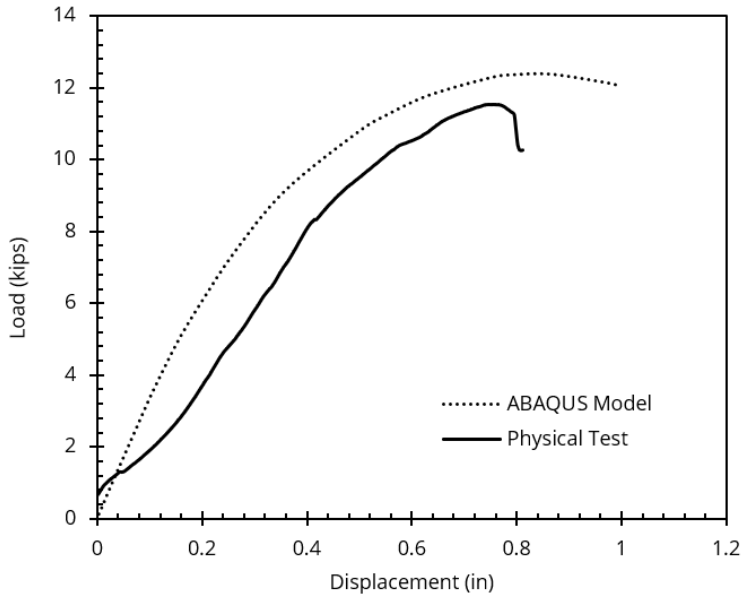

Table 3.6 *Sample ID and Variable Description for Specimens Analyzed in ABAQUS*

Sample ID	Rebar Diameter (in)	Joint Aperture (in)	Angle (°)	Fixed/Free
M1	0.5	0.125	15	Free
M2	0.5	0.25	15	Free
M3	0.5	0.5	15	Free
M4	0.5	0.75	15	Free
M5	0.5	1	15	Free
M6	0.625	0.125	15	Free
M7	0.625	0.25	15	Free
M8	0.625	0.5	15	Free
M9	0.625	0.75	15	Free
M10	0.625	1	15	Free
M11	0.75	0.125	15	Free
M12	0.75	0.25	15	Free
M13	0.75	0.5	15	Free
M14	0.75	0.75	15	Free
M15	0.75	1	15	Free

Chapter 4 Results and Discussion

Rock slopes in Tennessee are often reinforced with grouted steel anchors oriented to be loaded in shear and not tension. The purpose of this work is to confirm the assumptions used in the design of rock slopes reinforced with grouted steel anchors and to determine the joint aperture where bending instead of shear failure occurs. This has been achieved through the means of large-scale direct shear testing and numerical modeling. This chapter provides an overview of the data analysis process, background on theoretical shear and bending capacity for steel dowels, and concludes with a design chart for use in the determination of dowel capacity (ultimate resisting force) with relation to dowel properties and joint aperture

4.1 Ultimate Resisting Force Determination

The ultimate resisting force, Fy, for each specimen was determined using the load and displacement data collected for each specimen. Shear force was applied to the physical specimens until either the specimen showed signs of failure or the equipment reached capacity at 22 kips. The resulting data was plotted as shown in Figure 4.1 with displacement on the horizontal axis and load on the vertical axis. Ultimate resisting force was taken as the peak value of the plotted data.

Figure 4.1 *Load vs. Displacement Plot Showing Peak Shear Resistance (Ultimate Resisting Force) Determination*

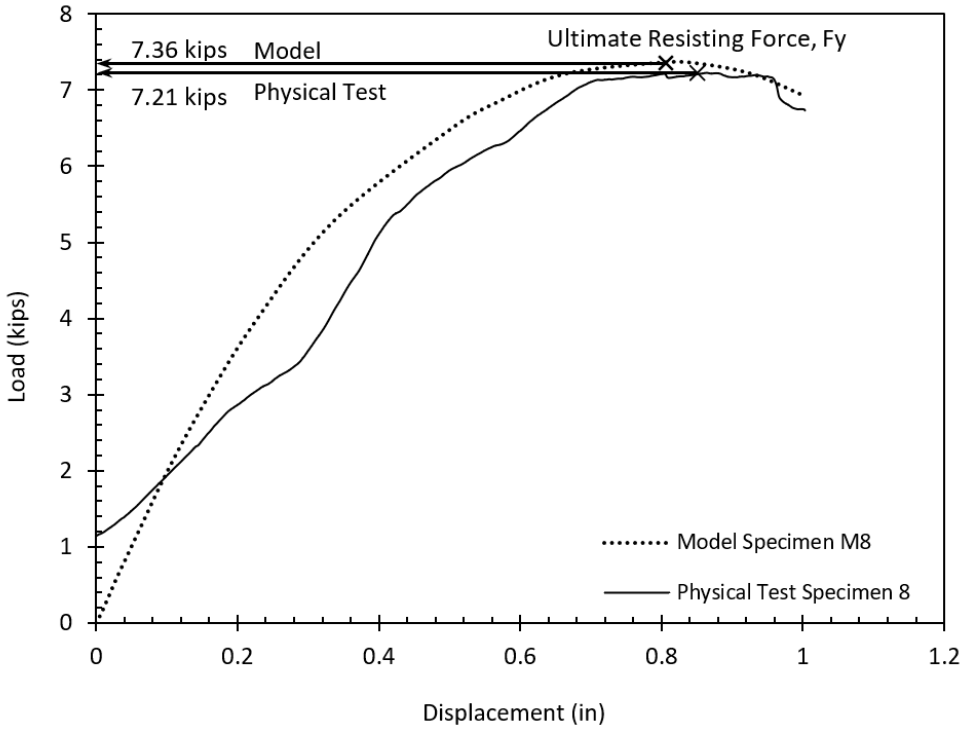

The results of this analysis can be found in Table 4.1. It is to be noted that not all 29 physical specimens have been included in Table 4.1. In the case of repeated specimens, one representative data set for each variable configuration has been included to provide an evenly weighted distribution of results. Load-displacement curves for the cases listed in Table 4.1 can

be found in Appendix A. The analysis for modeling results was conducted using the same process. The test cases and ultimate resisting forces used for analysis are summarized in Table 4.2. The load-displacement response curves for all modeled cases can be found in Appendix B.

Table 4.1 *Variable description and ultimate resisting force for physical test specimens used in analysis*

Physical Test Sample ID	Rebar Diameter (in)	Joint Aperture (in)	Angle (°)	Fixed/Free	Physical Test Fy (kips)
1	0.5	0.25	15	Free	22
2	0.5	0.5	15	Free	17.8
3	0.75	0.75	15	Free	22
4 b	0.625	0.75	15	Free	7.99
5 b	0.625	0.25	15	Free	7.34
6 a	0.625	0.5	0	Free	7.92
7 b	0.75	0.25	15	Free	11.52
8	0.625	0.5	15	Free	7.21
9b	0.75	0.5	15	Free	10.75
10b	0.625	0.5	30	Free	7.45
11b	0.5	0.75	15	Free	4.06
12	0.625	0.25	15	Fixed	10.2
13b	0.625	0.5	15	Fixed	8.39
14b	0.625	0.75	15	Fixed	7.58

Note. "a" denotes a repeated test, not randomly selected, and "b" designates a randomly selected retest.

Table 4.2 *Variable description and ultimate resisting force for modeled test specimens used in analysis*

Model Sample ID	Corresponding Physical Test ID (if applicable)	Rebar Diameter (in)	Joint Aperture (in)	Angle (°)	Fixed/ Free	Model Fy (kips)
M1	n/a	0.5	0.125	15	Free	7.37
M2	1	0.5	0.25	15	Free	7.05
M3	2	0.5	0.5	15	Free	5.75
M4	11b	0.5	0.75	15	Free	4.92
M5	n/a	0.5	1	15	Free	4.00
M6	n/a	0.625	0.125	15	Free	9.29
M7	5b	0.625	0.25	15	Free	7.69
M8	8	0.625	0.5	15	Free	7.36
M9	4b	0.625	0.75	15	Free	6.54
M10	n/a	0.625	1	15	Free	5.59
M11	n/a	0.75	0.125	15	Free	12.44
M12	7b	0.75	0.25	15	Free	12.37
M13	9b	0.75	0.5	15	Free	9.21
M14	3	0.75	0.75	15	Free	8.43
M15	n/a	0.75	1	15	Free	7.25

4.2 Strain Gage Results

Strain gages were applied along the length of each dowel prior to testing with the aim of gathering data related directly to bending behavior. The results of the strain gage data were generally unusable for a variety of reasons, but primarily due to physical damage caused by concrete encasement process used to create the simulated rock joints. While pure bending analysis is not possible with truncated data, it is possible to deduce that there are peaks in strain in locations where bending is expected to occur.

Figure 4.2 provides the peak strain gage reading for seven strain gages located along the length of one dowel. The horizontal axis is the distance of the gage from the center of joint aperture with the negative numbers representing the distance below the joint (bottom block) and the positive number representing the distance above the joint (top block; see Figure 3.3), the vertical axis is the peak strain recorded for each gage. As expected, the strain is higher near the joint. This specimen was "free" meaning that the top half of the bar was un-bonded and the aperture size was 0.75 inches. Theoretically, this means that there should be double bending behavior (recall Figure 2.8) and the stress in the bottom block should be higher than the stress in the top block. This theory is confirmed by the data in Figure 4.2. Additionally, in double bending, the center of the joint will be pulled into pure tension, and as such, experience less strain than either side of the joint. This is also confirmed by the data in Figure 4.2.

Figure 4.2 *Peak Strain Distribution Along the Rebar for Specimen 3*

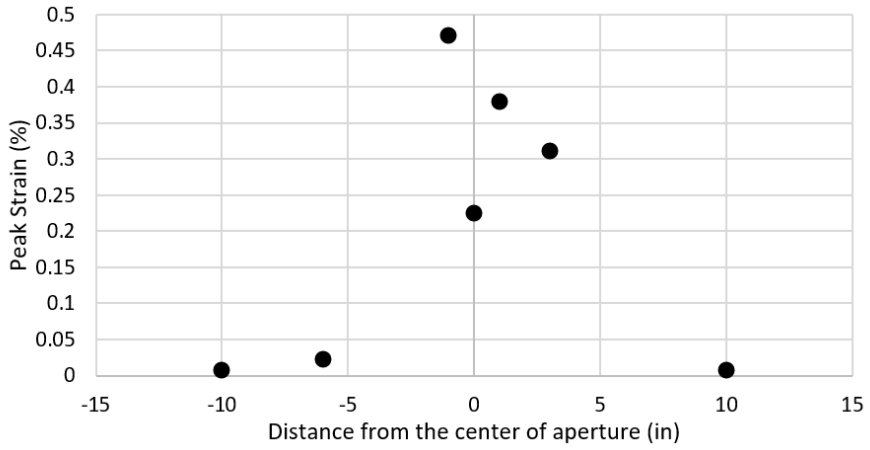

4.3 Theoretical Shear and Bending Calculations

A key purpose of this work is to determine the joint aperture at which the shear capacity of a given dowel must be reduced due to the influence of bending forces. To do this, first the shear capacity was calculated for each bar size and strength using the Equation 4.1 wherein Z_y is the shear strength of the bar, taken as 0.5Fy via the Tresca Criterion, and A_b is the cross-sectional area of the bar. This equation results in a single value for all joint aperture scenarios for a given bar.

$$F_{shear} = Z_y A_b \quad \text{(Eqn. 4.1)}$$

In order to get a more accurate prediction of capacity, the forces associated with bending must also be considered. Treating the portion of the dowel that crosses the joint aperture as a simply supported beam, bending stress can be calculated via Equation 4.2. Here M refers to the moment induced at the center of the joint, c is the distance from the neutral axis, or center, of the dowel, and I is the moment of inertia in the direction of bending.

$$\sigma_{Bending} = \frac{Mc}{I} \quad \text{(Eqn. 4.2)}$$

Moment is calculated by multiplying a force by a distance. In this case, the force is designated as $F_{bending}$ and the distance is half of the joint aperture (Eqn. 4.3).

$$M = F_{Bending}\,\frac{s}{2} = \frac{\sigma I}{c} \quad \text{(Eqn. 4.3)}$$

Finally, solving for $F_{bending}$ reveals an equation (Eqn. 4.4) that takes into account the characteristics of the dowel as well as the aperture spacing.

$$F_{Bending} = \frac{2F_y I}{cs} \quad \text{(Eqn. 4.4)}$$

It should be noted that any dilation in the joint will affect the cross-sectional area of the bar and increase this value along with c and I. Zero degrees dilation represents the most conservative case.

As an example, both F_{shear} and $F_{bending}$ have been calculated for a 60-ksi #8 dowel at a range of joint apertures, and the results are shown in Figure 4.3. Near the zero-aperture point, the bending capacity is higher than the shear capacity. This continues until an aperture value of approximately half of the dowel diameter where the bending values drop below the shear capacity line. When the bending values are higher than the shear values, the shear capacity governs. When the shear capacity values are higher than the bending values, the bending capacity governs.

Figure 4.3 *Theoretical shear and bending resistance in a grade 60 #8 dowel*

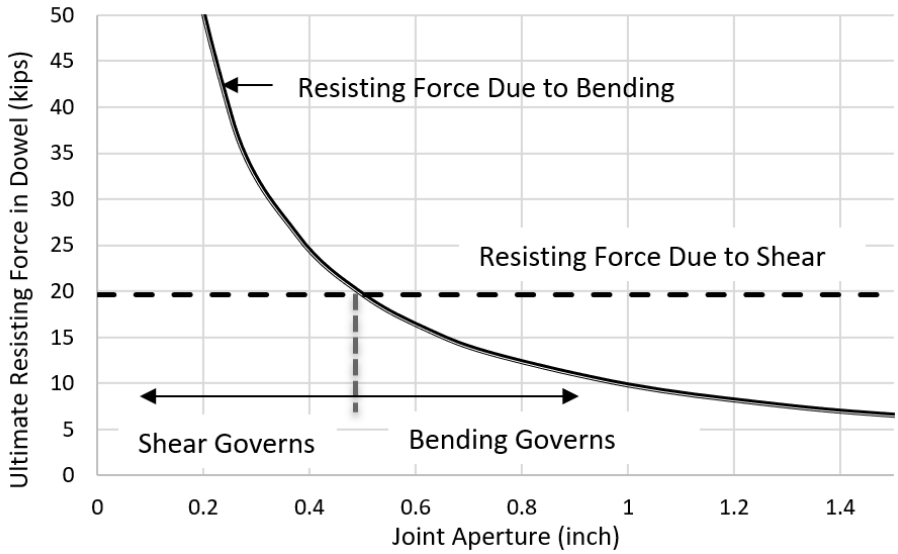

4.4 Comparison of Ultimate Resisting Force to Theoretical Shear and Bending Capacity

The ultimate resisting force for each specimen was determined according to section 4.1 and is given in Tables 4.1 and 4.2. Figure 4.4 takes the theory shown in Figure 4.3 and expands the results to include three dowel diameters, 0.5", 0.625", and 0.75". Recalling from Table 4.1, those are also the dowel diameters tested experimentally. The results of the physical testing as well as the results of modeling are shown as data points on top of the theoretical capacity lines in Figure 4.4. There are three notable outliers, but a majority of the data points follow the expected behavior.

Figure 4.4 *Ultimate Resisting Force as Compared to Theoretical Shear and Bending for 0.5", 0.625", and 0.75" Diameter Dowels*

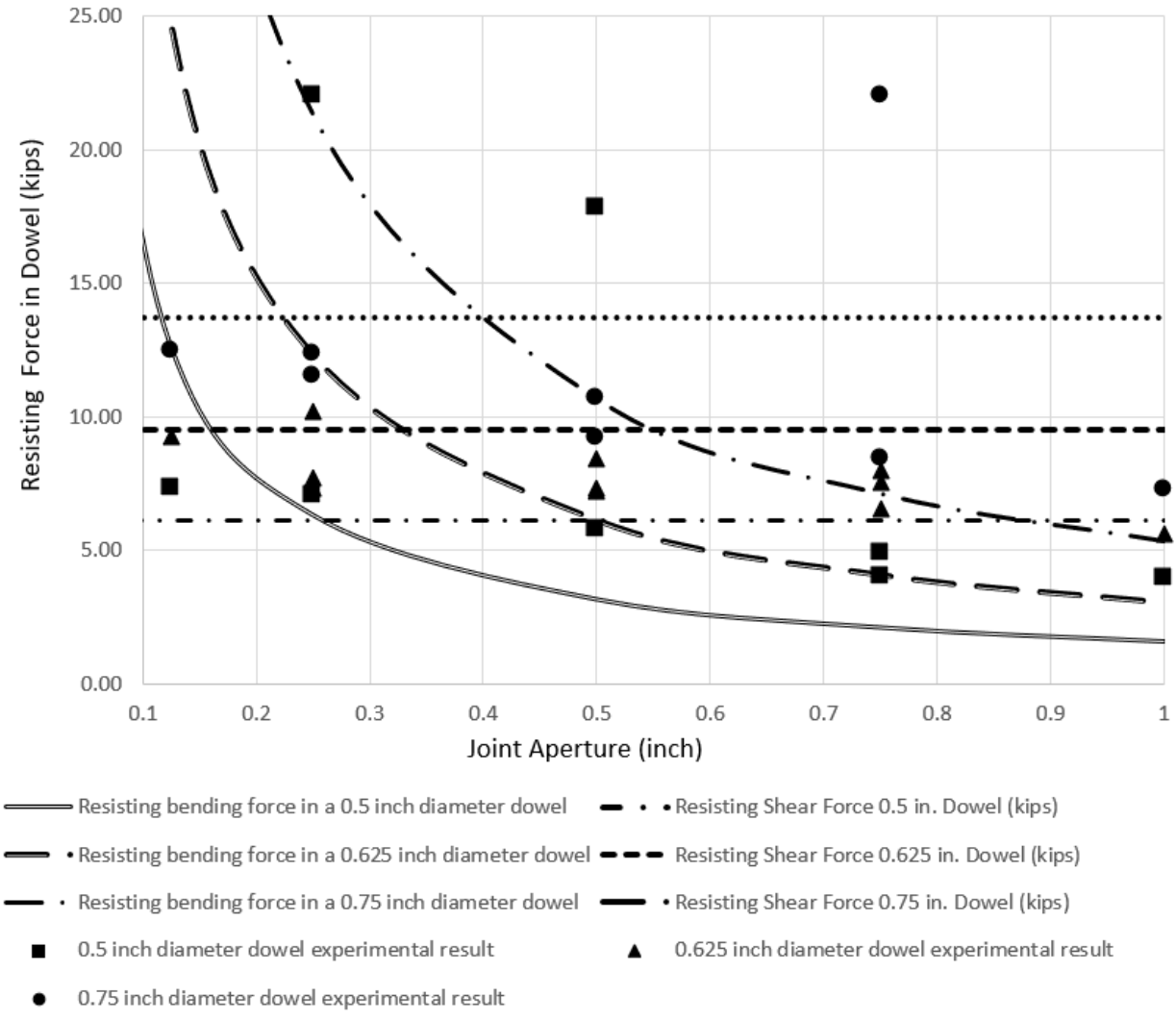

By breaking the data set down into individual bar diameter plots (Figures 4.5-4.7), it is apparent that the dowel performance aligns with the governing conditions provided in Figure 4.3. Figure 4.7 shows the strongest alignment, but all data sets show sufficient agreement to warrant the conservative use of the theoretical governing equations in the creation of a design chart (Figure 4.8.). It should be noted that the values in Figure 4.6 include both free and fixed condition specimens of which there is no notable difference in ultimate resisting force.

Figure 4.5 *Ultimate Resisting Force as Compared to Theoretical Shear and Bending for 0.5" Diameter Dowels*

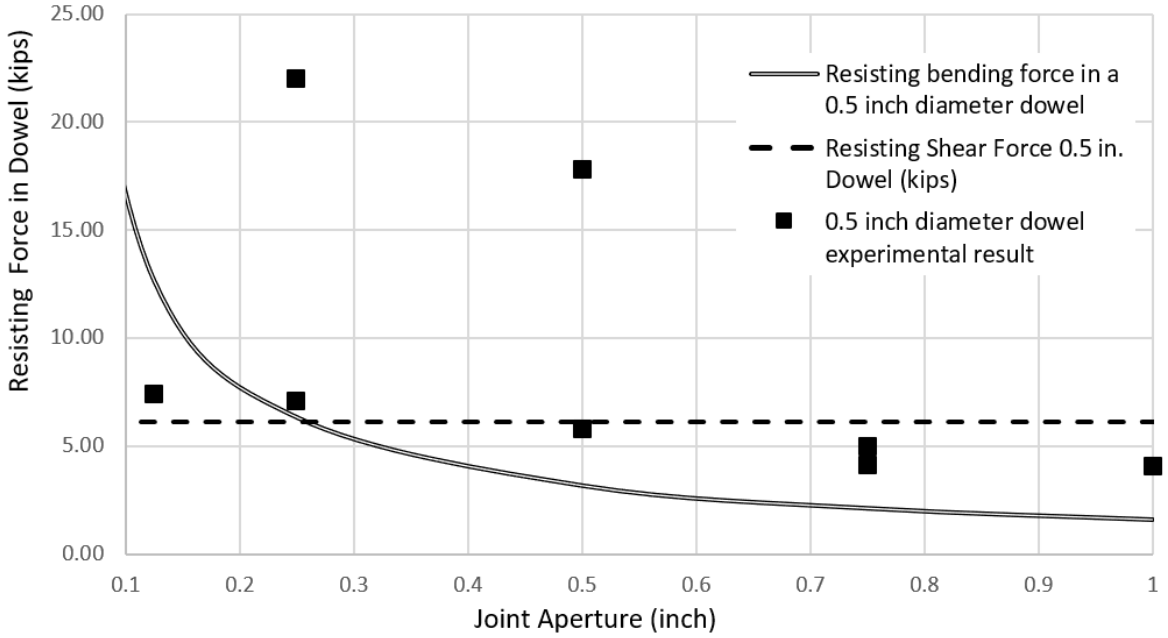

Figure 4.6 *Ultimate Resisting Force as Compared to Theoretical Shear and Bending for 0.625" Diameter Dowels*

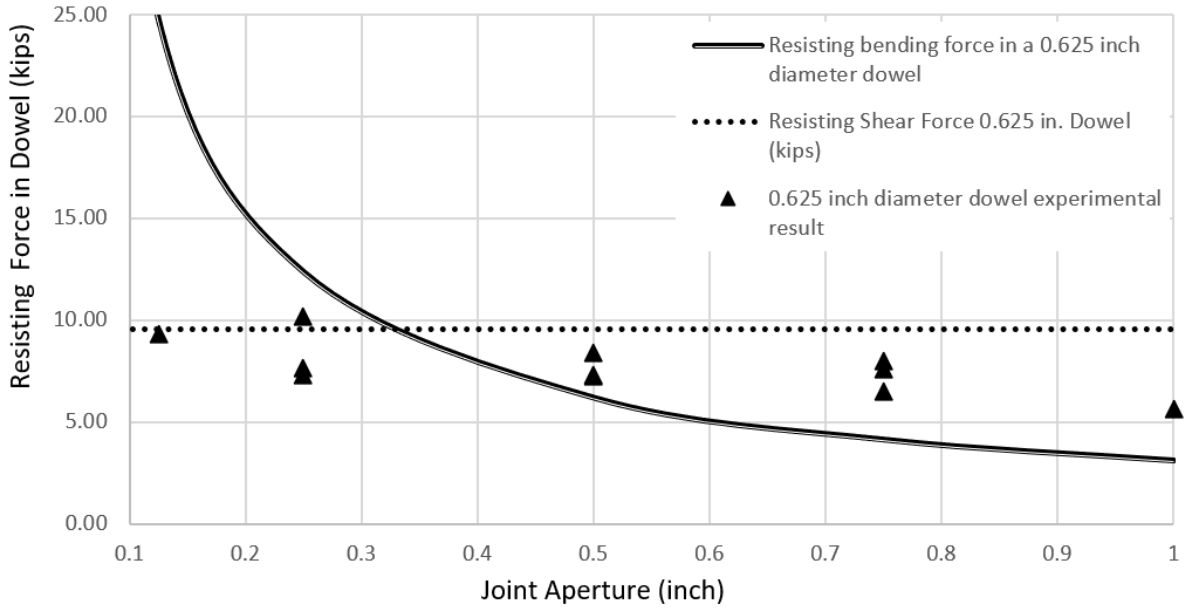

Figure 4.7 *Ultimate Resisting Force as Compared to Theoretical Shear and Bending for 0.75" Diameter Dowels*

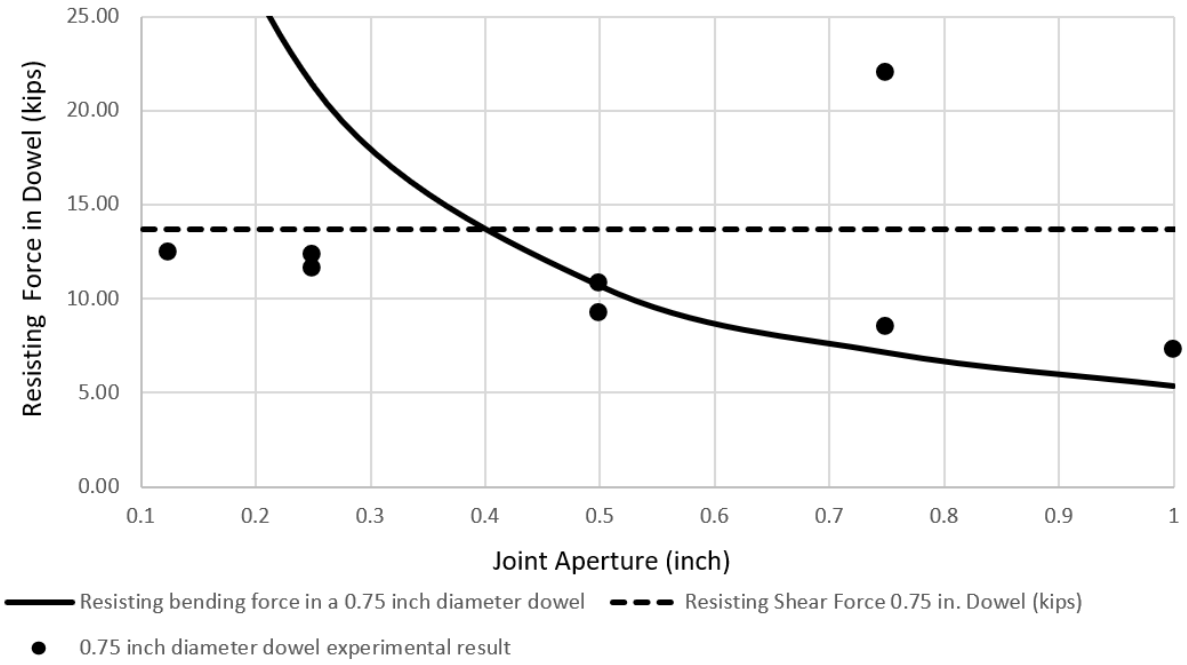

4.5 Un-Tensioned Dowel Capacity Design Chart

The results of this investigation are presented in a form of a design chart, where the reduction in capacity relative to the pure shear value can be determined based on an estimated joint spacing. This chart will be useful to TDOT engineers and geologists in Regions 1, 2, & 3 in terms of an additional approach to supplement tensioned rock bolts to mitigate rockfall hazards.

Given the confirmation provided through physical testing and numerical modeling, a design chart is presented (Figure 4.8.). TDOT has successfully utilized un-tensioned rock dowels in the past, typically deploying #8 and #10 bars of either grade 50 or 75. Though grades 50 and 75 are the most common grades used for rock dowels, a chart has also been included for grades 60 and 80 which are more prevalent in reinforcing steel (Figure 4.9). These bar sizes and strengths are included in the design chart with the intent of providing applicable information that can be implemented immediately. Curves for the #6 and #12 bars have also been included.

To use the chart, select a dowel size and grade. Then, find the estimated joint aperture on the horizontal axis and draw a vertical line straight up from the aperture value. The point at which the drawn vertical line crosses the line for the selected dowel diameter corresponds to the predicted resisting force for the dowel. Values for grade 50 dowels are read on the left vertical axis and values for grade 75 dowels are read on the right vertical axis.

Notes on inclination angle: The dowel inclination angle with respect to the joint increases the theoretical capacity of a dowel as it increases the subject cross-sectional area. This increase was not observed in the test results used to derive this design chart. Additionally, results in the literature (Spang & Egger, 1990) also failed to see a notable increase in dowel capacity as inclination increased for most cases. As a result, only the case of dowels installed perpendicular to the joint is given for design. This is also the most conservative configuration.

This chart will allow TDOT personnel responsible for developing rockfall mitigation measures to expand the application of un-tensioned rock dowels with increased confidence in their safety. Because these are more cost effective than tensioned rock anchors, a greater number of slopes can be remediated for the same cost.

Figure 4.8 *Un-Tensioned Dowel Shear Capacity Design Chart for Grade 50 and Grade 75 Rebar (Bar Angle of Inclination is Zero Degrees)*

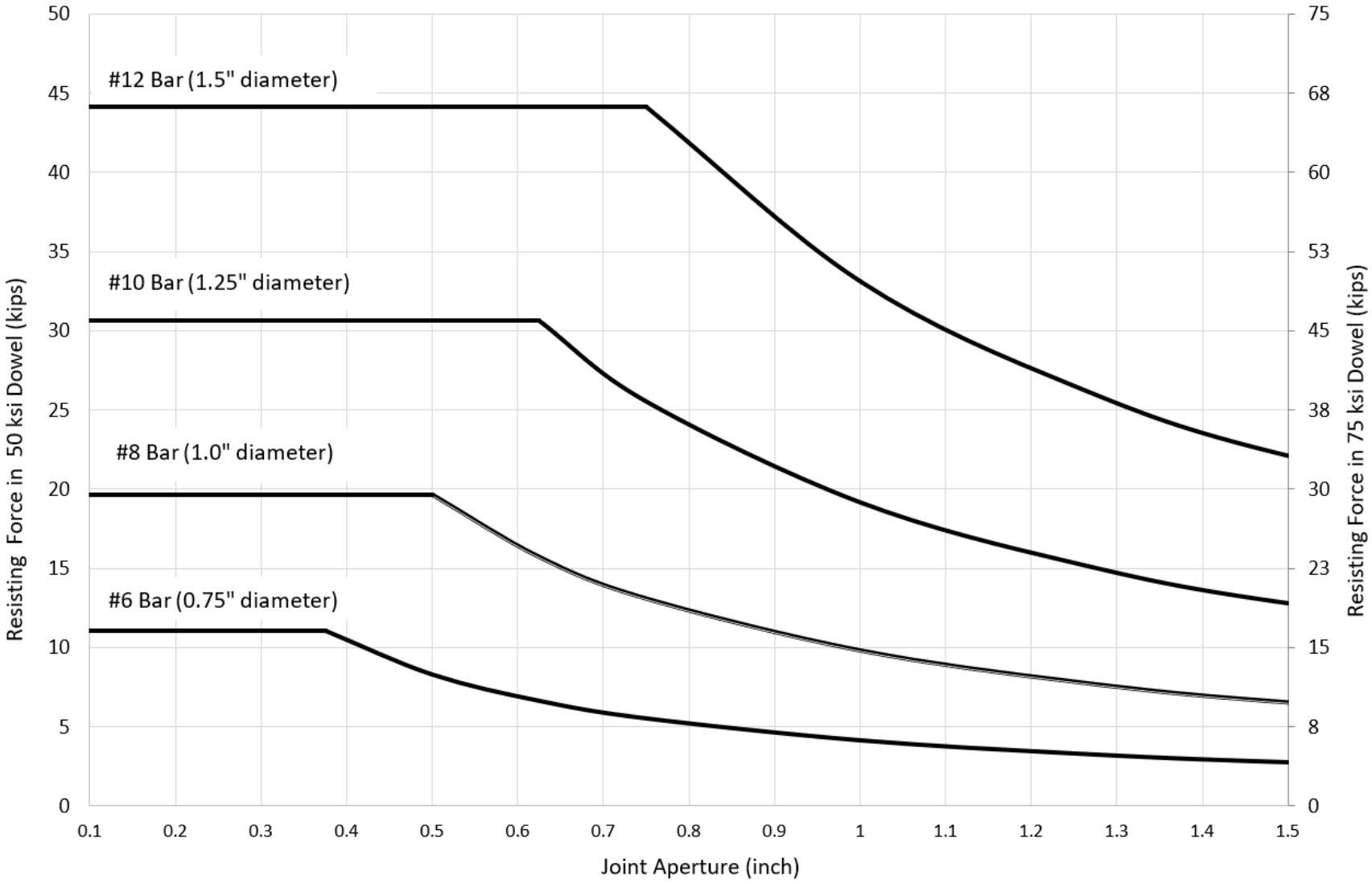

Figure 4.9 *Un-Tensioned Dowel Shear Capacity Design Chart for Grade 60 and Grade 80 Rebar (Bar Angle of Inclination is Zero Degrees)*

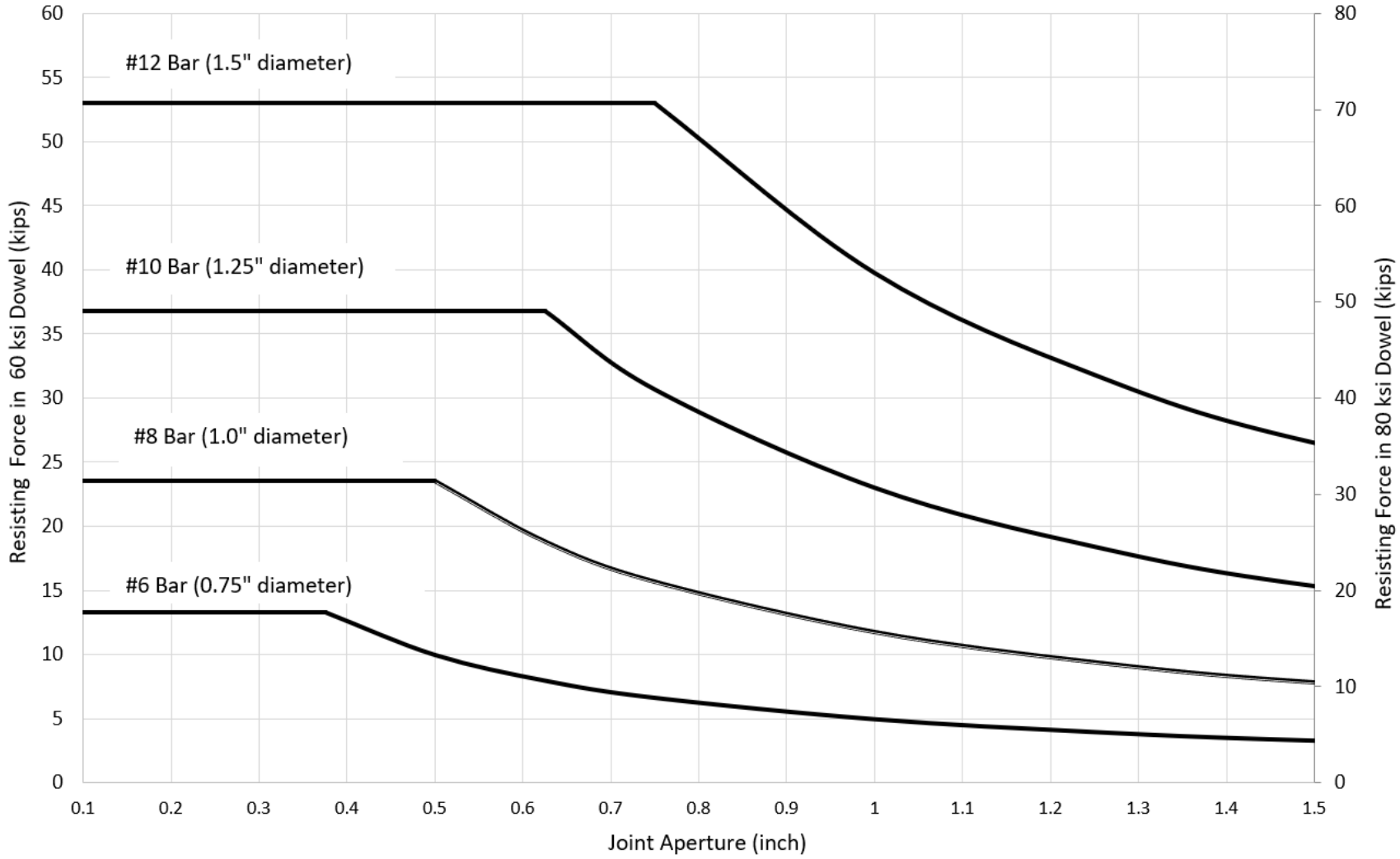

Chapter 5 Conclusions

In Tennessee, cut rock slopes with exposed discontinuities are often reinforced with grouted steel anchors. These elements are installed across the discontinuity to stabilize the system by immobilizing the rock material above the sliding surface (discontinuity). The function of the rock anchors is to resist shear loading rather than tension. However, the steel bar may experience bending in cases where the discontinuity is sufficiently large. The purpose of this study was to investigate the performance of simulated un-tensioned dowel-jointed rock block systems subjected to shear loading and evaluate whether bending likely occurred as well as its contribution to the reduction in dowel capacity. The performance of simulated un-tensioned dowel-jointed rock block systems subjected to shear loading was investigated through physical testing and numerical simulations. The dowelled rock block system response was studied as a function of aperture size (joint spacing), dowel diameter, and dowel angle of inclination with respect to the joint normal. A total of 29 physical experiments were conducted using large concrete blocks to simulate the jointed rock material and steel rebars to simulate the dowels. A large-scale direct shear apparatus was used to apply shear loading. A corresponding numerical model was developed to generate additional results by extending the test dowel size and joint thickness. An additional 15 test cases were tested using the numerical model. The results from the experimental and numerical studies were used to develop a design chart describing the shear capacity of a given diameter dowel which identifies the threshold between the pure shear capacity and the reduced capacity due to bending effects as a function of joint thickness.

The main conclusions derived from this study are:

- The rebar double bending phenomenon (formation of plastic hinges) was inferred from the strain gage data in the case of a large aperture size (joint spacing of 0.75 inches). However, this observation is limited given most of the collected strain gage data for other test cases was unusable due to physical damage caused by concrete encasement process.
- Bending reduces the dowel shear capacity by a quantity related to bar size and aperture size.
- Bending begins to occur at an aperture size relative to bar diameter and strength.
- Based on the conducted physical tests and numerical analyses results, dowel response is in good agreement with the governing equations for theoretical shear and bending conditions. All data sets show sufficient agreement to warrant the conservative use of the theoretical shear and bending governing equations in the creation of the developed design chart (Figure 4.8 and Figure 4.9).
- The dowel inclination angle with respect to the joint increases the theoretical capacity of a dowel as it increases the subject cross-sectional area. In this study, dowel inclination angle had little influence on ultimate shear resistance based on the test results used to derive this design chart. This finding is in agreement with results found in the literature (Spang & Egger, 1990).
- Free and fixed dowel placement show no real difference in resistance. In other words, the bonding condition of the rebar in the upper block did not significantly influence the ultimate shear resistance of the rebar, regardless of size or joint opening size.

This investigation integrated both physical testing and numerical modeling results. Yet, much more work on this topic remains. The nature of the large-scale physical testing inherently meant that each experiment would take a significant amount of time (mold construction, concrete curing, etc.). However, while only a limited number of tests could be completed, several important insights were gained. Development of the numerical model was necessary to supplement laboratory-obtained results. Furthermore, the developed design chart will be useful to TDOT engineers and geologists in Regions 1, 2, & 3 as an additional approach to supplement tensioned rock bolts to mitigate rockfall hazards.

One significant limitation of this work is that the study focused on planar-type failure modes (which may include wedge failure mode). While rock anchors are typically applied to planar and wedge failure modes, mitigation for other failure modes (circular sliding, toppling, differential weathering) are not addressed here. Other limitations include the relatively low number of variables addressed in this study. For example, the compressive strength of the surrounding rock material and interface friction at the discontinuity impact the resistance of the dowelled-jointed rock system.

The following recommendations are made based on the findings of this study:

- Un-tensioned dowels may be safely used to mitigate rock masses exhibiting the potential of planar type failures. However, consideration must be given to whether relative rock movement has already taken place, compressive strength of the surrounding rock, number of dowels proposed, extent of discontinuities, etc.
- The design chart should be used as an additional approach to rock stabilization in particularly dangerous areas. Because dowels are more cost effective than tensioned rock anchors, a greater number of slopes can be remediated for the same cost.
- A survey of the use of rock anchors/dowels in every state should be completed. This would be beneficial in the development of a national standard or guidelines.

References

Andrew, R.D. & Pierson, L.A. (2012). Stabilization of rockfall. In A.K. Turner & R.L. Schuster (Eds.), *Rockfall characterization and control* (pp. 468-493). Transportation Research Board.

Chau, K.T., Wong, R.H. C., Liu, J. & Lee, C.F. (2003). Rockfall hazard analysis for Hong Kong based on rockfall inventory. *Rock Mechanics and Rock Engineering*. 36(5), 383–408. doi: 10.1007/s00603-002-0035-z

Deere, D.U. & Miller, R.P. (1966). Engineering classifications and index properties for intact rock. Technical Report No. AFWL-TR 65-116, Air Force Weapons Laboratory, Kirtland Air Force Base, New Mexico.

Dudziak, S., Jackiewicz-Rek, W., & Kozyra, Z. (2021). On the calibration of a numerical model for concrete-to-concrete interface. *Materials*. 14(23), 7204.

Eiriksson, H.J., Bessason, B., & Unnthorsson, R. (2018). Uniaxial and lateral strain behavior of ribbed reinforcement bars inspected with digital image correlation. *Structural Concrete*. 19(6), 1992-2003.

Federal Highway Administration (FHWA). (1993). Rockfall hazard rating system: Participant's manual. NHI Course No. 130220. Publication No. FHWA SA-93-057. National Highway Institute.

Ferrero, A.M. (1995). The shear strength of reinforced rock joints. *International Journal of Rock Mechanics and Mining Sciences & Geomechanics*. 32(6), 595-605.

Genikomsou, A.S., & Polak, M.A. (2015). Finite element analysis of punching shear of concrete slabs using damaged plasticity model in ABAQUS. *Engineering Structures*, 98, 38-48.

Higgins, J.D. & Andrew, R.D. (2012). Site characterization. In A.K. Turner & R.L. Schuster (Eds.), *Rockfall characterization and control* (pp. 177-211). Transportation Research Board.

Hungr, O., Evans, S.G. and Hazzard, J. (1999). Magnitude and frequency of rock falls and rock slides along the main transportation corridors of southwestern British Columbia. *Canadian Geotechnical Journal*. 36(2), pp. 224–238. doi: 10.1139/t98-106.

Kmiecik, P., & Kamiński, M. (2011). Modelling of reinforced concrete structures and composite structures with concrete strength degradation taken into consideration. *Archives of Civil and Mechanical Engineering.* 11(3), 623-636.

Liu, C.H. & Li, Y.Z. (2017). Analytical study of the mechanical behavior of fully grouted bolts in bedding rock slopes. *Rock Mechanics and Rock Engineering*. 50, 2413-2423.

Mathern, A., & Yang, J. (2021). A practical finite element modeling strategy to capture cracking and crushing behavior of reinforced concrete structures. *Materials*, 14(3), 506

Mauldon, M., Drumm, E., Dunne, W.E., Bateman, V., Rose, B., and Kim, M. (2007). *Rockfall management system for Tennessee: Final project report.* (Contract # RES 1189 CUT 236). Tennessee Department of Transportation. https://www.tn.gov/content/dam/tn/tdot/hq-materials-tests/geotech/TN_RMS_Final_Report.pdf

Moore, H.L. (1986). Wedge failures along Tennessee highways in the Appalachian region: Their occurrence and correction. *Bulletin of the Association of Engineering Geologists*. 23(4), 441-460. https://doi-org.utk.idm.oclc.org/10.2113/gseegeosci.xxiii.4.441

Norrish, N. I. and Wyllie, D.C. (1996). *Rock slope stability analysis*. In Turner, A. K. and Schuster, R. L. (eds.), Landslides: Investigation and Mitigation: Transportation Research Board Special Report 247, National Research Council, Washington, DC, pp. 391–425.

Pierson, L.A. & Vierling, M.P. (2012). Mitigation selection. In A.K. Turner & R.L. Schuster (Eds.), *Rockfall characterization and control* (pp. 445-456). Transportation Research Board.

Prado, F. S., Stucchi, F. R., & Meneghetti, L. C. (2021). Numerical analysis of high-strength concrete columns interconnected by normal-strength concrete floor. *Latin American Journal of Solids and Structures*. 18(8), e413, 1-25.

Simons, N., Menzies, B., and Matthews, M. (2007). *A short course in soil and rock slope engineering*. Thomas Telford, Ltd.

Spang, K. & Egger, P. (1990). Action of fully-grouted bolts in jointed rock and factors of influence. *Rock Mechanics and Rock Engineering*. 23, 201-229.

Tennessee State Government. (2022). https://www.tn.gov/content/dam/tn/environment/geology/images/geology_geologic-map-lg.jpg. Accessed March 21, 2022.

United States Geological Survey (USGS) (2021). How many deaths result from landslides each year? *Natural Hazards*. https://www.usgs.gov/faqs/how-many-deaths-result-landslides-each-year?qt-news_science_products=0#qt-news_science_products. Accessed September 23, 2021.

Vandewater, C.J., Dunne, W.M., Mauldon, M., Drumm, E.C., and Bateman, V. (2005). Classifying and assessing the geologic contribution to rockfall hazard. *Environmental & Engineering Geoscience*, 11(2), 141-154.

Walkinshaw, J. (1992). Landslide correction costs on U.S. state highways systems. *Transportation Research Record*, 1343, 36-41.

Wyllie, D.C. (2018). *Rock slope engineering: Civil applications* (5th ed.). CRC Press. Taylor & Francis Group.

Wyllie, D.C. and Mah, C.W. (1981). *Rock slope engineering* (4th ed.). Institution of Mining and Metallurgy.

Wyllie, D.C. & Norrish, N.I. (1996). Stabilization of rock slopes. In A.K. Turner & R.L. Schuster (Eds.), *Landslides: Investigation and mitigation* (pp.474-503). Transportation Research Board.

Appendix A: Specimen Laboratory Test Conditions and Measured Load-Displacement Responses

This appendix includes relevant contextual and load-deformation response information for all laboratory tested concrete block specimens. Each specimen consists of two concrete blocks with an encased rebar. The specimens were tested in a large–scale direct shear apparatus as described in Chapter 3 of this report. The top concrete block of each specimen was fixed while the bottom block was free to move in response to the applied shear load (constant displacement rate of 1mm/min). A constant normal load of 800 lb was applied. The following terminology is used in this Appendix. See also Figure A.1.

Aperture Size (s): This is the size of the opening between the upper and lower concrete blocks measured perpendicular to adjacent block faces. The aperture size was maintained by placing smooth steel rods (spacer bars) in the aperture.

Rebar Inclination Angle (θ): The angle at which the rebar was placed in the concrete block specimen with respect to the aperture (joint) normal.

Peak Load: System failure load. The peak load is indicated by a global maximum after which the load values decrease with increasing displacement.

Maximum Load: In cases where the system failure was not reached, the maximum applied load was obtained instead. This occurred for tests in which actuator capacity was less than the system failure load. If the applied load reached the actuator capacity, the test was terminated at that point.

Rebar Bonding Condition: In the free (unbonded/un-grouted) condition, the portion of the rebar above the aperture was free to move along the rebar length to ensure that a pure bending load is applied to the rebar. A select number of test cases were repeated in which the upper portion of the rebar was fixed (bonded/grouted) so that tension developed as the aperture deformed.

Concrete Compressive Strength: Compressive strength of the specimens was obtained by testing three concrete cylinders (4" x 8") on the same day as the testing of the specimens. Compressive strength was taken as the average value of the unconfined compressive strength values of the three cylinders. The cylinders were cast from the same concrete mix batch as the specimens.

Specimen Number and Designation: The test cases selected for the laboratory study were tested in a random order. The specimen number indicates the order in which the specimen was tested. The designation following the specimen number indicates the inclination angle, rebar number, aperture size, and specimen number as follows:

Specimen 1 (15-04-25-01): inclination angle = 15°, rebar # = #4, aperture size = 0.25", 01 = first specimen tested. For specimens with "a" or "b", "a" designates a selected retest and "b" designates a random test.

Figure A.1 *Schematic of a Specimen Showing Aperture Size (s) and Rebar Inclination Angle with Respect to the Aperture (Joint) Normal*

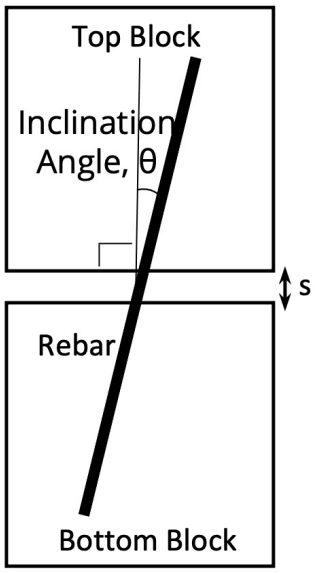

Specimen/Sample ID 1 (15-04-25-01)

Date Cast: 11-14-2020
Date Tested: 12-19-2020
Concrete Compressive Strength: 11330 psi
Peak Load: 22 kips
Actuator Capacity: 22 kips

Rebar Diameter: 0.5 inches (#4)
Rebar Inclination Angle (θ): 15°
Aperture Size: 0.25 inches
Rebar Bonding Condition: Free (un-grouted)

Note: Actuator capacity was reached prior to system failure. Thus, peak load is taken as the actuator capacity.

Figure A.2 *Shear load-shear displacement curve for Specimen 1: rebar inclination angle = 15°, rebar diameter = 0.5 inches, and aperture size = 0.25 inches.*

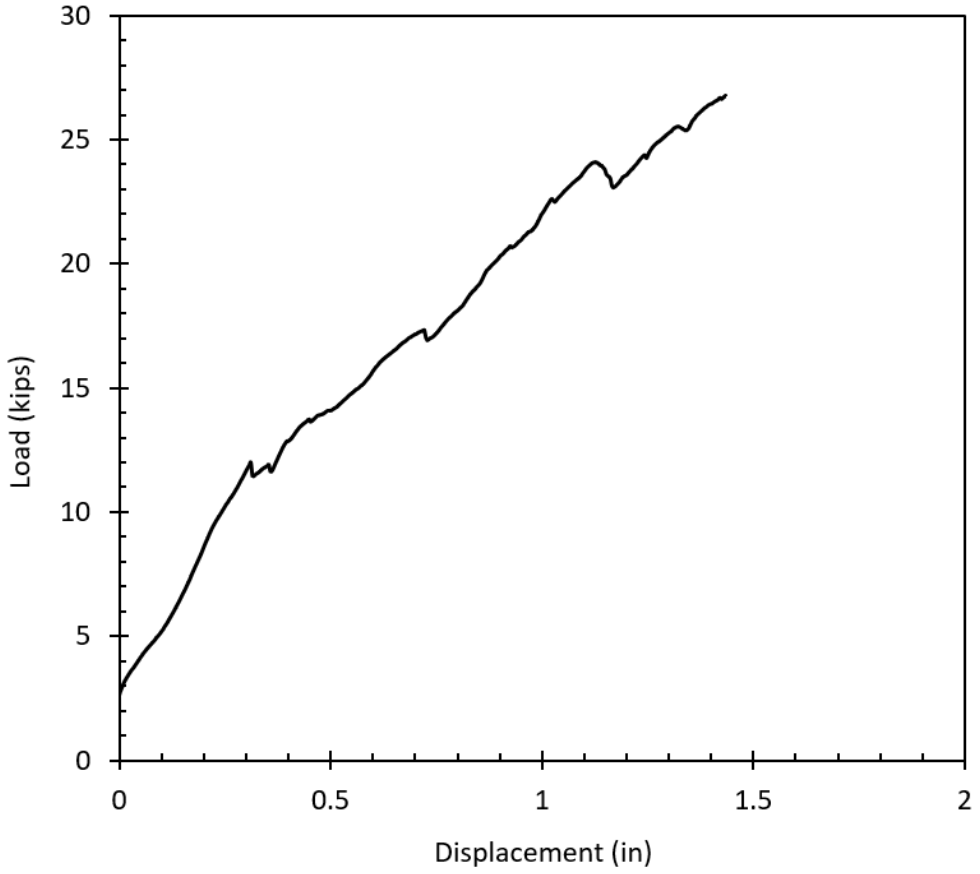

Specimen/Sample ID 2 (15-04-50-02)

Date Cast: 12-20-2020
Date Tested: 01-13-2021
Concrete Compressive Strength: 11650 psi
Peak Load: 17.8 kips
Actuator Capacity: 22 kips

Rebar Diameter: 0.5 inches (#4)
Rebar Inclination Angle (θ): 15°
Aperture Size: 0.5 inches
Rebar Bonding Condition: Free (un-grouted)

Figure A.3 *Shear load-shear displacement curve for Specimen 2: rebar inclination angle = 15°, rebar diameter = 0.5 inches, and aperture size = 0.5 inches.*

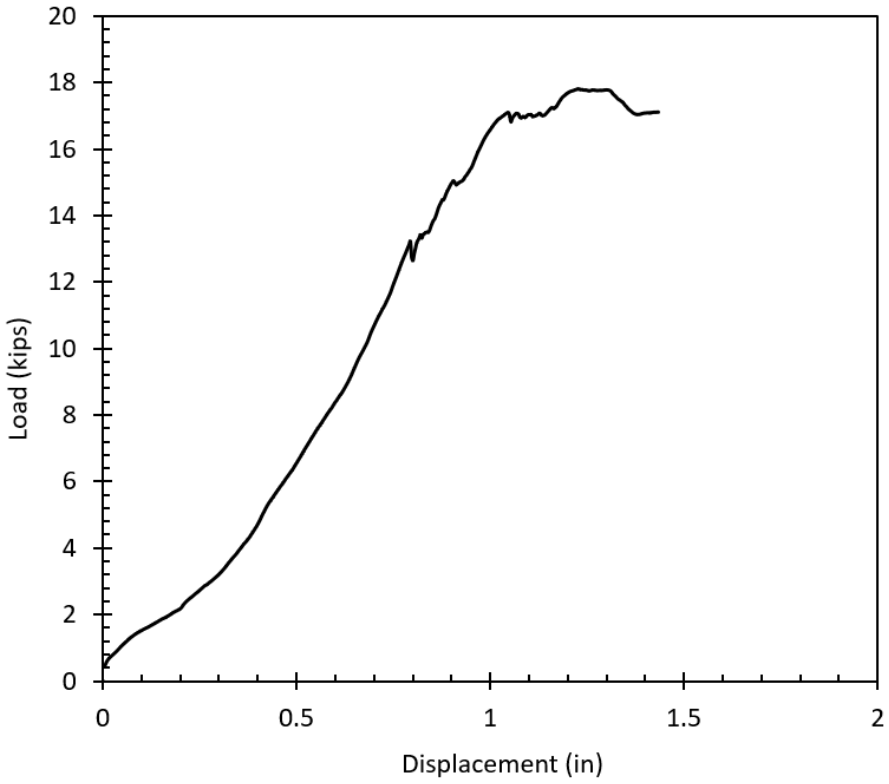

Specimen/Sample ID 2a (15-04-50-02-a)

Date Cast: 04-24-2021
Date Tested: 05-16-2021
Concrete Compressive Strength: 10720 psi
Peak Load: 1.48 kips
Actuator Capacity: 22 kips

Rebar Diameter: 0.5 inches (#4)
Rebar Inclination Angle (θ): 15°
Aperture Size: 0.5 inches
Rebar Bonding Condition: Free (un-grouted)
a: designates a repeated test, not randomly selected

Figure A.4 *Shear load-shear displacement curve for Specimen 2a: rebar inclination angle = 15°, rebar diameter = 0.5 inches, and aperture size = 0.5 inches.*

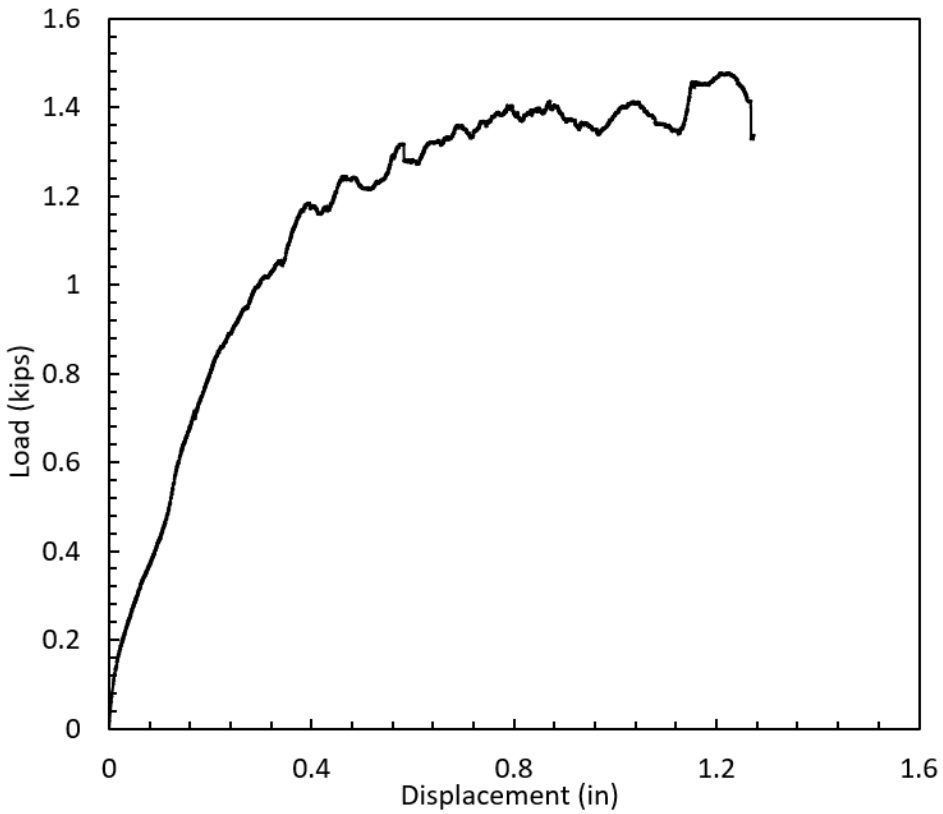

Specimen/Sample ID 3 (15-06-75-03)

Date Cast: 02-20-2021
Date Tested: 03-11-2021
Concrete Compressive Strength: 10820 psi
Peak Load: 22 kips
Actuator Capacity: 22 kips

Rebar Diameter: 0.75 inches (#6)
Rebar Inclination Angle (θ): 15°
Aperture Size: 0.75 inches
Rebar Bonding Condition: Free (un-grouted)

Note: Actuator capacity was reached prior to system failure. Thus, peak load is taken as the actuator capacity.

Figure A.5 *Shear load-shear displacement curve for Specimen 3: rebar inclination angle = 15°, rebar diameter = 0.75 inches, and aperture size = 0.75 inches.*

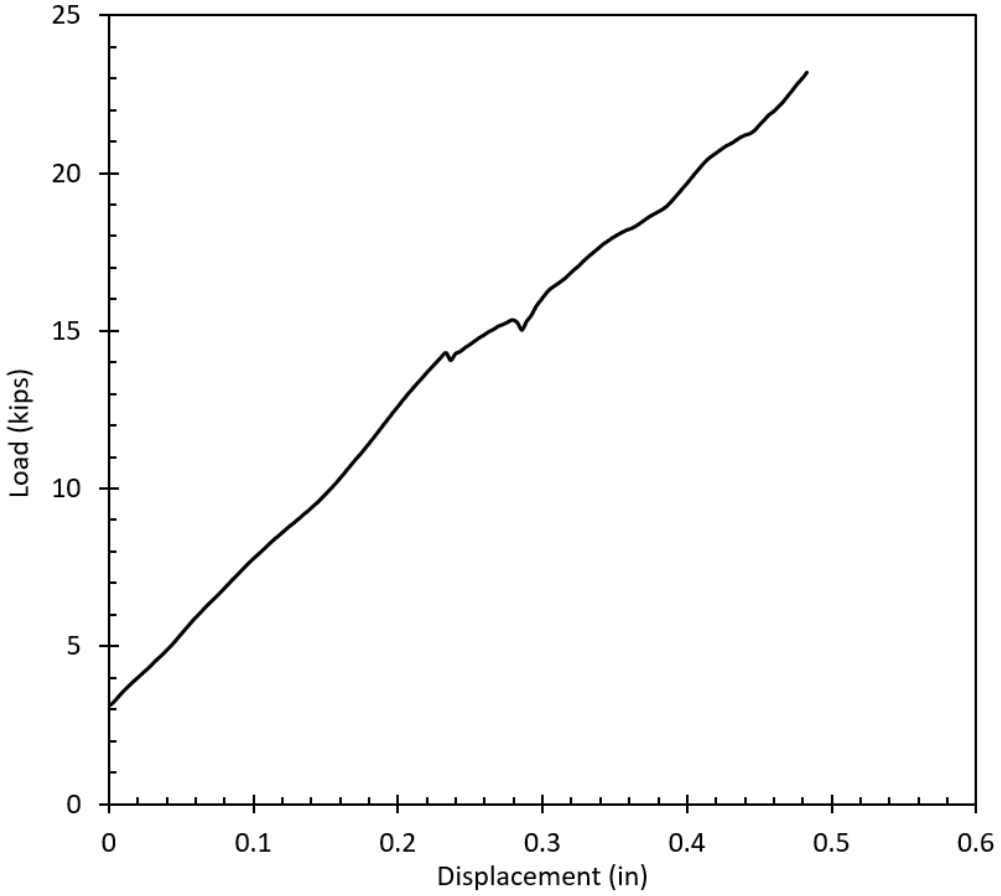

Specimen/Sample ID 4 (15-05-75-04)

Date Cast: 02-27-2021
Date Tested: 03-13-2021
Concrete Compressive Strength: 10840 psi
Peak Load: 22 kips
Actuator Capacity: 22 kips

Rebar Diameter: 0.625 inches (#5)
Rebar Inclination Angle (θ): 15°
Aperture Size: 0.75 inches
Rebar Bonding Condition: Free (un-grouted)

Note: Actuator capacity was reached prior to system failure. Thus, peak load is taken as the actuator capacity.

Figure A.6 *Shear load-shear displacement curve for Specimen 4: rebar inclination angle = 15°, rebar diameter = 0.625 inches, and aperture size = 0.75 inches.*

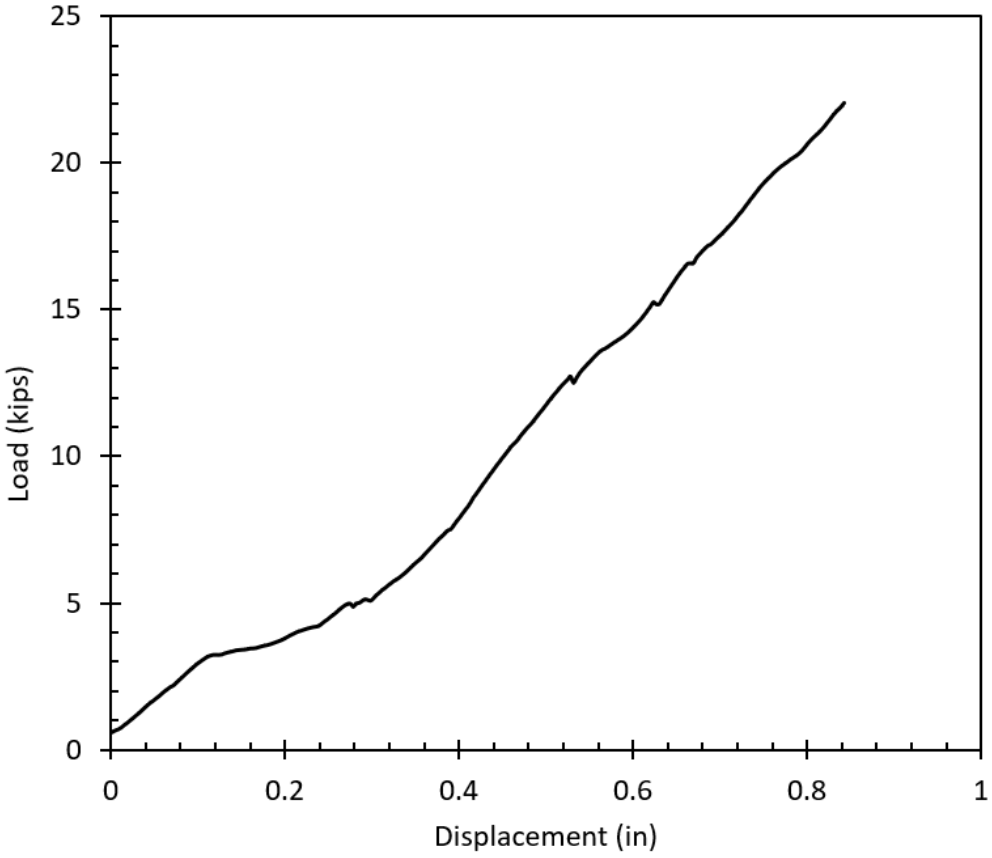

Specimen/Sample ID 4a (15-05-75-04-a)

Date Cast: 07-24-2021
Date Tested: 08-09-2021
Concrete Compressive Strength: 11280 psi
Peak Load: 7.5 kips
Actuator Capacity: 22 kips

Rebar Diameter: 0.625 inches (#5)
Rebar Inclination Angle (θ): 15°
Aperture Size: 0.75 inches
Rebar Bonding Condition: Free (un-grouted)
a: designates a repeated test, not randomly selected

Figure A.7 *Shear load-shear displacement curve for Specimen 4a: rebar inclination angle = 15°, rebar diameter = 0.625 inches, and aperture size = 0.75 inches.*

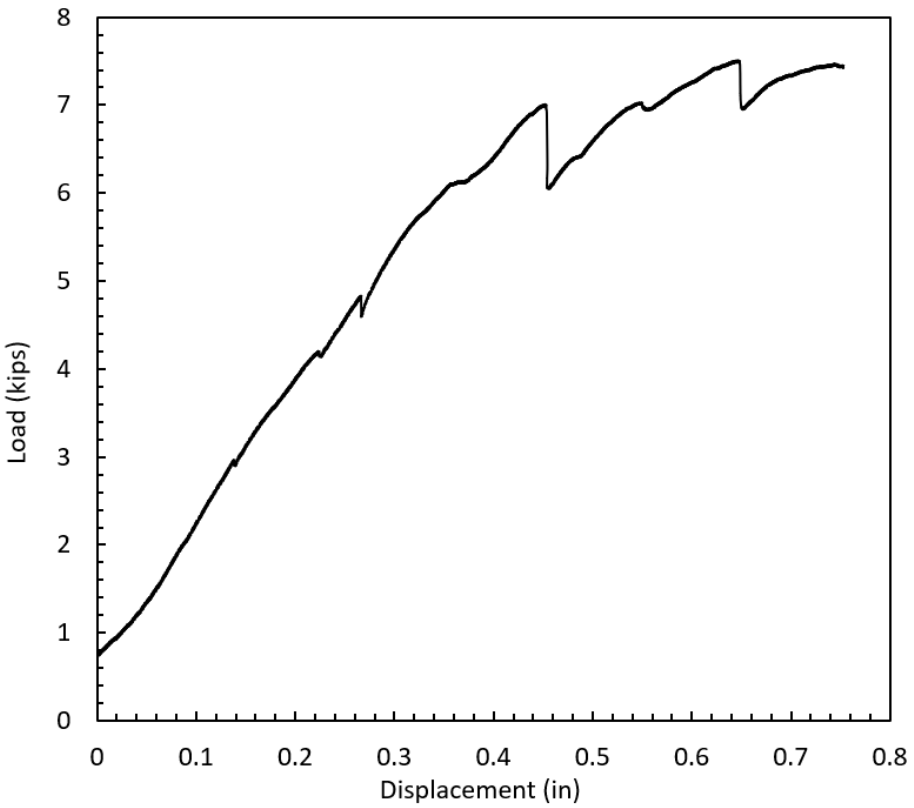

Specimen/Sample ID 4b (15-05-75-04-b)

Date Cast: 11-06-2021	Rebar Diameter: 0.625 inches (#5)
Date Tested: 11-23-2021	Rebar Inclination Angle (θ): 15°
Concrete Compressive Strength: 11920 psi	Aperture Size: 0.75 inches
Peak Load: 7.99 kips	Rebar Bonding Condition: Free (un-grouted)
Actuator Capacity: 22 kips	b: designates a randomly selected retest

Figure A.8 *Shear load-shear displacement curve for Specimen 4b: rebar inclination angle = 15°, rebar diameter = 0.625 inches, and aperture size = 0.75 inches.*

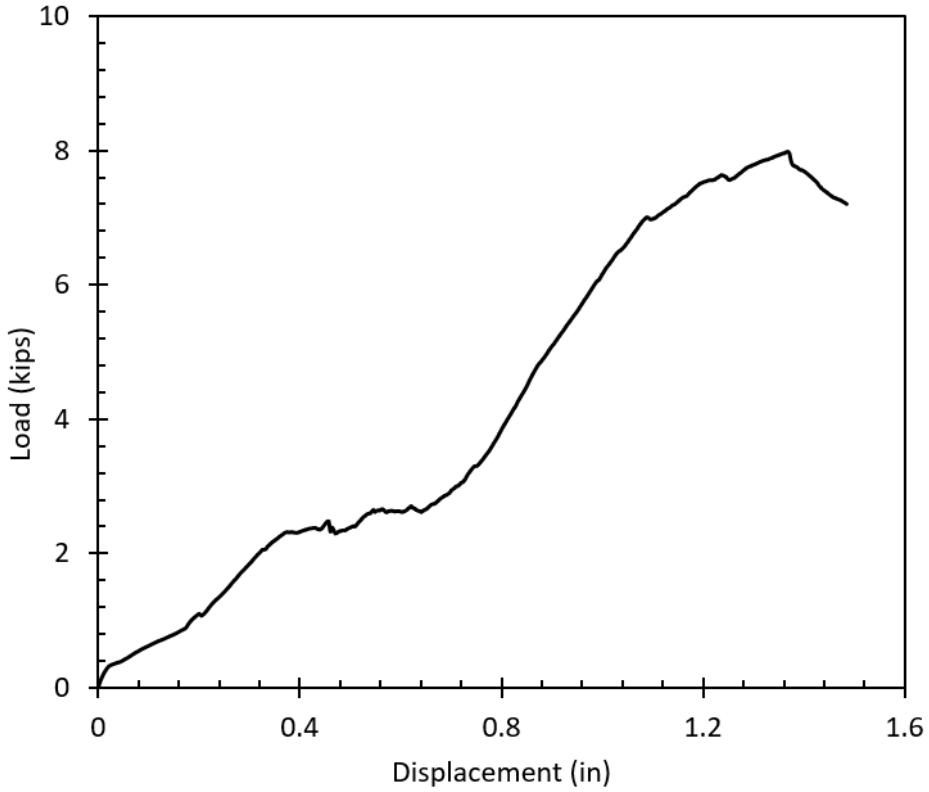

Specimen/Sample ID 5 (15-05-25-05)

Date Cast: 03-20-2021
Date Tested: 04-14-2021
Concrete Compressive Strength: 12860 psi
Peak Load: 8.55 kips
Actuator Capacity: 22 kips

Rebar Diameter: 0.625 inches (#5)
Rebar Inclination Angle (θ): 15°
Aperture Size: 0.25 inches
Rebar Bonding Condition: Free (un-grouted)

Figure A.9 *Shear load-shear displacement curve for Specimen 5: rebar inclination angle = 15°, rebar diameter = 0.625 inches, and aperture size = 0.25 inches.*

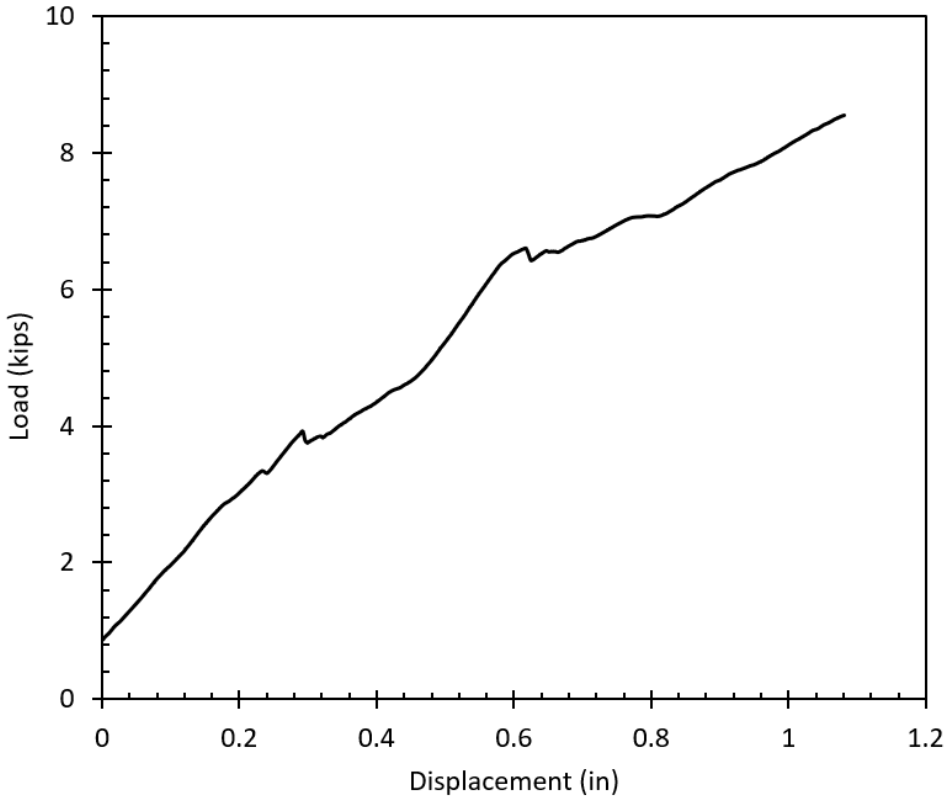

Specimen/Sample ID 5b (15-05-25-05-b)

Date Cast: 10-09-2021	Rebar Diameter: 0.625 inches (#5)
Date Tested: 11-08-2021	Rebar Inclination Angle (θ): 15°
Concrete Compressive Strength: 12090 psi	Aperture Size: 0.25 inches
Peak Load: 7.34 kips	Rebar Bonding Condition: Free (un-grouted)
Actuator Capacity: 22 kips	b: designates a randomly selected retest

Figure A.10 *Shear load-shear displacement curve for Specimen 5b: rebar inclination angle = 15°, rebar diameter = 0.625 inches, and aperture size = 0.25 inches.*

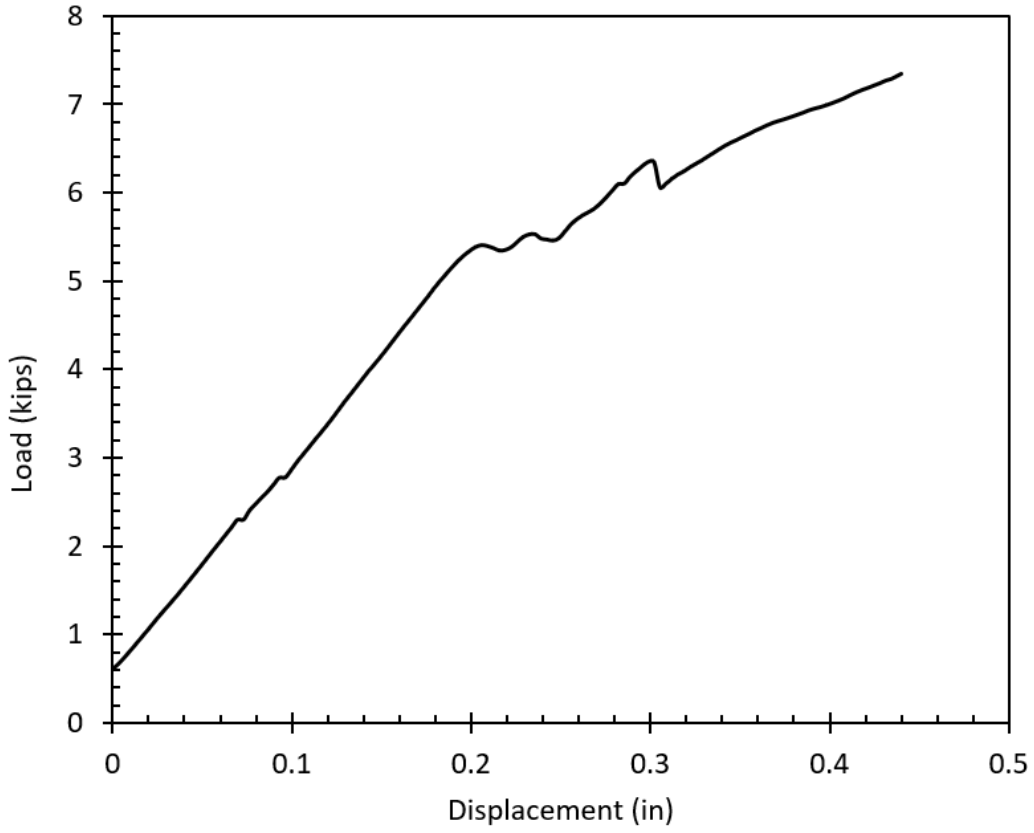

Specimen/Sample ID 6 (00-05-50-06)

Date Cast: 03-27-2021
Date Tested: 04-25-2021
Concrete Compressive Strength: 12970 psi
Peak Load: 6.8 kips
Actuator Capacity: 22 kips

Rebar Diameter: 0.625 inches (#5)
Rebar Inclination Angle (θ): 0°
Aperture Size: 0.5 inches
Rebar Bonding Condition: Free (un-grouted)

Figure A.11 *Shear load-shear displacement curve for Specimen 6: rebar inclination angle = 0°, rebar diameter = 0.625 inches, and aperture size = 0.5 inches.*

Specimen/Sample ID 6a (00-05-50-06-a)

Date Cast: 05-17-2021
Date Tested: 06-18-2021
Concrete Compressive Strength: 12220 psi
Peak Load: 7.92 kips
Actuator Capacity: 22 kips

Rebar Diameter: 0.625 inches (#5)
Rebar Inclination Angle (θ): 0°
Aperture Size: 0.5 inches
Rebar Bonding Condition: Free (un-grouted)
a: designates a repeated test, not randomly selected

Figure A.12 *Shear load-shear displacement curve for Specimen 6a: rebar inclination angle = 0°, rebar diameter = 0.625 inches, and aperture size = 0.5 inches.*

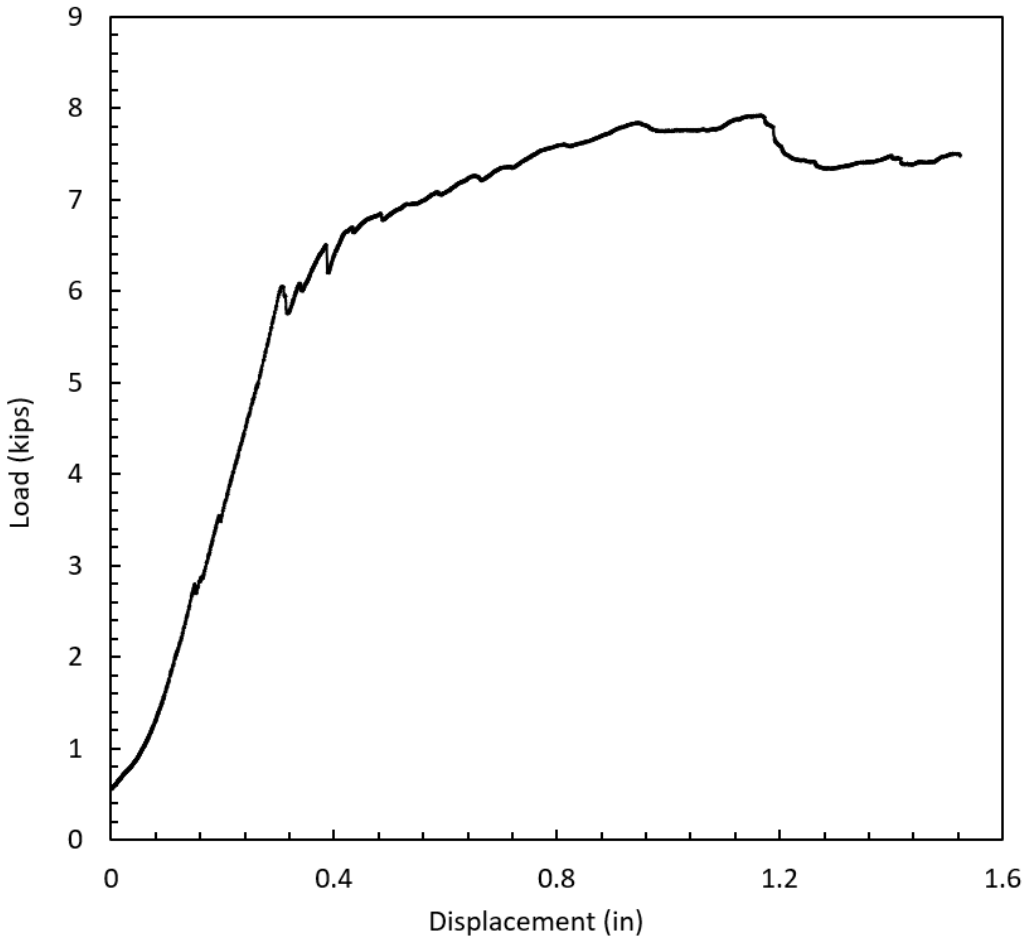

Specimen/Sample ID 7 (15-06-25-07)

Date Cast: 04-11-2021
Date Tested: 05-03-2021
Concrete Compressive Strength: 11140 psi
Peak Load: 11 kips
Actuator Capacity: 22 kips

Rebar Diameter: 0.75 inches (#6)
Rebar Inclination Angle (θ): 15°
Aperture Size: 0.25 inches
Rebar Bonding Condition: Free (un-grouted)

Figure A.13 *Shear load-shear displacement curve for Specimen 7: rebar inclination angle = 15°, rebar diameter = 0.75 inches, and aperture size = 0.25 inches.*

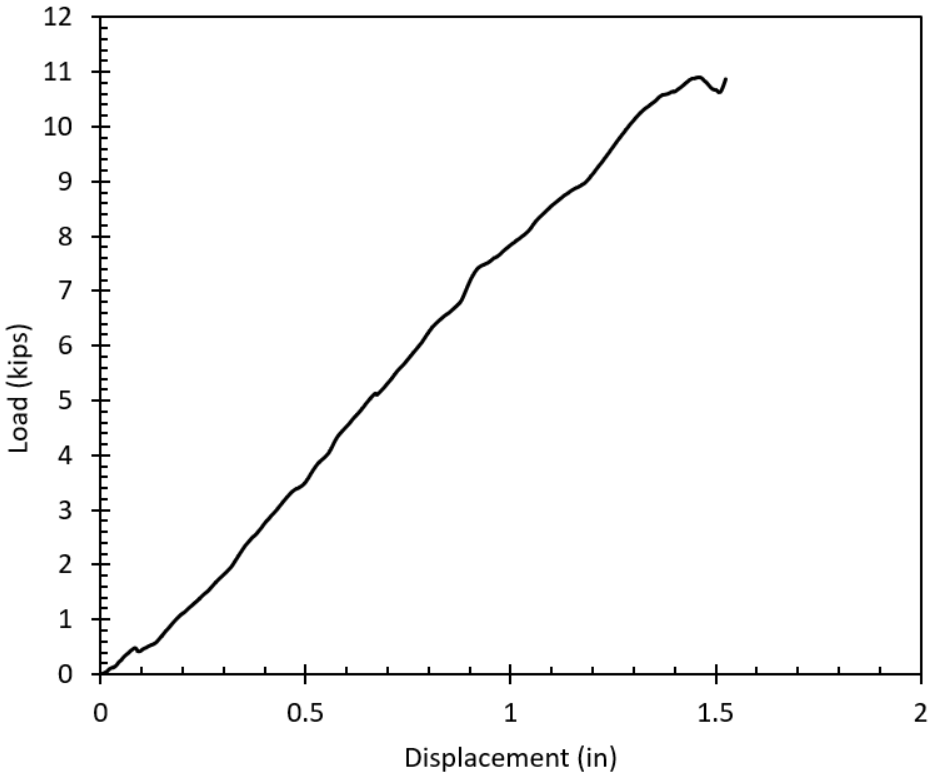

Specimen/Sample ID 7a (15-06-25-07-a)

Date Cast: 06-19-2021
Date Tested: 07-14-2021
Concrete Compressive Strength: 12200 psi
Peak Load: 12.2 kips

Actuator Capacity: 22 kips

Rebar Diameter: 0.75 inches (#6)
Rebar Inclination Angle (θ): 15°
Aperture Size: 0.25 inches
Rebar Bonding Condition: Free (un grouted)
a: designates a repeated test, not randomly selected

Figure A.14 *Shear load-shear displacement curve for Specimen 7a: rebar inclination angle = 15°, rebar diameter = 0.75 inches, and aperture size = 0.25 inches.*

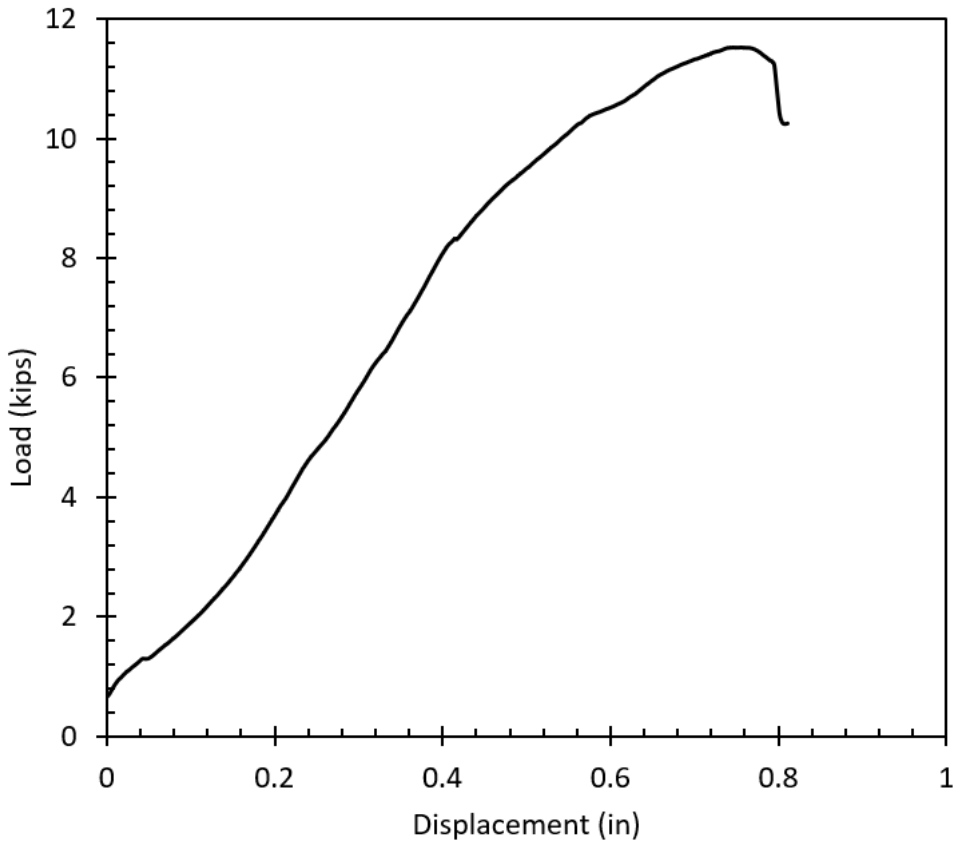

Specimen/Sample ID 7b (15-06-25-07-b)

Date Cast: 11-09-2021
Date Tested: 12-11-2021
Concrete Compressive Strength: 11830 psi
Peak Load: 11.52 kips
Actuator Capacity: 22 kips

Rebar Diameter: 0.75 inches (#6)
Rebar Inclination Angle (θ): 15°
Aperture Size: 0.25 inches
Rebar Bonding Condition: Free (un-grouted)
b: designates a randomly selected retest

Figure A.15 *Shear load-shear displacement curve for Specimen 7b: rebar inclination angle = 15°, rebar diameter = 0.75 inches, and aperture size = 0.25 inches.*

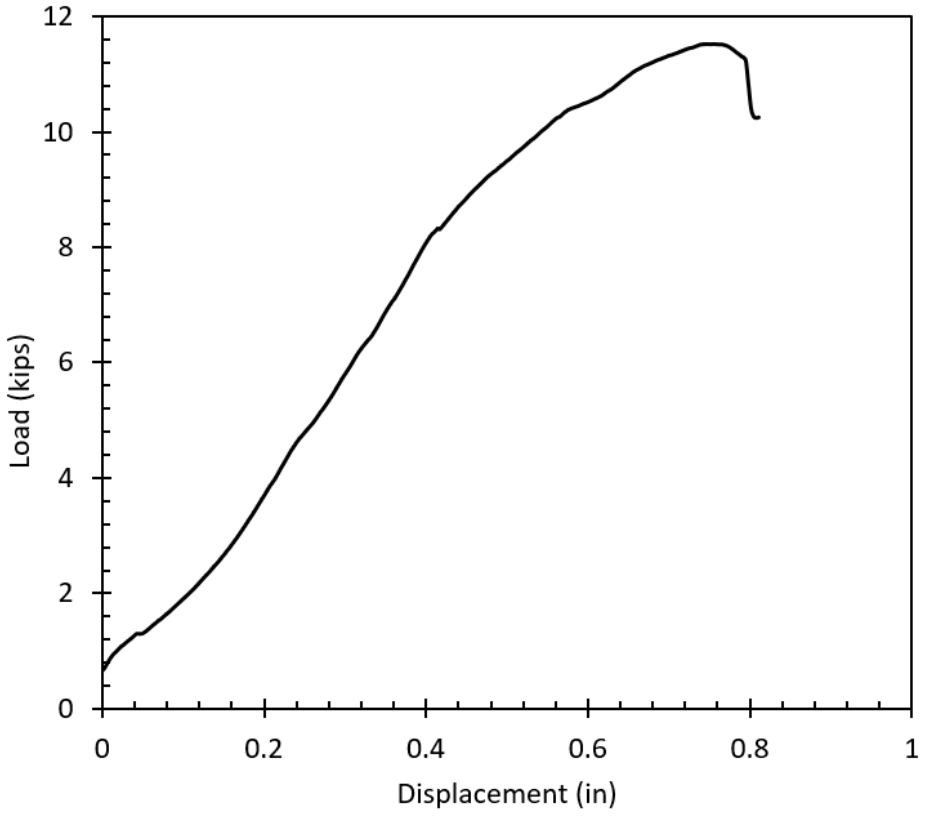

Specimen/Sample ID 8 (15-05-50-08)

Date Cast: 05-08-2021
Date Tested: 05-23-2021
Concrete Compressive Strength: 11040 psi
Peak Load: 7.21 kips
Actuator Capacity: 22 kips

Rebar Diameter: 0.625 inches (#5)
Rebar Inclination Angle (θ): 15°
Aperture Size: 0.5 inches
Rebar Bonding Condition: Free (un-grouted)

Figure A.16 *Shear load-shear displacement curve for Specimen 8: rebar inclination angle = 15°, rebar diameter = 0.625 inches, and aperture size = 0.5 inches.*

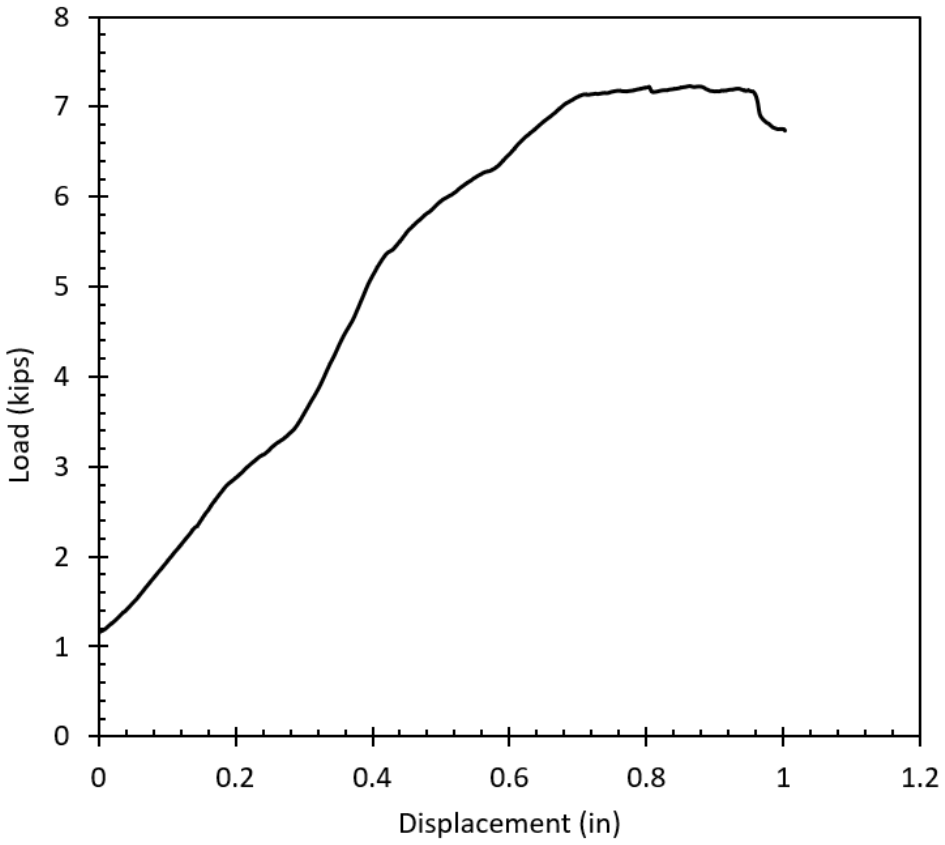

Specimen/Sample ID 8a (15-05-50-08-a)

Date Cast: 06-05-2021
Date Tested: 06-25-2021
Concrete Compressive Strength: 11060 psi
Peak Load: 4.45 kips

Actuator Capacity: 22 kips

Rebar Diameter: 0.625 inches (#5)
Rebar Inclination Angle (θ): 15°
Aperture Size: 0.5 inches
Rebar Bonding Condition: Free (un-grouted)
a: designates a repeated test, not randomly selected

Figure A.17 *Shear load-shear displacement curve for Specimen 8a: rebar inclination angle = 15°, rebar diameter = 0.625 inches, and aperture size = 0.5 inches.*

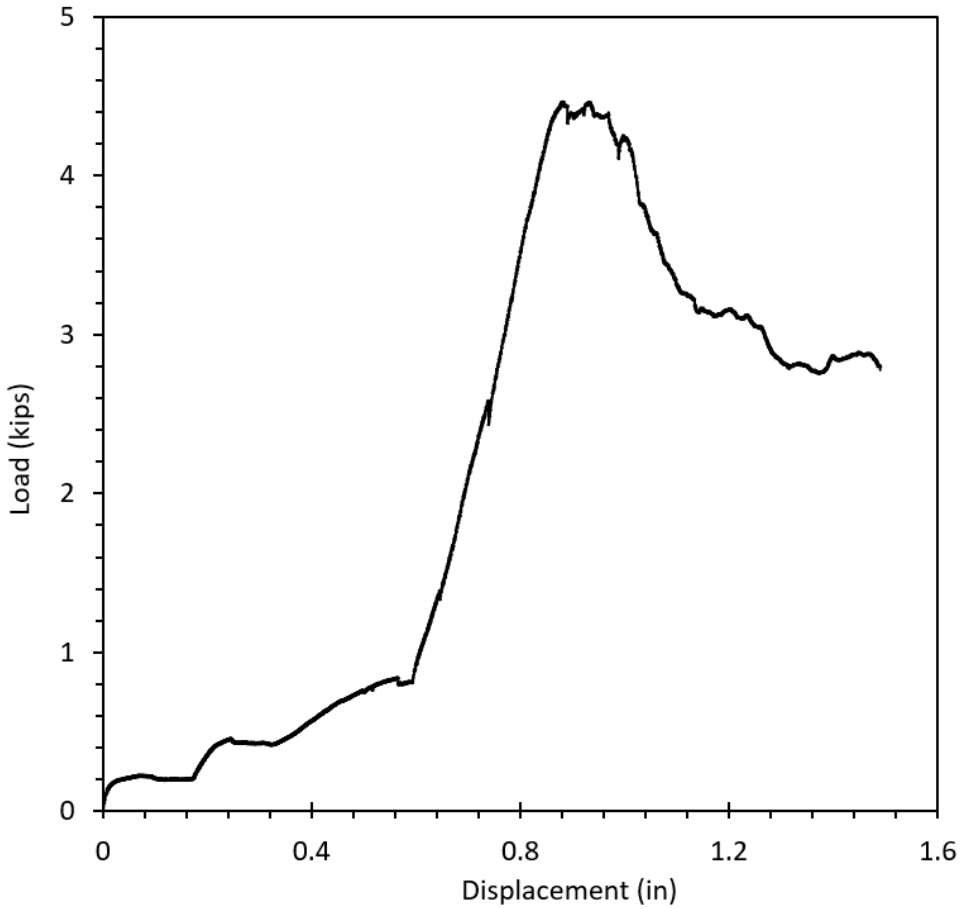

Specimen/Sample ID 9 (15-06-50-09)

Date Cast: 05-11-2021
Date Tested: 05-29-2021
Concrete Compressive Strength: 11250 psi
Peak Load: 13.1 kips
Actuator Capacity: 22 kips

Rebar Diameter: 0.75 inches (#6)
Rebar Inclination Angle (θ): 15°
Aperture Size: 0.5 inches
Rebar Bonding Condition: Free (un-grouted)

Figure A.18 *Shear load-shear displacement curve for Specimen 9: rebar inclination angle = 15°, rebar diameter = 0.75 inches, and aperture size = 0.5 inches.*

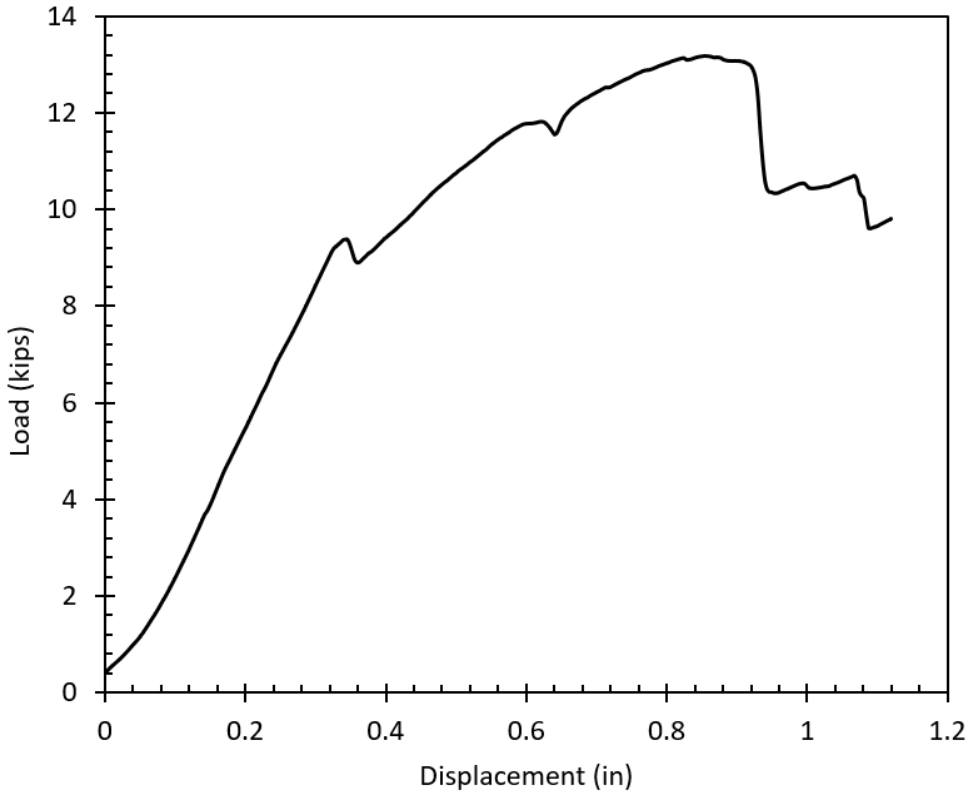

Specimen/Sample ID 9a (15-06-50-09-a)

Date Cast: 06-12-2021
Date Tested: 07-01-2021
Concrete Compressive Strength: 11130 psi
Peak Load: 2.6 kips
Actuator Capacity: 22 kips

Rebar Diameter: 0.75 inches (#6)
Rebar Inclination Angle (θ): 15°
Aperture Size: 0.5 inches
Rebar Bonding Condition: Free (un-grouted)
a: designates a repeated test, not randomly selected

Figure A.19 *Shear load-shear displacement curve for Specimen 9a: rebar inclination angle = 15°, rebar diameter = 0.75 inches, and aperture size = 0.5 inches.*

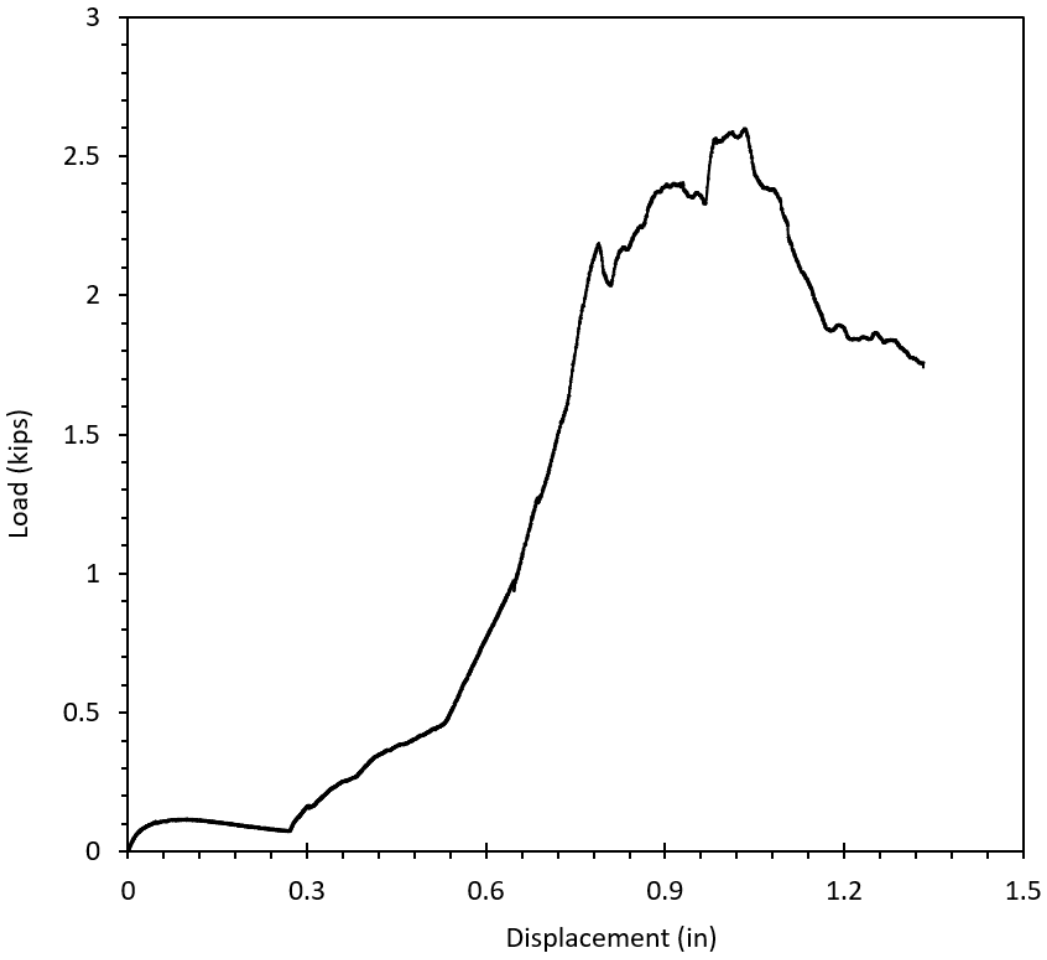

Specimen/Sample ID 9b (15-06-50-09-b)

Date Cast: 11-01-2021	Rebar Diameter: 0.75 inches (#6)
Date Tested: 11-19-2021	Rebar Inclination Angle (θ): 15°
Concrete Compressive Strength: 10580 psi	Aperture Size: 0.5 inches
Peak Load: 10.75 kips	Rebar Bonding Condition: Free (un-grouted)
Actuator Capacity: 22 kips	b: designates a randomly selected retest

Figure A.20 *Shear load-shear displacement curve for Specimen 9b: rebar inclination angle = 15°, rebar diameter = 0.75 inches, and aperture size = 0.5 inches.*

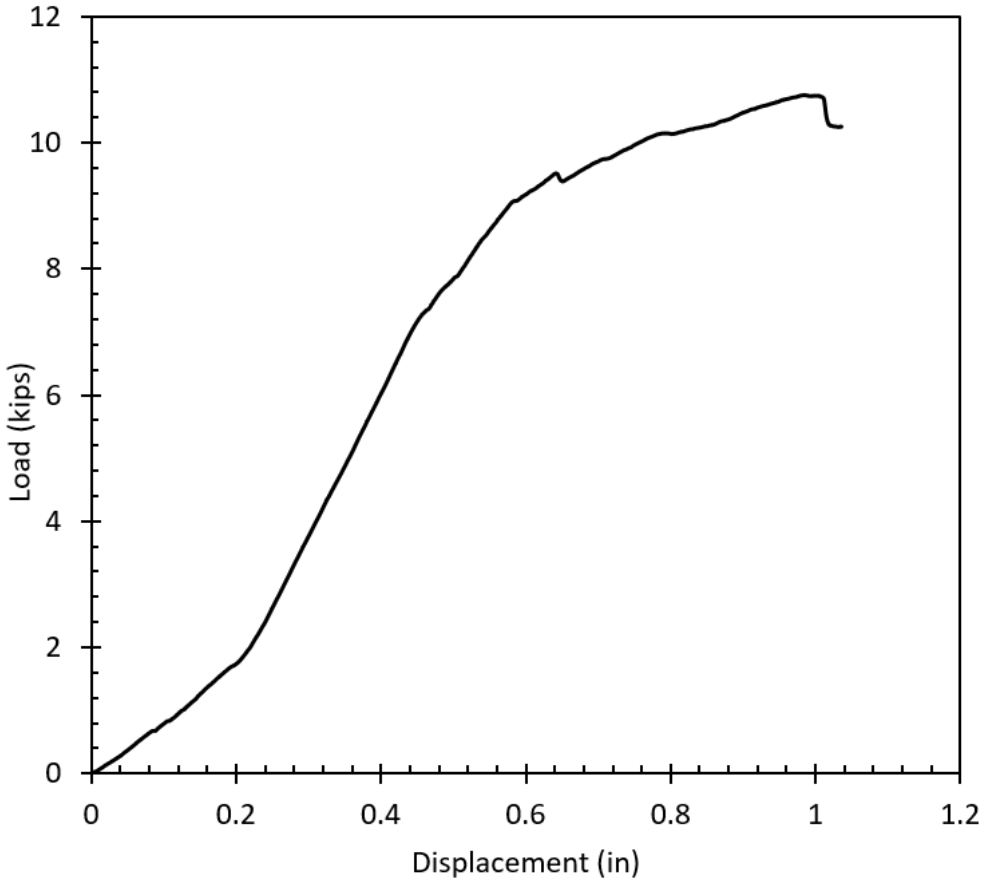

Specimen/Sample ID 10 (30-05-50-10)

Date Cast: 05-20-2021
Date Tested: 06-03-2021
Concrete Compressive Strength: 10720 psi
Peak Load: 2.17 kips
Actuator Capacity: 22 kips

Rebar Diameter: 0.625 inches (#5)
Rebar Inclination Angle (θ): 30°
Aperture Size: 0.5 inches
Rebar Bonding Condition: Free (un-grouted)

Figure A.21 *Shear load-shear displacement curve for Specimen 10: rebar inclination angle = 15°, rebar diameter = 0.625 inches, and aperture size = 0.5 inches.*

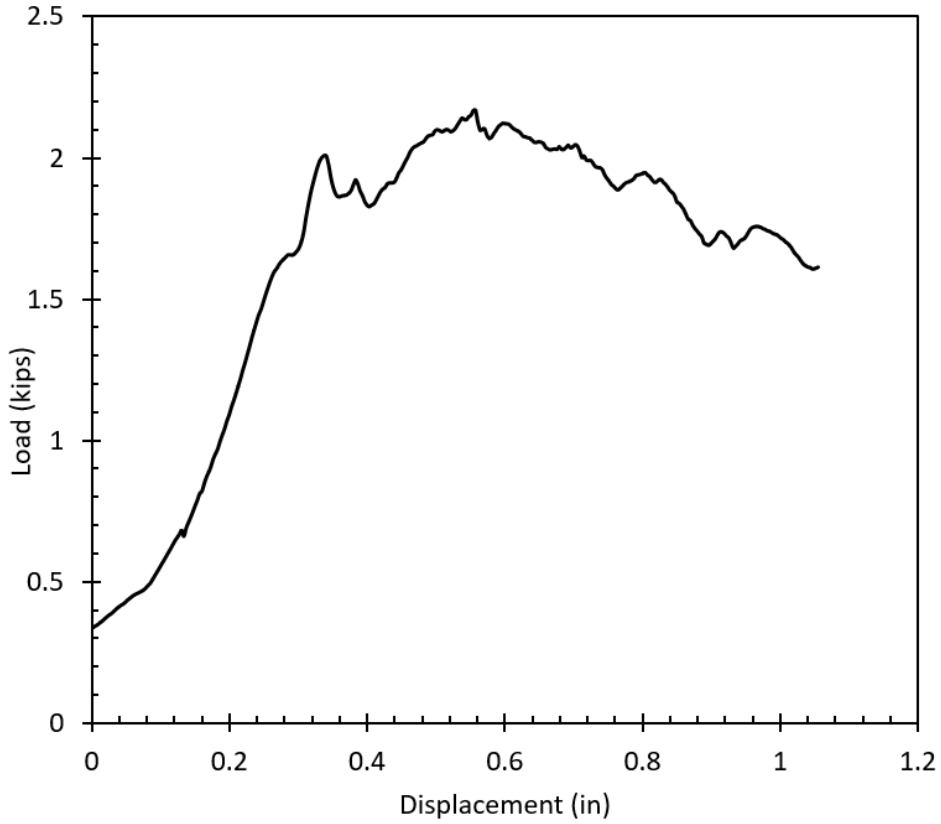

Specimen/Sample ID 10a (30-05-50-10-a)

Date Cast: 06-26-2021
Date Tested: 07-24-2021
Concrete Compressive Strength: 12270 psi
Peak Load: 7.95 kips
Actuator Capacity: 22 kips

Rebar Diameter: 0.625 inches (#5)
Rebar Inclination Angle (θ): 30°
Aperture Size: 0.5 inches
Rebar Bonding Condition: Free (un-grouted)
a: designates a repeated test, not randomly selected

Figure A.22 *Shear load-shear displacement curve for Specimen 10a: rebar inclination angle = 30°, rebar diameter = 0.625 inches, and aperture size = 0.5 inches.*

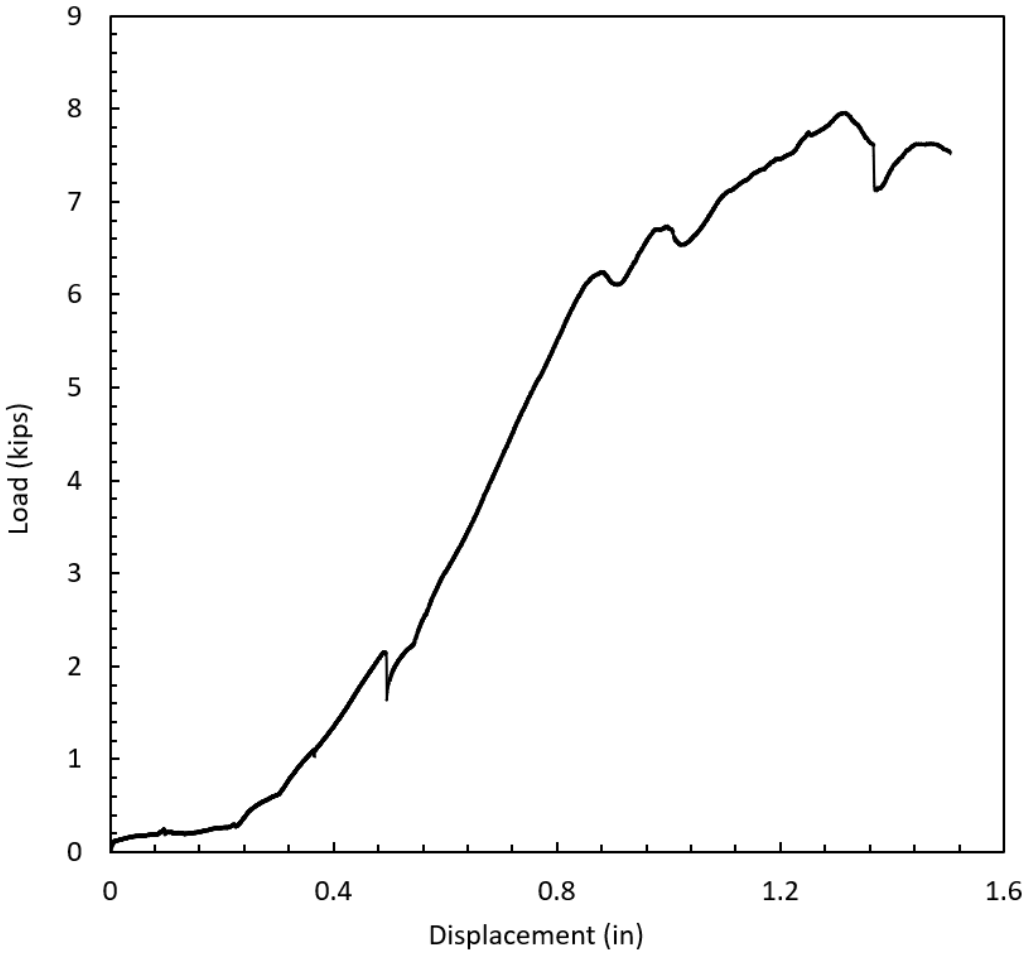

Specimen/Sample ID 10b (30-05-50-10-b)

Date Cast: 11-09-2021
Date Tested: 12-17-2021
Concrete Compressive Strength: 12140 psi
Peak Load: 7.45 kips
Actuator Capacity: 22 kips

Rebar Diameter: 0.625 inches (#5)
Rebar Inclination Angle (θ): 30°
Aperture Size: 0.5 inches
Rebar Bonding Condition: Free (un-grouted)
b: designates a randomly selected retest

Figure A.23 *Shear load-shear displacement curve for Specimen 10b: rebar inclination angle = 15°, rebar diameter = 0.625 inches, and aperture size = 0.5 inches.*

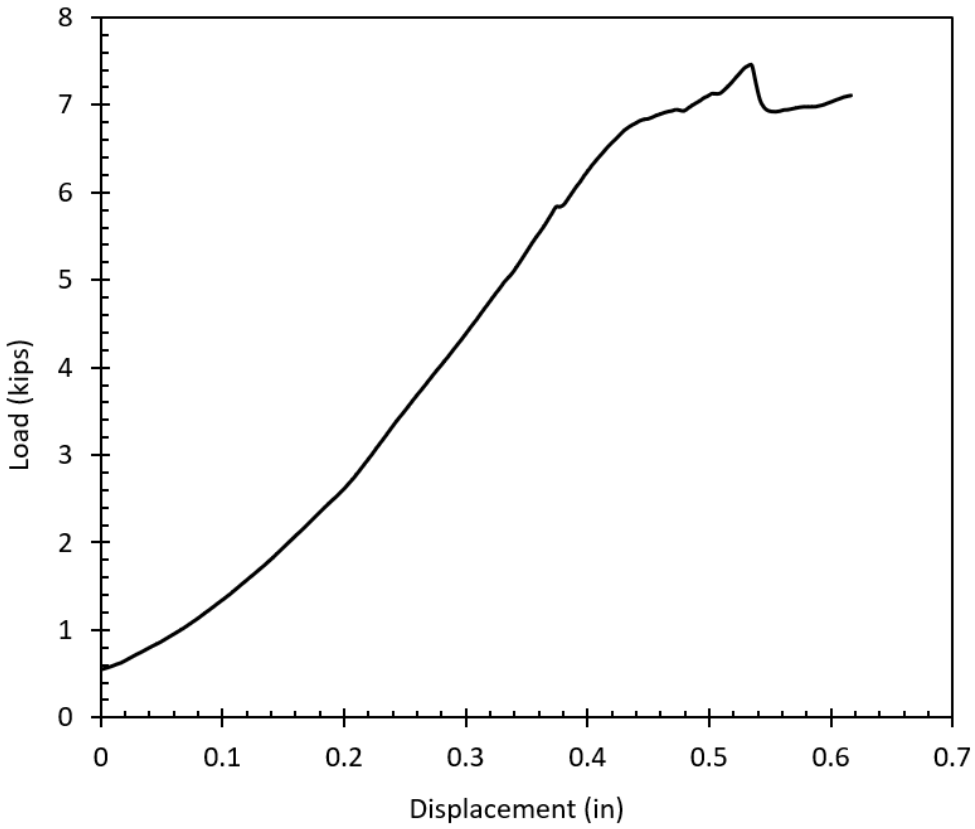

Specimen/Sample ID 11 (15-04-75-11)

Date Cast: 07-15-2021
Date Tested: 08-10-2021
Concrete Compressive Strength: 10850 psi
Peak Load: 4.04 kips
Actuator Capacity: 22 kips

Rebar Diameter: 0.5 inches (#4)
Rebar Inclination Angle (θ): 15°
Aperture Size: 0.75 inches
Rebar Bonding Condition: Free (un-grouted)

Figure A.24 *Shear load-shear displacement curve for Specimen 11: rebar inclination angle = 15°, rebar diameter = 0.5 inches, and aperture size = 0.75 inches.*

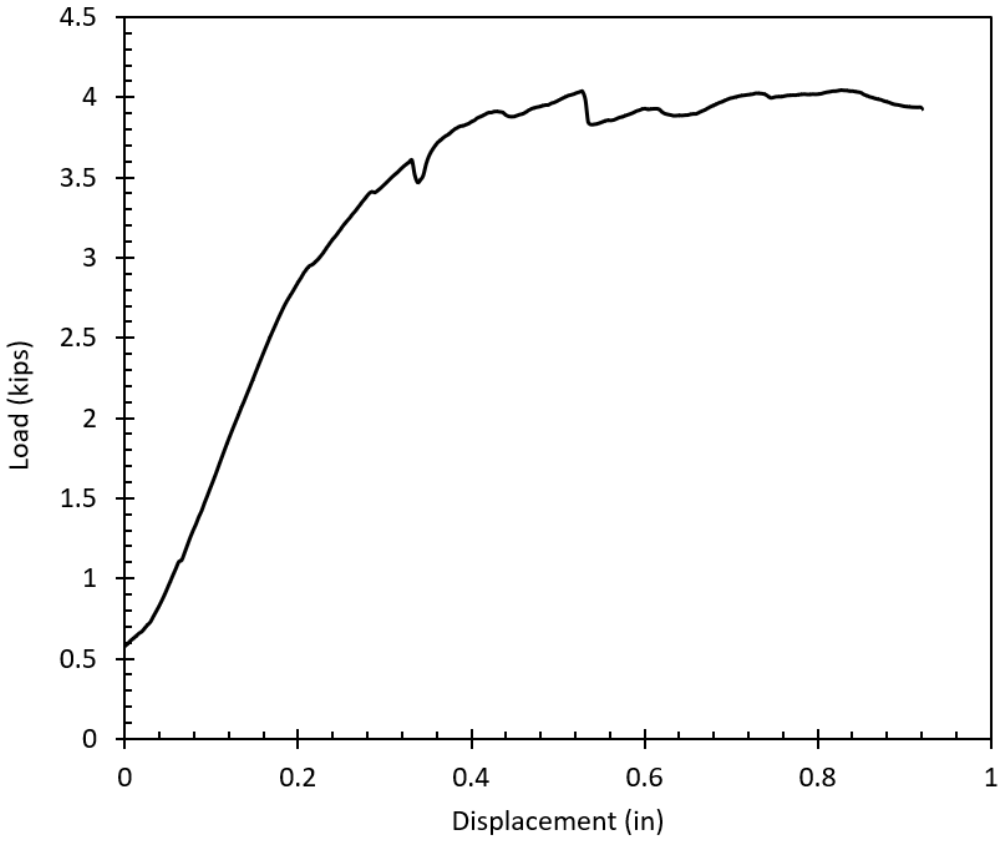

Specimen/Sample ID 11b (15-04-75-11-b)

Date Cast: 11-12-2021
Date Tested: 12-17-2021
Concrete Compressive Strength: 12310 psi
Peak Load: 4.06 kips
Actuator Capacity: 22 kips

Rebar Diameter: 0.5 inches (#4)
Rebar Inclination Angle (θ): 15°
Aperture Size: 0.75 inches
Rebar Bonding Condition: Free (un-grouted)
b: designates a randomly selected retest

Figure A.25 *Shear load-shear displacement curve for Specimen11b: rebar inclination angle = 15°, rebar diameter = 0.5 inches, and aperture size = 0.75 inches.*

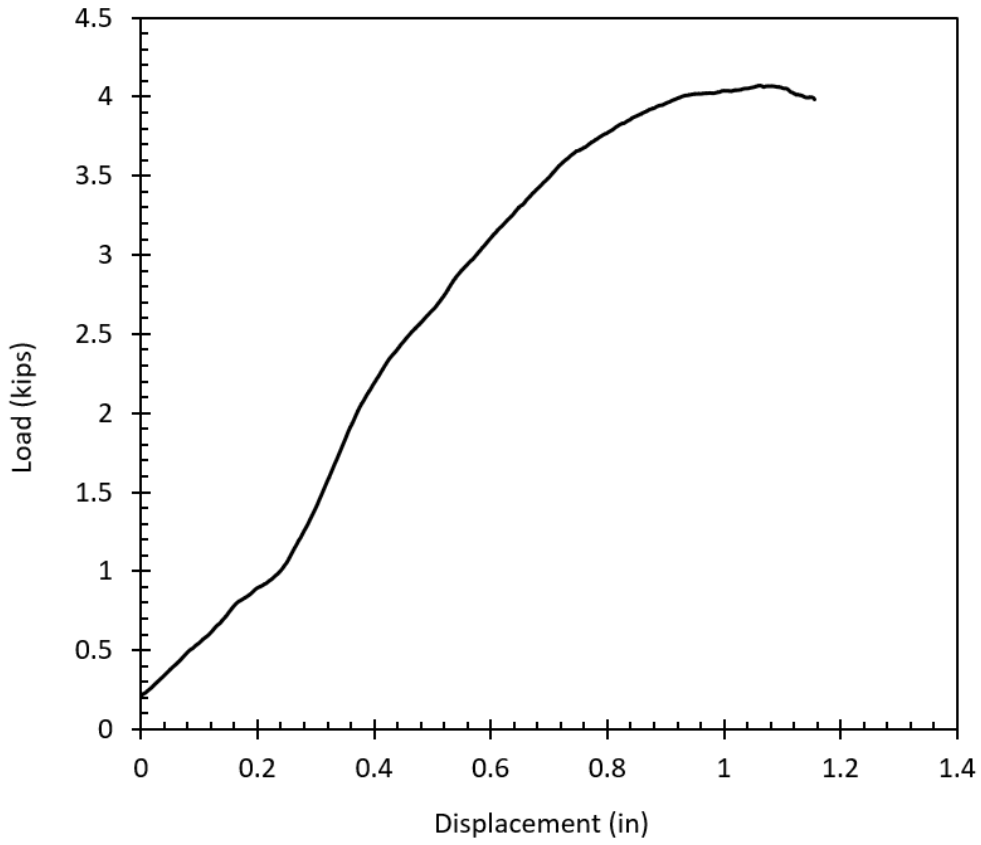

Specimen/Sample ID 12 (15-05-25-12)

Date Cast: 11-12-2021
Date Tested: 12-21-2021
Concrete Compressive Strength: 11020 psi
Peak Load: 10.2 kips
Actuator Capacity: 22 kips

Rebar Diameter: 0.625 inches (#5)
Rebar Inclination Angle (θ): 15°
Aperture Size: 0.25 inches
Rebar Bonding Condition: Fixed (grouted)

Figure A.26 *Shear load-shear displacement curve for Specimen 12: rebar inclination angle = 15°, rebar diameter = 0.625 inches, and aperture size = 0.25 inches.*

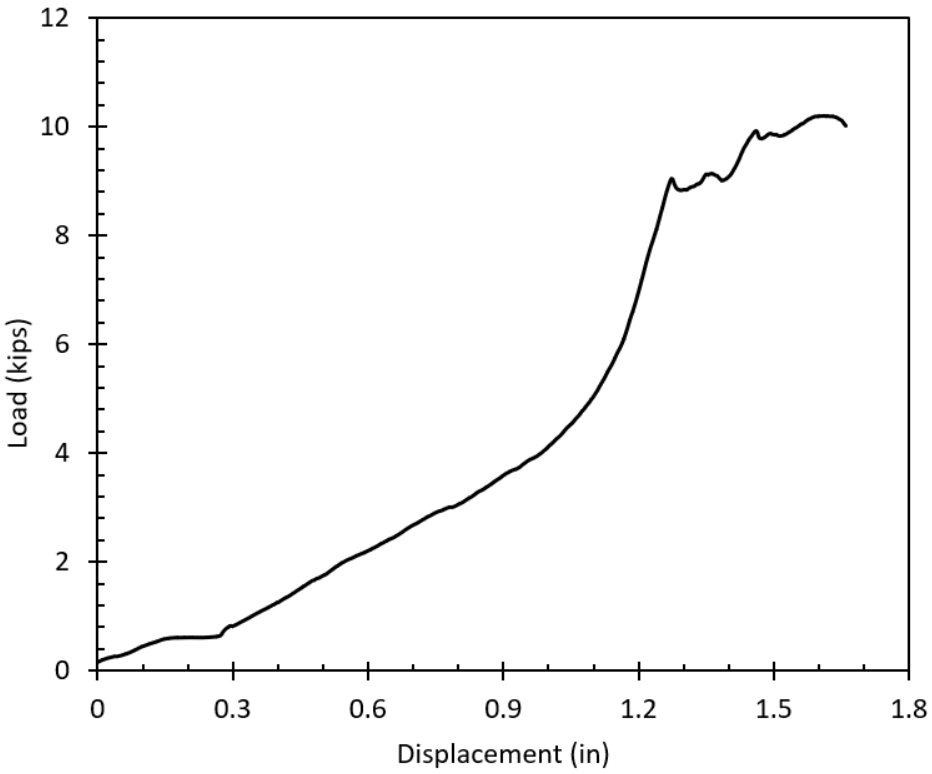

Specimen/Sample ID 13 (15-05-50-13)

Date Cast: 07-17-2021
Date Tested: 10-18-2021
Concrete Compressive Strength: 12030 psi
Peak Load: 8.75 kips
Actuator Capacity: 22 kips

Rebar Diameter: 0.625 inches (#5)
Rebar Inclination Angle (θ): 15°
Aperture Size: 0.5 inches
Rebar Bonding Condition: Fixed (grouted)

Figure A.27 *Shear load-shear displacement curve for Specimen 13: rebar inclination angle = 15°, rebar diameter = 0.625 inches, and aperture size = 0.5 inches.*

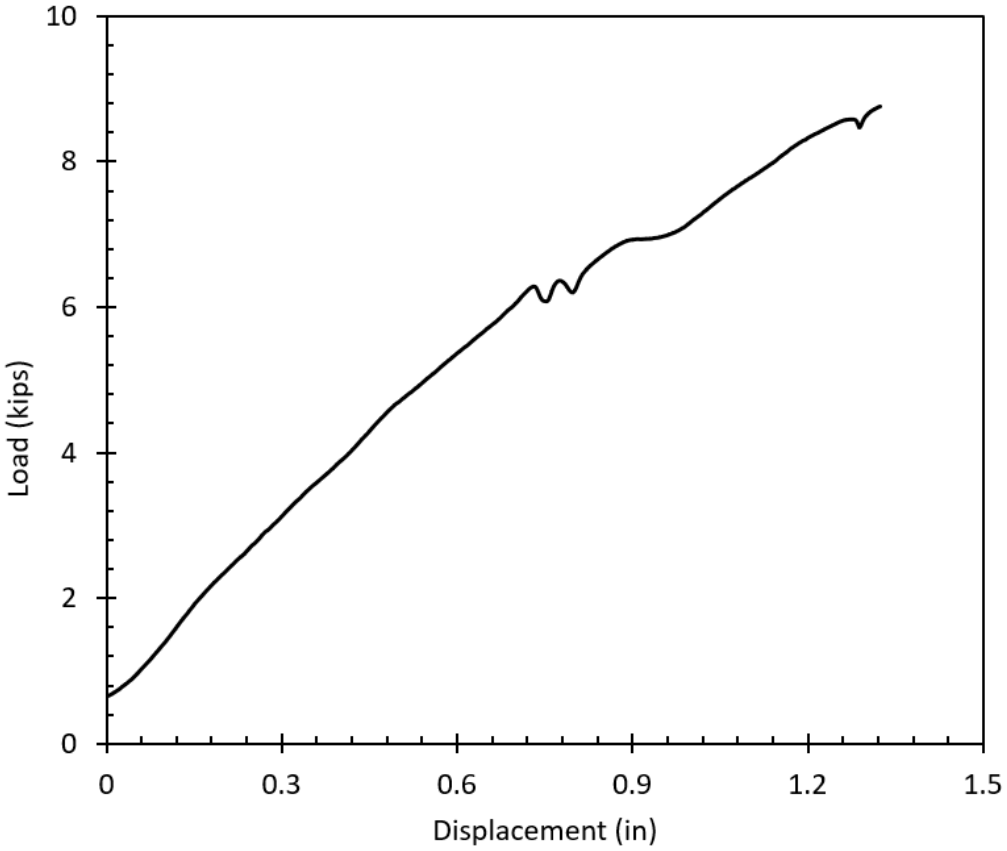

Specimen/Sample ID 13b (15-05-50-13-b)

Date Cast: 11-09-2021	Rebar Diameter: 0.625 inches (#5)
Date Tested: 12-21-2021	Rebar Inclination Angle (θ): 15°
Concrete Compressive Strength: 11970 psi	Aperture Size: 0.5 inches
Peak Load: 8.39 kips	Rebar Bonding Condition: Fixed (grouted)
Actuator Capacity: 22 kips	b: designates a randomly selected retest

Figure A.28 *Shear load-shear displacement curve for Specimen 13b: rebar inclination angle = 15°, rebar diameter = 0.625 inches, and aperture size = 0.5 inches.*

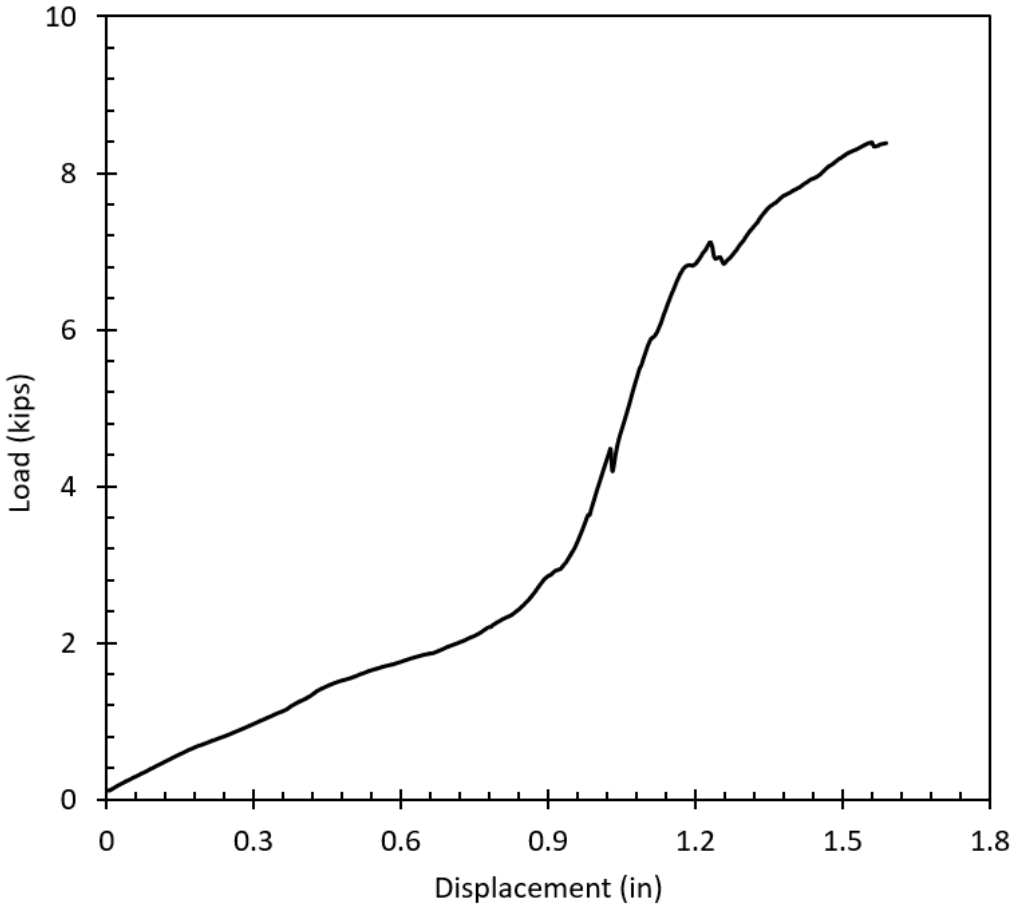

Specimen/Sample ID 14 (15-05-75-14)

Date Cast: 08-07-2021
Date Tested: 12-21-2021
Concrete Compressive Strength: 11670 psi
Peak Load: 6.18 kips
Actuator Capacity: 22 kips

Rebar Diameter: 0.625 inches (#5)
Rebar Inclination Angle (θ): 15°
Aperture Size: 0.75 inches
Rebar Bonding Condition: Fixed (grouted)

Figure A.29 *Shear load-shear displacement curve for Specimen 14: rebar inclination angle = 15°, rebar diameter = 0.625 inches, and aperture size = 0.75 inches.*

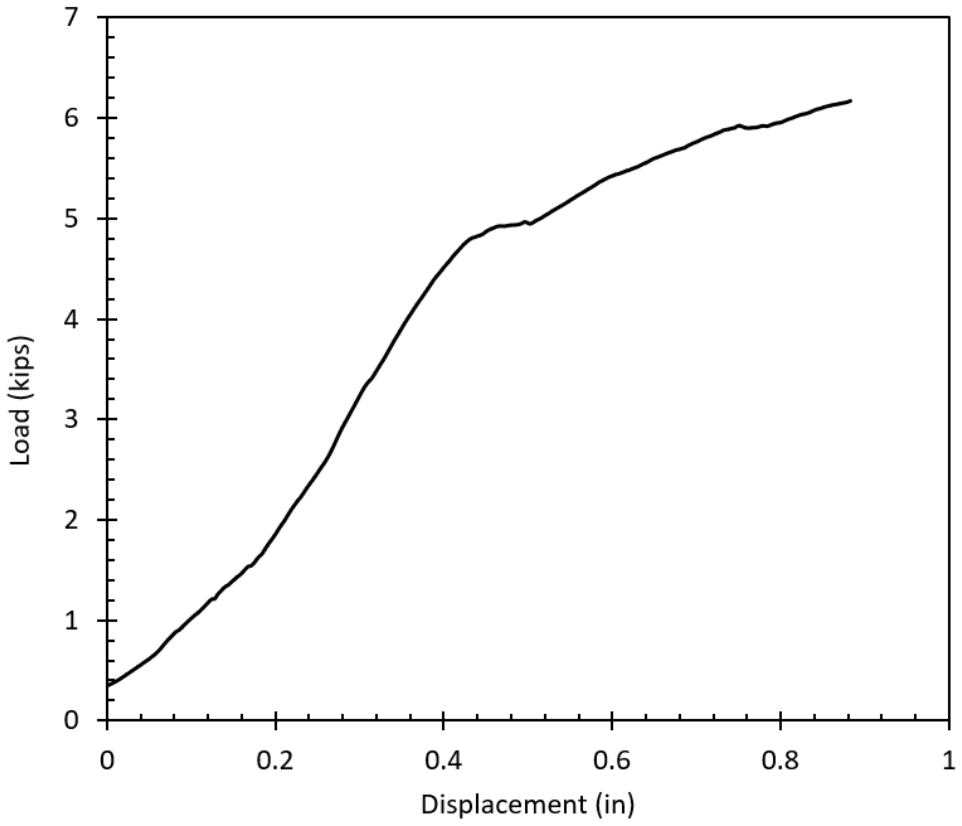

Specimen/Sample ID 14b (15-05-75-14-b)

Date Cast: 11-12-2021
Date Tested: 12-21-2021
Concrete Compressive Strength: 12480 psi
Peak Load: 7.58 kips
Actuator Capacity: 22 kips

Rebar Diameter: 0.625 inches (#5)
Rebar Inclination Angle (θ): 15°
Aperture Size: 0.75 inches
Rebar Bonding Condition: Fixed (grouted)
b: designates a randomly selected retest

Figure A.30 *Shear load-shear displacement curve for Specimen 14b: rebar inclination angle = 15°, rebar diameter = 0.625 inches, and aperture size = 0.75 inches.*

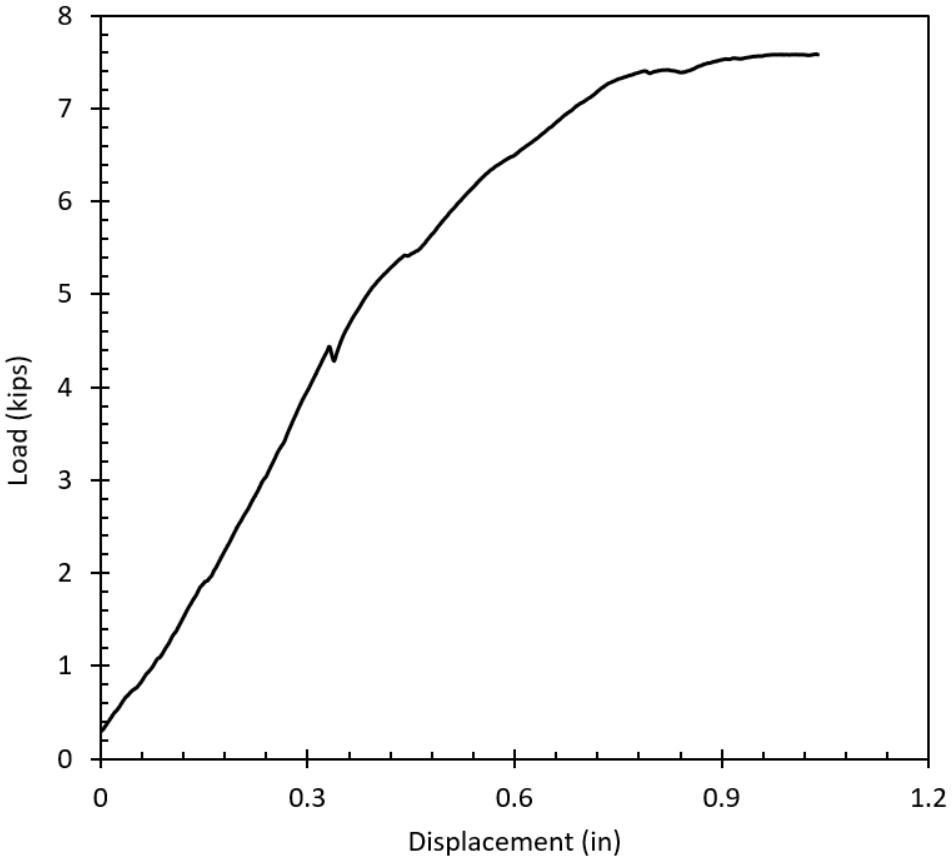

Appendix B: Numerical Model Derived Load-Displacement Responses

This appendix includes load-deformation response information for all modeled concrete block specimens. Each specimen consists of two concrete blocks with an encased rebar. A numerical model of the physical testing set-up was developed to supplement the experimental results from the direct shear testing and increase the robustness of the developed design chart. ABAQUS FEA software was used to simulate the large-scale direct shear tests performed in the laboratory. A 3D Finite Element model was adopted for analysis in ABAQUS. The concrete blocks were modelled with dimensions of 20″ × 20″ × 20″ (50.8 cm x 50.8 cm x 50.8cm) with various aperture sizes to simulate the physical testing conditions. Note that the model dimensions are slightly different from those of the actual concrete blocks but have a minimal influence on the results. Further details regarding the model testing conditions are given in section 3.7 of this report. For the model specimens corresponding to a physically-tested specimen(s), both the physical testing and modeled load-displacement results are shown for comparison.

Specimen M1

Rebar Diameter: 0.5 inches (#4)	No Corresponding Physical Test
Rebar Bonding Condition: Free (un-grouted)	Rebar Inclination Angle (θ): 15°
Peak Load: 7.37 kips	Aperture Size: 0.125 inches

Figure B.1 *Shear load-shear displacement curve for Specimen M1: rebar inclination angle = 15°, rebar diameter = 0.5 inches, and aperture size = 0.125 inches.*

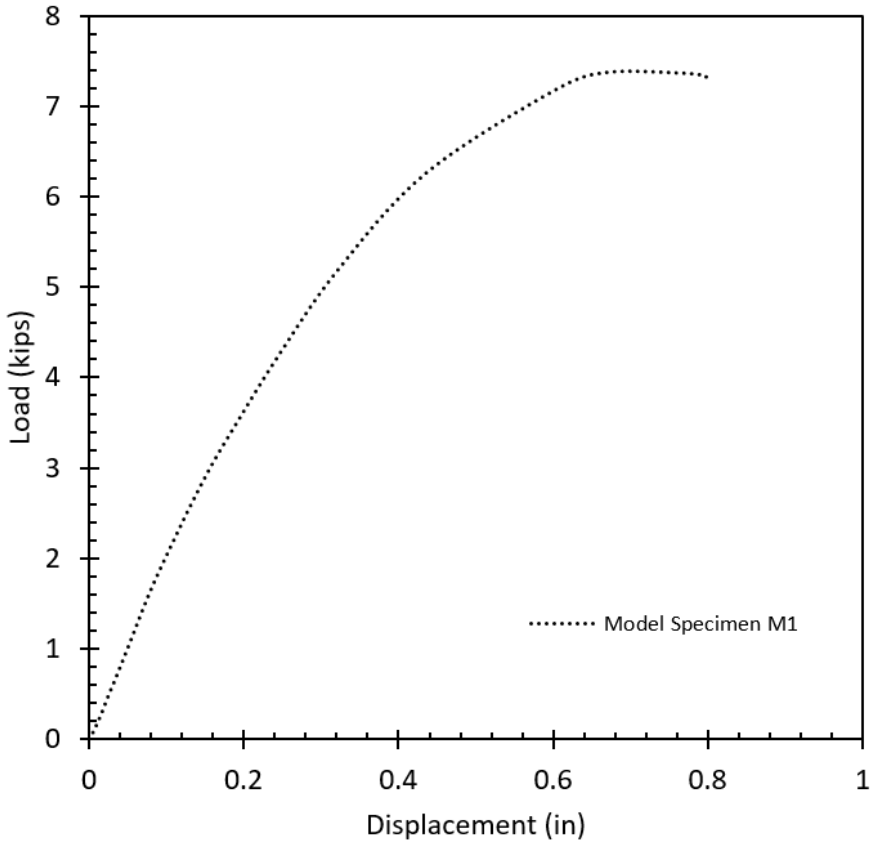

Specimen M2

Rebar Diameter: 0.5 inches (#4)	Corresponding Physical Test Specimen 1
Rebar Bonding Condition: Free (un-grouted)	Rebar Inclination Angle (θ): 15°
Peak Load: 7.05 kips	Aperture Size: 0.25 inches

Figure B.2 *Shear load-shear displacement curve for Specimen M2 and Specimen 1: rebar inclination angle = 15°, rebar diameter = 0.5 inches, and aperture size = 0.25 inches.*

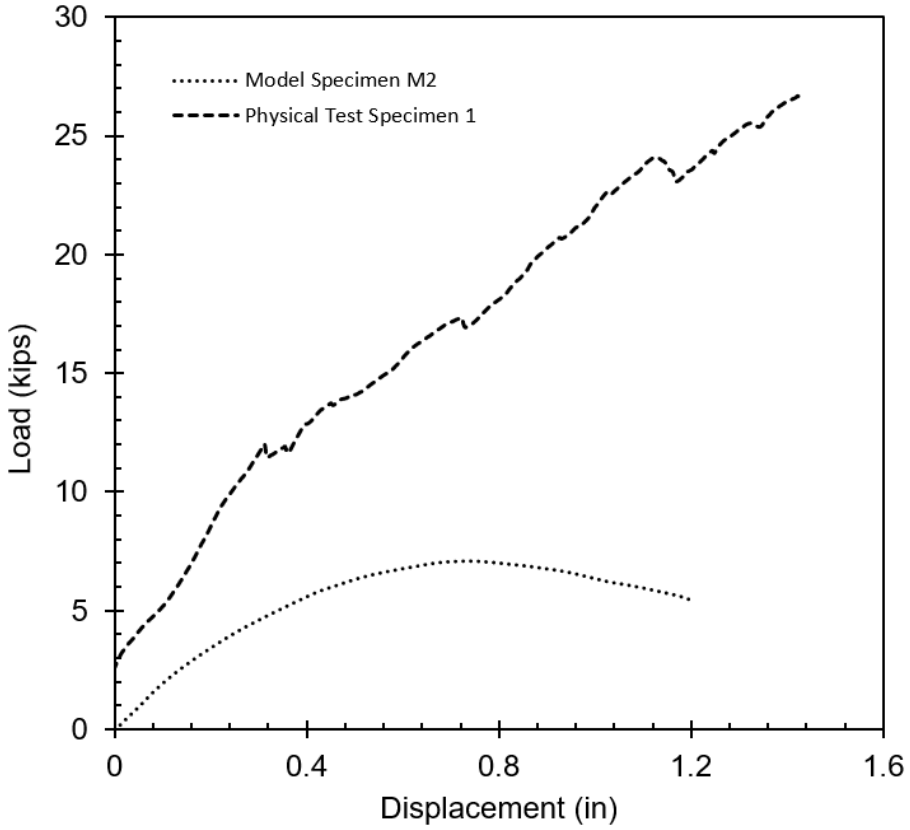

Specimen M3

Rebar Diameter: 0.5 inches (#4)	Corresponding Physical Test Specimen 2
Rebar Bonding Condition: Free (un-grouted)	Rebar Inclination Angle (θ): 15°
Peak Load: 5.75 kips	Aperture Size: 0.5 inches

Figure B.3 *Shear load-shear displacement curve for Specimen M3 and Specimen 2: rebar inclination angle = 15°, rebar diameter = 0.5 inches, and aperture size = 0.5 inches.*

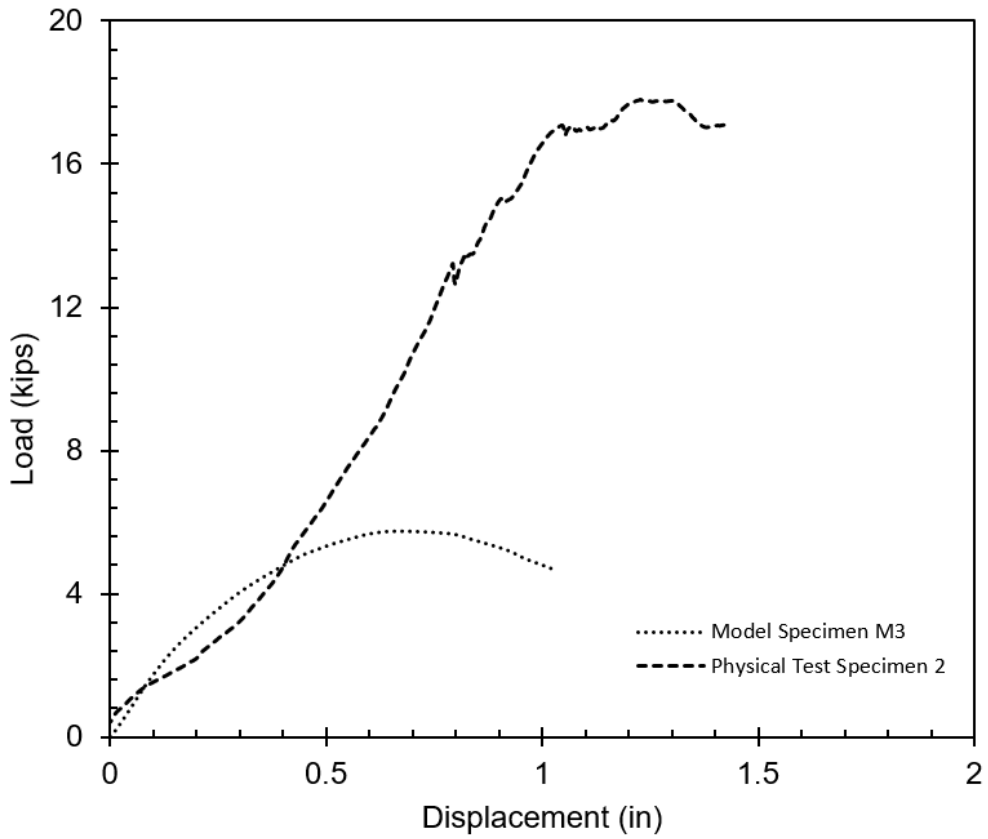

Specimen M4

Rebar Diameter: 0.5 inches (#4)
Rebar Bonding Condition: Free (un-grouted)
Peak Load: 4.92 kips
Corresponding Physical Test Specimen 11b
Rebar Inclination Angle (θ): 15°
Aperture Size: 0.75 inches

Figure B.4 *Shear load-shear displacement curve for Specimen M4 and Specimen 11b: rebar inclination angle = 15°, rebar diameter = 0.5 inches, and aperture size = 0.75 inches.*

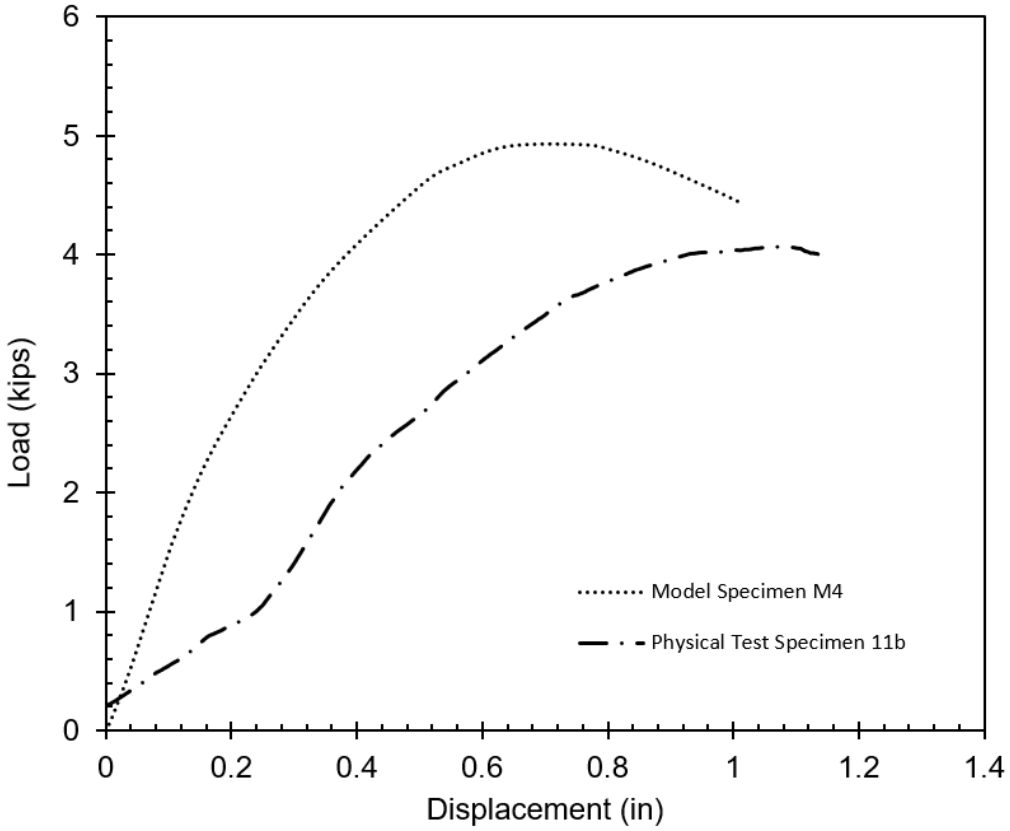

Specimen M5

Rebar Diameter: 0.5 inches (#4)	No Corresponding Physical Test
Rebar Bonding Condition: Free (un-grouted)	Rebar Inclination Angle (θ): 15°
Peak Load: 4.00 kips	Aperture Size: 1 inch

Figure B.5 *Shear load-shear displacement curve for Specimen M5: rebar inclination angle = 15°, rebar diameter = 0.5 inches, and aperture size = 1 inch.*

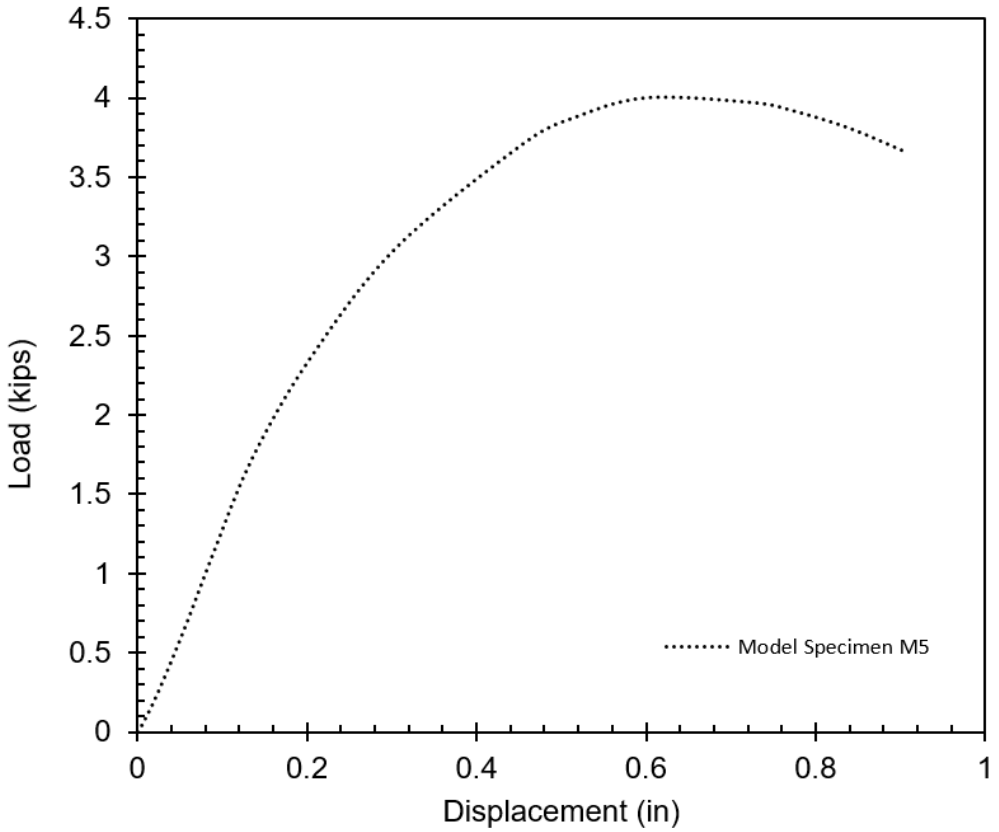

Specimen M6

Rebar Diameter: 0.625 inches (#5)	No Corresponding Physical Test
Rebar Bonding Condition: Free (un-grouted)	Rebar Inclination Angle (θ): 15°
Peak Load: 9.29 kips	Aperture Size: 0.125 inches

Figure B.6 *Shear load-shear displacement curve for Specimen M6: rebar inclination angle = 15°, rebar diameter = 0.625 inches, and aperture size = 0.125 inches.*

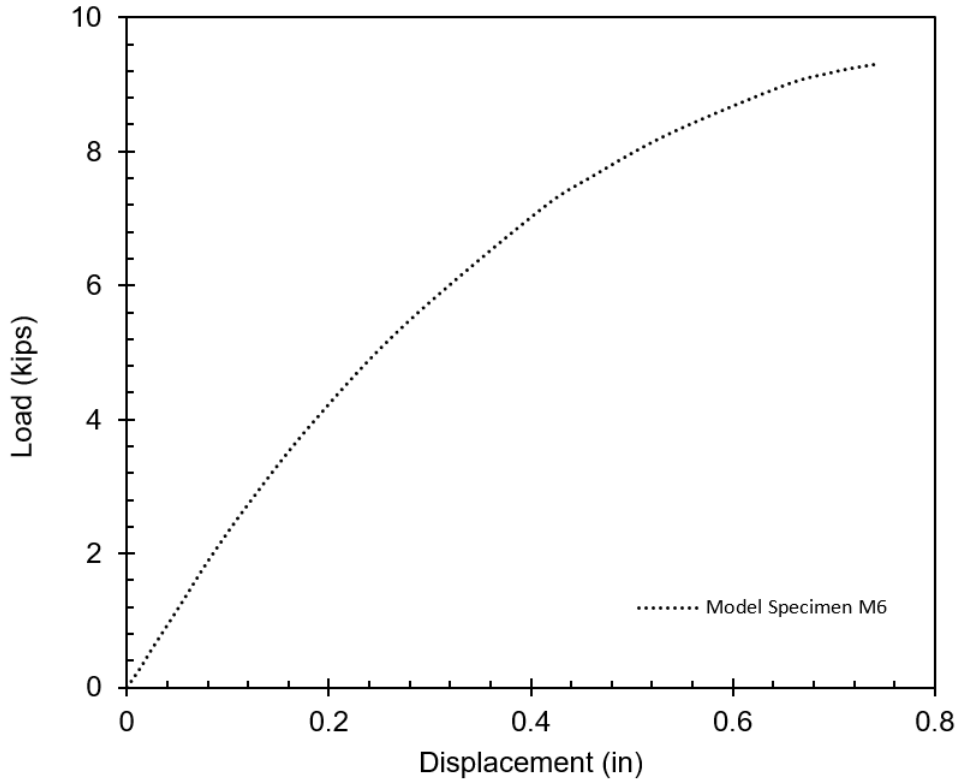

Specimen M7

Rebar Diameter: 0.625 inches (#5)
Rebar Bonding Condition: Free (un-grouted)
Peak Load: 7.69 kips
Corresponding Physical Test Specimen 5b
Rebar Inclination Angle (θ): 15°
Aperture Size: 0.25 inches

Figure B.7 *Shear load-shear displacement curve for Specimen M7 and Specimen 5b: rebar inclination angle = 15°, rebar diameter = 0.625 inches, and aperture size = 0.25 inches.*

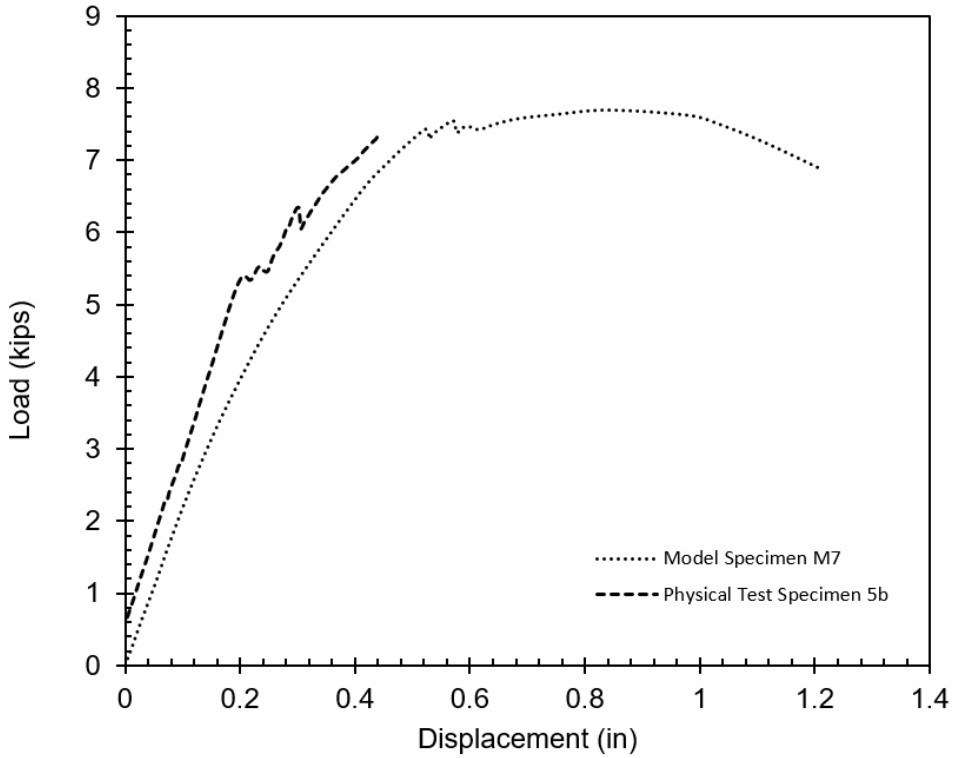

Specimen M8

Rebar Diameter: 0.625 inches (#5)	Corresponding Physical Test Specimen 8
Rebar Bonding Condition: Free (un-grouted)	Rebar Inclination Angle (θ): 15°
Peak Load: 7.36 kips	Aperture Size: 0.5 inches

Figure B.8 *Shear load-shear displacement curve for Specimen M8: rebar inclination angle = 15°, rebar diameter = 0.625 inches, and aperture size = 0.5 inches.*

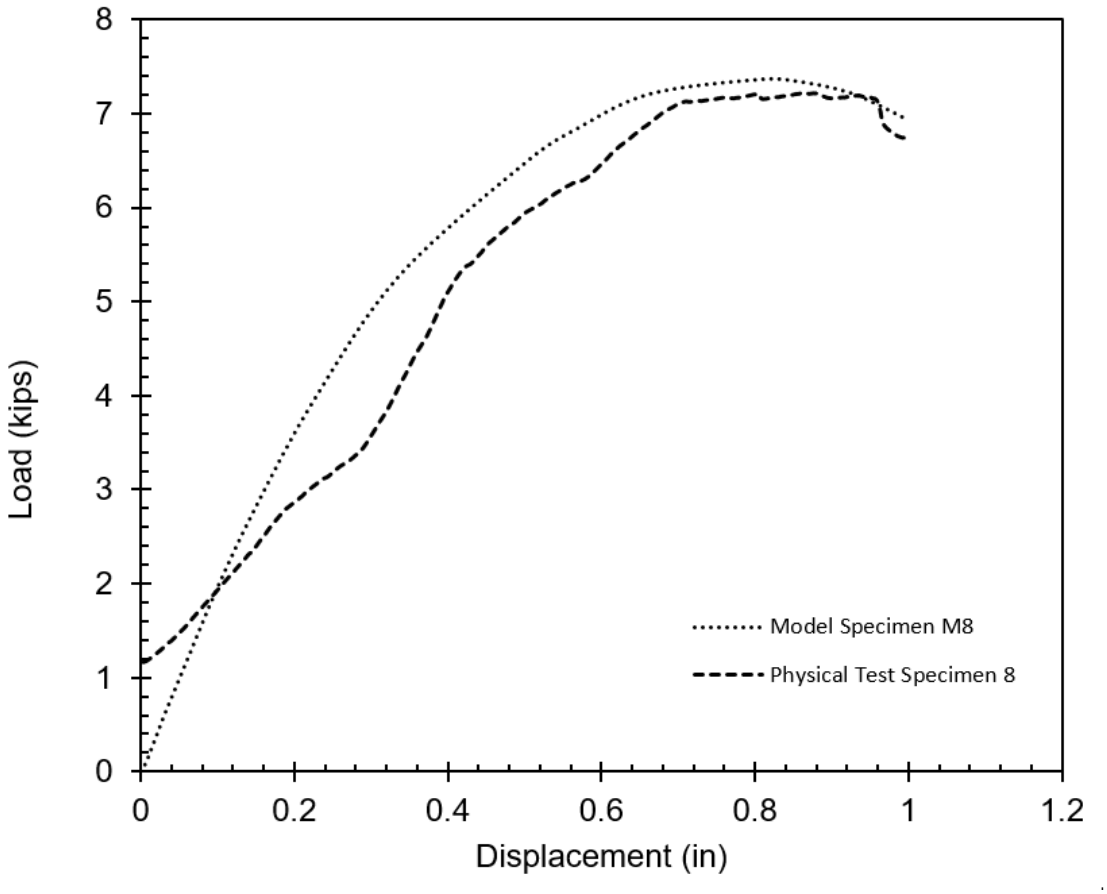

Specimen M9

Rebar Diameter: 0.625 inches (#5)	Corresponding Physical Test Specimen 4b
Rebar Bonding Condition: Free (un-grouted)	Rebar Inclination Angle (θ): 15°
Peak Load: 6.54 kips	Aperture Size: 0.75 inches

Figure B.9 *Shear load-shear displacement curve for Specimen M9 and Specimen 4b: rebar inclination angle = 15°, rebar diameter = 0.625 inches, and aperture size = 0.75 inches.*

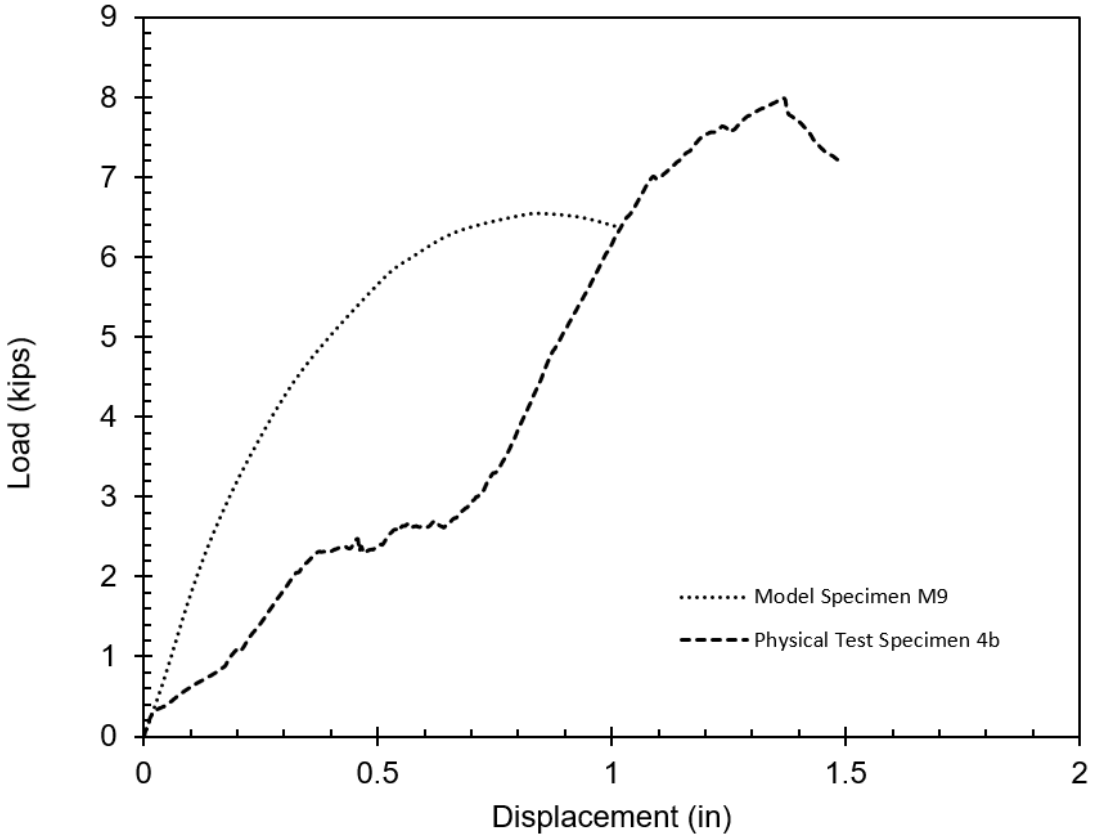

Specimen M10

Rebar Diameter: 0.625 inches (#5)	No Corresponding Physical Test
Rebar Bonding Condition: Free (un-grouted)	Rebar Inclination Angle (θ): 15°
Peak Load: 5.59 kips	Aperture Size: 1 inch

Figure B.10 *Shear load-shear displacement curve for Specimen M10: rebar inclination angle = 15°, rebar diameter = 0.625 inches, and aperture size = 1 inch.*

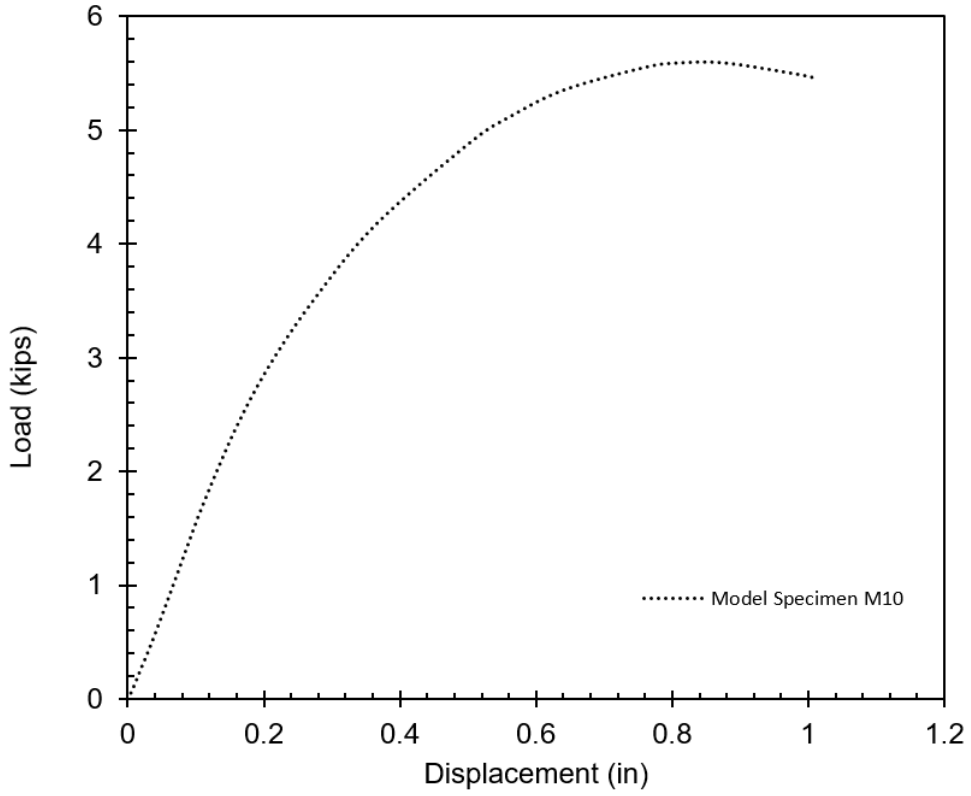

Specimen M11

Rebar Diameter: 0.75 inches (#6)	No Corresponding Physical Test
Rebar Bonding Condition: Free (un-grouted)	Rebar Inclination Angle (θ): 15°
Peak Load: 12.44 kips	Aperture Size: 0.125 inches

Figure B.11 *Shear load-shear displacement curve for Specimen M11: rebar inclination angle = 15°, rebar diameter = 0.75 inches, and aperture size = 0.125 inches.*

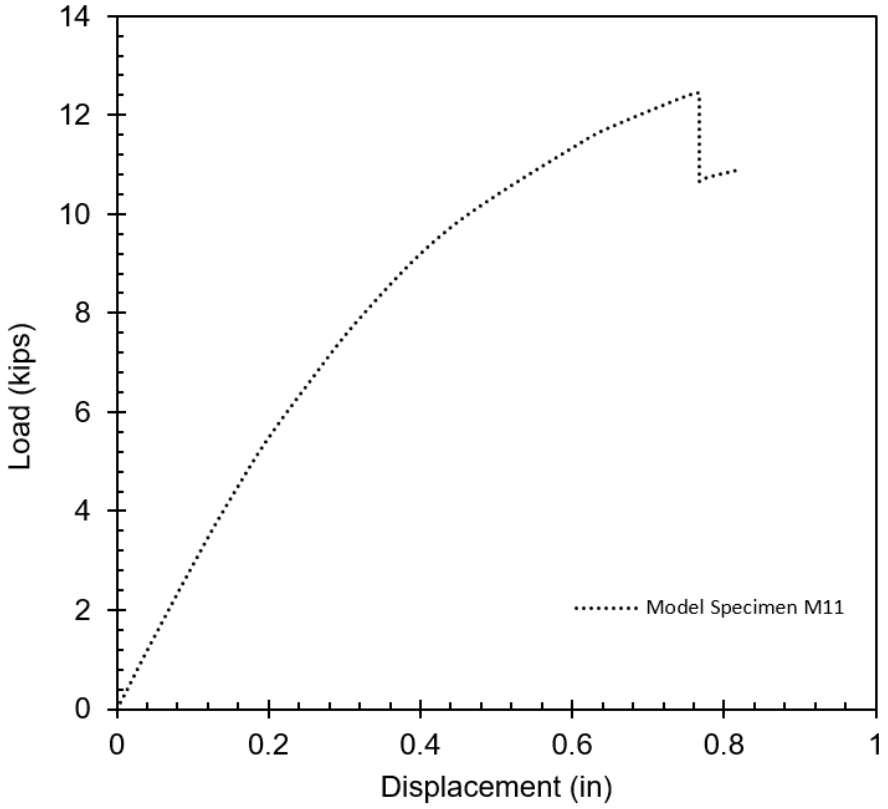

Specimen M12

Rebar Diameter: 0.75 inches (#6)	Corresponding Physical Test Specimen 7b
Rebar Bonding Condition: Free (un-grouted)	Rebar Inclination Angle (θ): 15°
Peak Load: 12.37 kips	Aperture Size: 0.25 inches

Figure B.12 *Shear load-shear displacement curve for Specimen M12: rebar inclination angle = 15°, rebar diameter = 0.75 inches, and aperture size = 0.25 inches.*

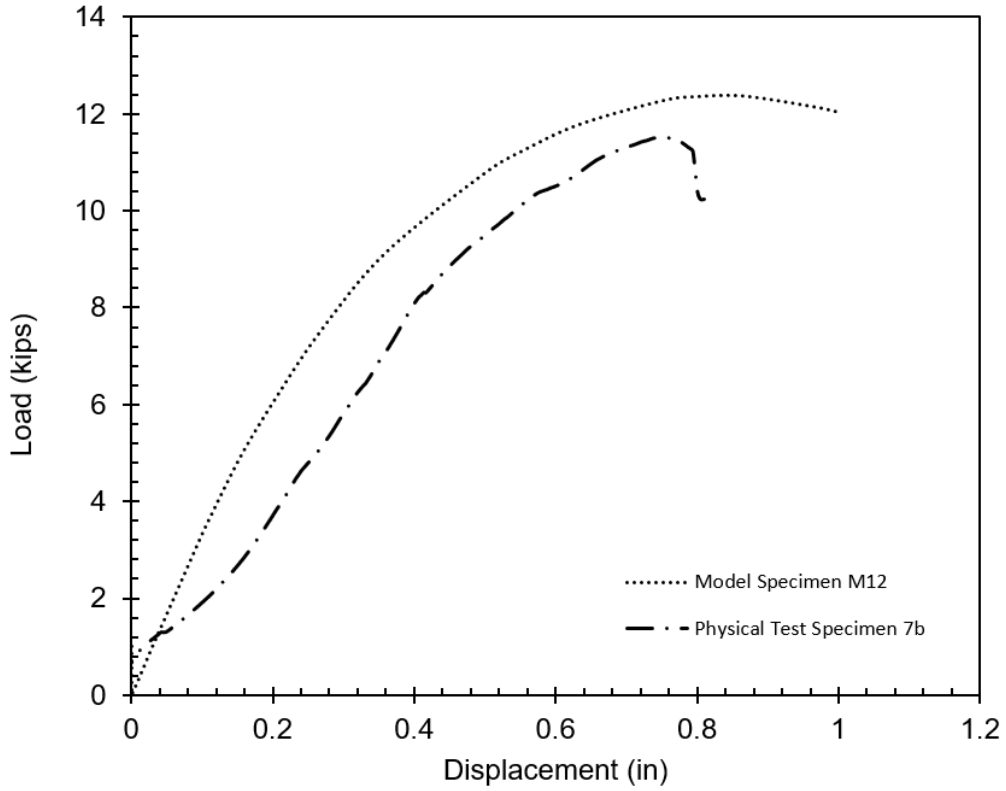

Specimen M13

Rebar Diameter: 0.75 inches (#6)	Corresponding Physical Test Specimen 9b
Rebar Bonding Condition: Free (un-grouted)	Rebar Inclination Angle (θ): 15°
Peak Load: 9.21 kips	Aperture Size: 0.5 inches

Figure B.13 *Shear load-shear displacement curve for Specimen M13 and Specimen 9b: rebar inclination angle = 15°, rebar diameter = 0.75 inches, and aperture size = 0.5 inches.*

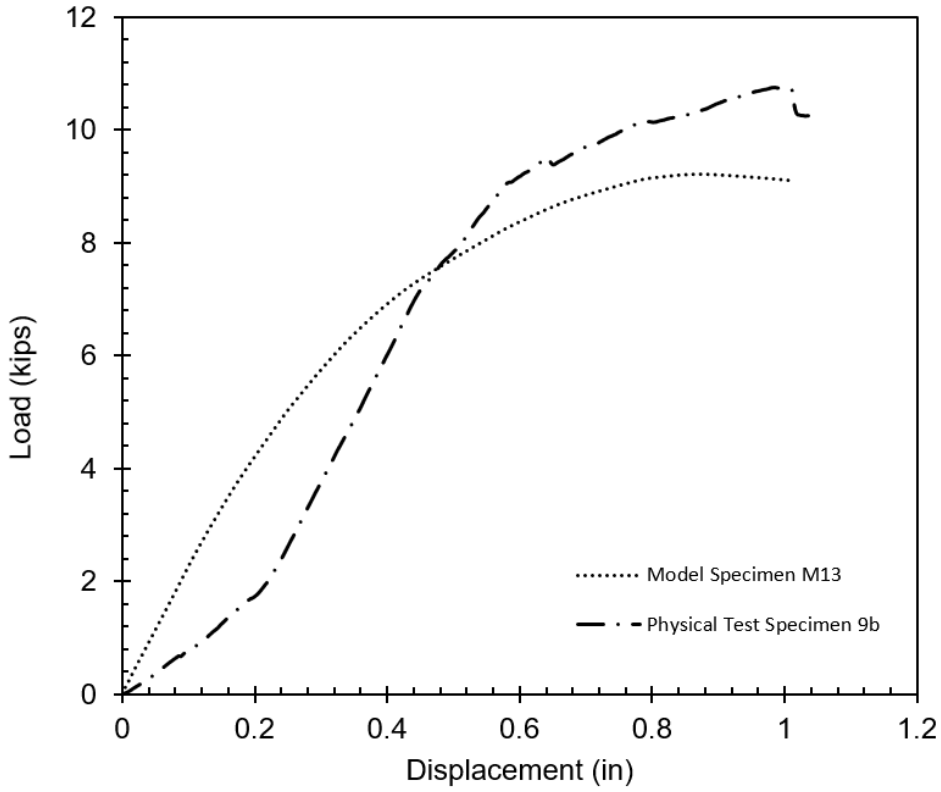

Specimen M14

Rebar Diameter: 0.75 inches (#6)	Corresponding Physical Test Specimen 3
Rebar Bonding Condition: Free (un-grouted)	Rebar Inclination Angle (θ): 15°
Peak Load: 8.43 kips	Aperture Size: 0.75 inches

Figure B.14 *Shear load-shear displacement curve for Specimen M14 and Specimen 3: rebar inclination angle = 15°, rebar diameter = 0.75 inches, and aperture size = 0.75 inches.*

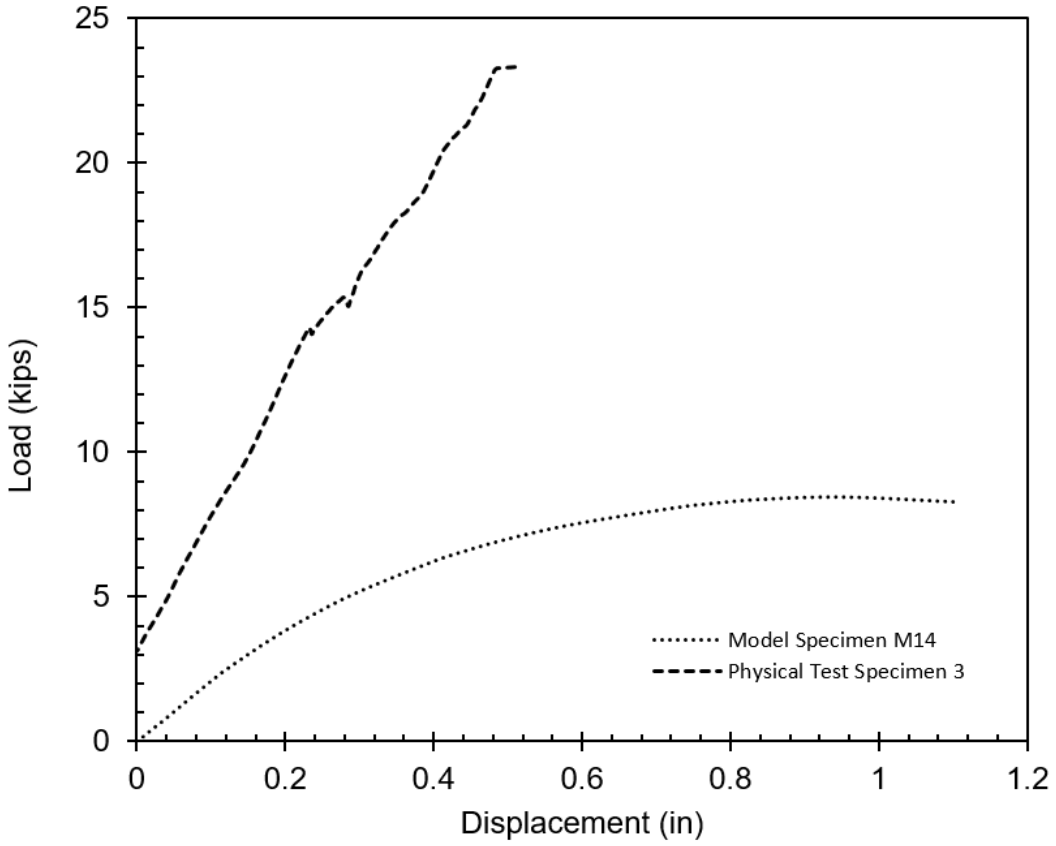

Specimen M15

Rebar Diameter: 0.75 inches (#6)	No Corresponding Physical Test
Rebar Bonding Condition: Free (un-grouted)	Rebar Inclination Angle (θ): 15°
Peak Load: 7.25 kips	Aperture Size: 1 inch

Figure B.15 *Shear load-shear displacement curve for Specimen M15: rebar inclination angle = 15°, rebar diameter = 0.75 inches, and aperture size = 1 inch.*

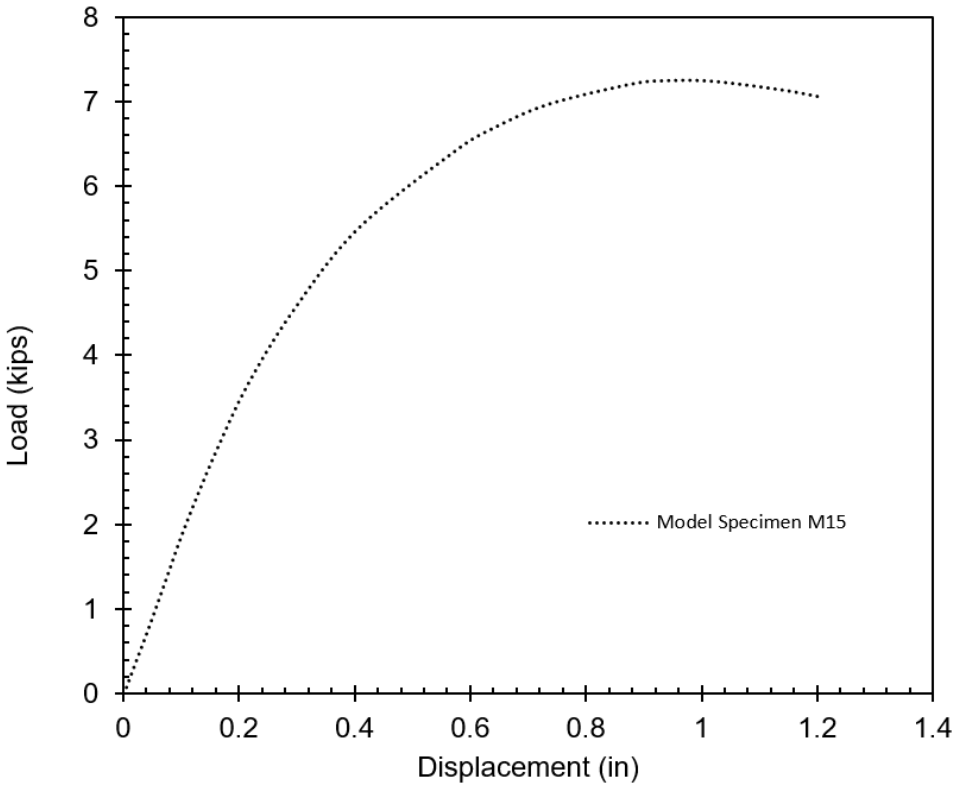

Appendix C: Rebar Certified Mill Test Reports

Figure C.1 *Mill Certificate for #4 rebar (1 of 3).*

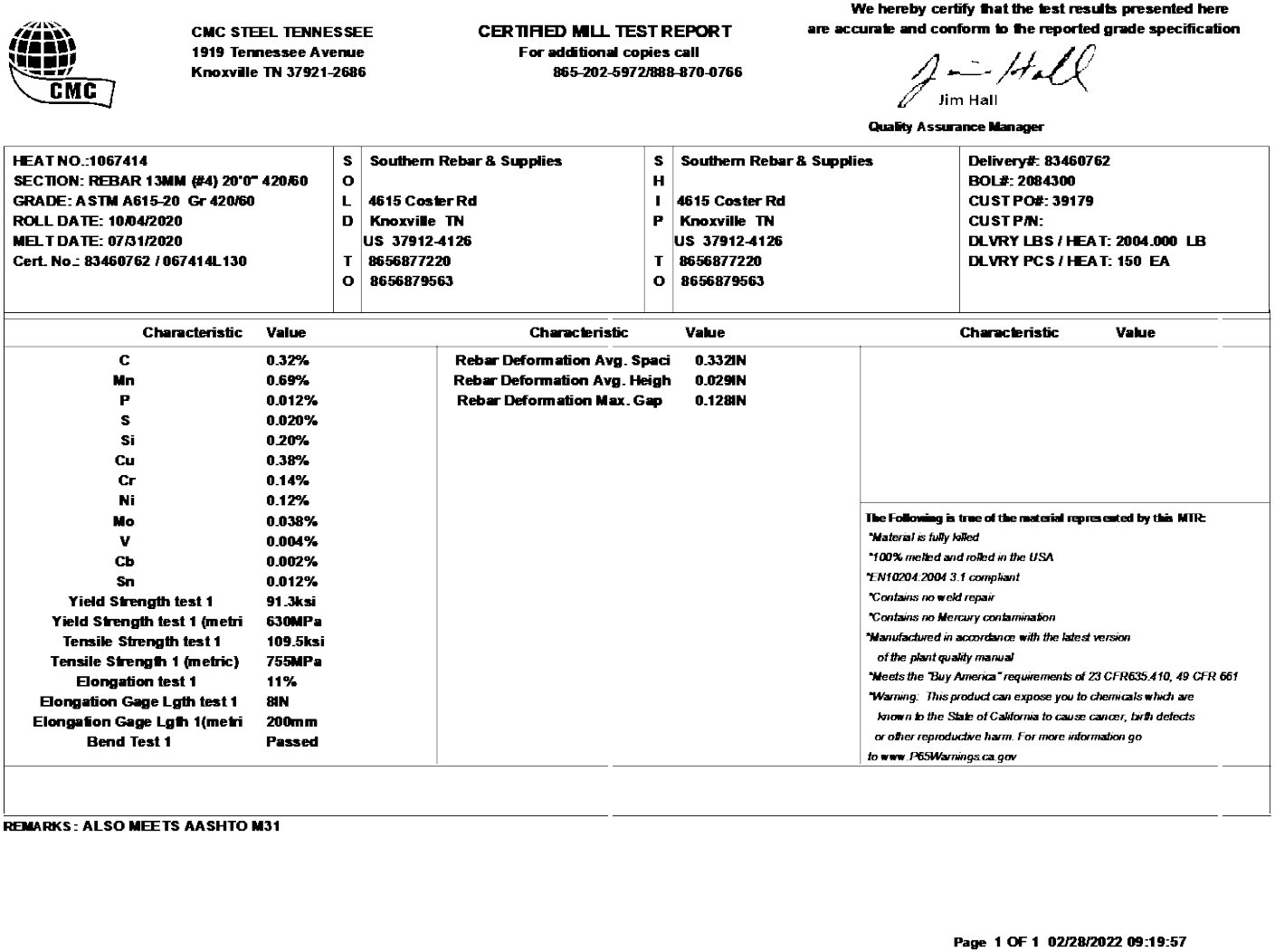

CMC STEEL TENNESSEE
1919 Tennessee Avenue
Knoxville TN 37921-2686

CERTIFIED MILL TEST REPORT
For additional copies call
865-202-5972/888-870-0766

We hereby certify that the test results presented here are accurate and conform to the reported grade specification

Jim Hall
Quality Assurance Manager

HEAT NO.:1067414 SECTION: REBAR 13MM (#4) 20'0" 420/60 GRADE: ASTM A615-20 Gr 420/60 ROLL DATE: 10/04/2020 MELT DATE: 07/31/2020 Cert. No.: 83460762 / 067414L130	S O L D T O	Southern Rebar & Supplies 4615 Coster Rd Knoxville TN US 37912-4126 8656877220 8656879563	S H I P T O	Southern Rebar & Supplies 4615 Coster Rd Knoxville TN US 37912-4126 8656877220 8656879563	Delivery#: 83460762 BOL#: 2084300 CUST PO#: 39179 CUST P/N: DLVRY LBS / HEAT: 2004.000 LB DLVRY PCS / HEAT: 150 EA	

Characteristic	Value	Characteristic	Value	Characteristic	Value
C	0.32%	Rebar Deformation Avg. Spaci	0.332IN		
Mn	0.69%	Rebar Deformation Avg. Heigh	0.029IN		
P	0.012%	Rebar Deformation Max. Gap	0.128IN		
S	0.020%				
Si	0.20%				
Cu	0.38%				
Cr	0.14%				
Ni	0.12%				
Mo	0.038%			The Following is true of the material represented by this MTR:	
V	0.004%			*Material is fully killed	
Cb	0.002%			*100% melted and rolled in the USA	
Sn	0.012%			*EN10204:2004 3.1 compliant	
Yield Strength test 1	91.3ksi			*Contains no weld repair	
Yield Strength test 1 (metri	630MPa			*Contains no Mercury contamination	
Tensile Strength test 1	109.5ksi			*Manufactured in accordance with the latest version of the plant quality manual	
Tensile Strength 1 (metric)	755MPa			*Meets the "Buy America" requirements of 23 CFR635.410, 49 CFR 661	
Elongation test 1	11%			*Warning: This product can expose you to chemicals which are known to the State of California to cause cancer, birth defects or other reproductive harm. For more information go to www.P65Warnings.ca.gov	
Elongation Gage Lgth test 1	8IN				
Elongation Gage Lgth 1(metri	200mm				
Bend Test 1	Passed				

REMARKS: ALSO MEETS AASHTO M31

Page 1 OF 1 02/28/2022 09:19:57

Figure C.2 *Mill Certificate for #4 rebar (2 of 3).*

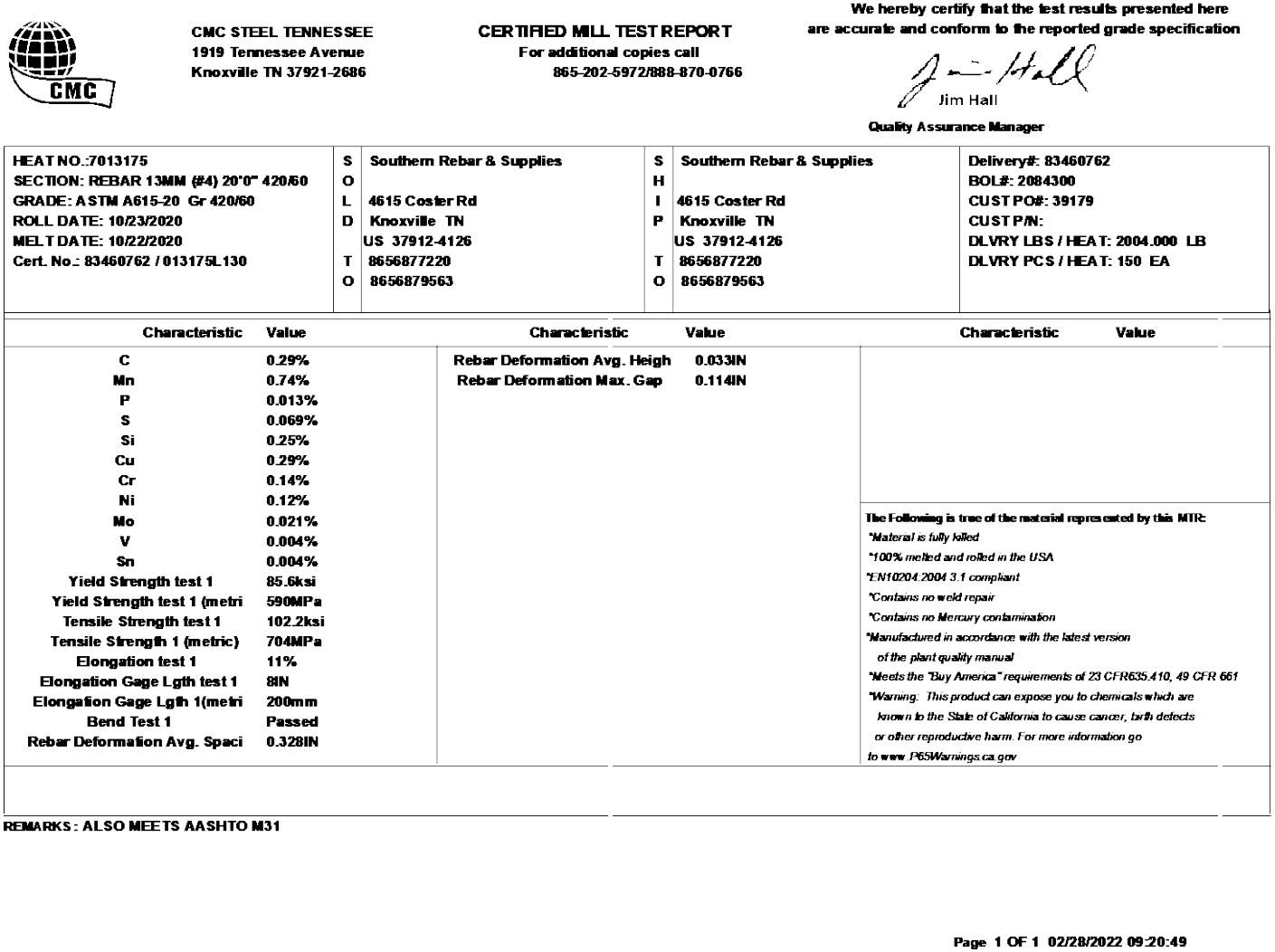

CMC STEEL TENNESSEE
1919 Tennessee Avenue
Knoxville TN 37921-2686

CERTIFIED MILL TEST REPORT
For additional copies call
865-202-5972/888-870-0766

We hereby certify that the test results presented here are accurate and conform to the reported grade specification

Jim Hall
Quality Assurance Manager

HEAT NO.:7013175 SECTION: REBAR 13MM (#4) 20'0" 420/60 GRADE: ASTM A615-20 Gr 420/60 ROLL DATE: 10/23/2020 MELT DATE: 10/22/2020 Cert. No.: 83460762 / 013175L130	SOLD TO	Southern Rebar & Supplies 4615 Coster Rd Knoxville TN US 37912-4126 8656877220 8656879563	SHIP TO	Southern Rebar & Supplies 4615 Coster Rd Knoxville TN US 37912-4126 8656877220 8656879563	Delivery#: 83460762 BOL#: 2084300 CUST PO#: 39179 CUST P/N: DLVRY LBS / HEAT: 2004.000 LB DLVRY PCS / HEAT: 150 EA

Characteristic	Value	Characteristic	Value	Characteristic	Value
C	0.29%	Rebar Deformation Avg. Heigh	0.033IN		
Mn	0.74%	Rebar Deformation Max. Gap	0.114IN		
P	0.013%				
S	0.069%				
Si	0.25%				
Cu	0.29%				
Cr	0.14%				
Ni	0.12%				
Mo	0.021%				
V	0.004%				
Sn	0.004%				
Yield Strength test 1	85.6ksi				
Yield Strength test 1 (metri	590MPa				
Tensile Strength test 1	102.2ksi				
Tensile Strength 1 (metric)	704MPa				
Elongation test 1	11%				
Elongation Gage Lgth test 1	8IN				
Elongation Gage Lgth 1(metri	200mm				
Bend Test 1	Passed				
Rebar Deformation Avg. Spaci	0.328IN				

The Following is true of the material represented by this MTR:
*Material is fully killed
*100% melted and rolled in the USA
*EN10204:2004 3.1 compliant
*Contains no weld repair
*Contains no Mercury contamination
*Manufactured in accordance with the latest version of the plant quality manual
*Meets the "Buy America" requirements of 23 CFR635.410, 49 CFR 661
*Warning: This product can expose you to chemicals which are known to the State of California to cause cancer, birth defects or other reproductive harm. For more information go to www.P65Warnings.ca.gov

REMARKS: ALSO MEETS AASHTO M31

Page 1 OF 1 02/28/2022 09:20:49

Figure C.3 *Mill Certificate for #4 rebar (3 of 3).*

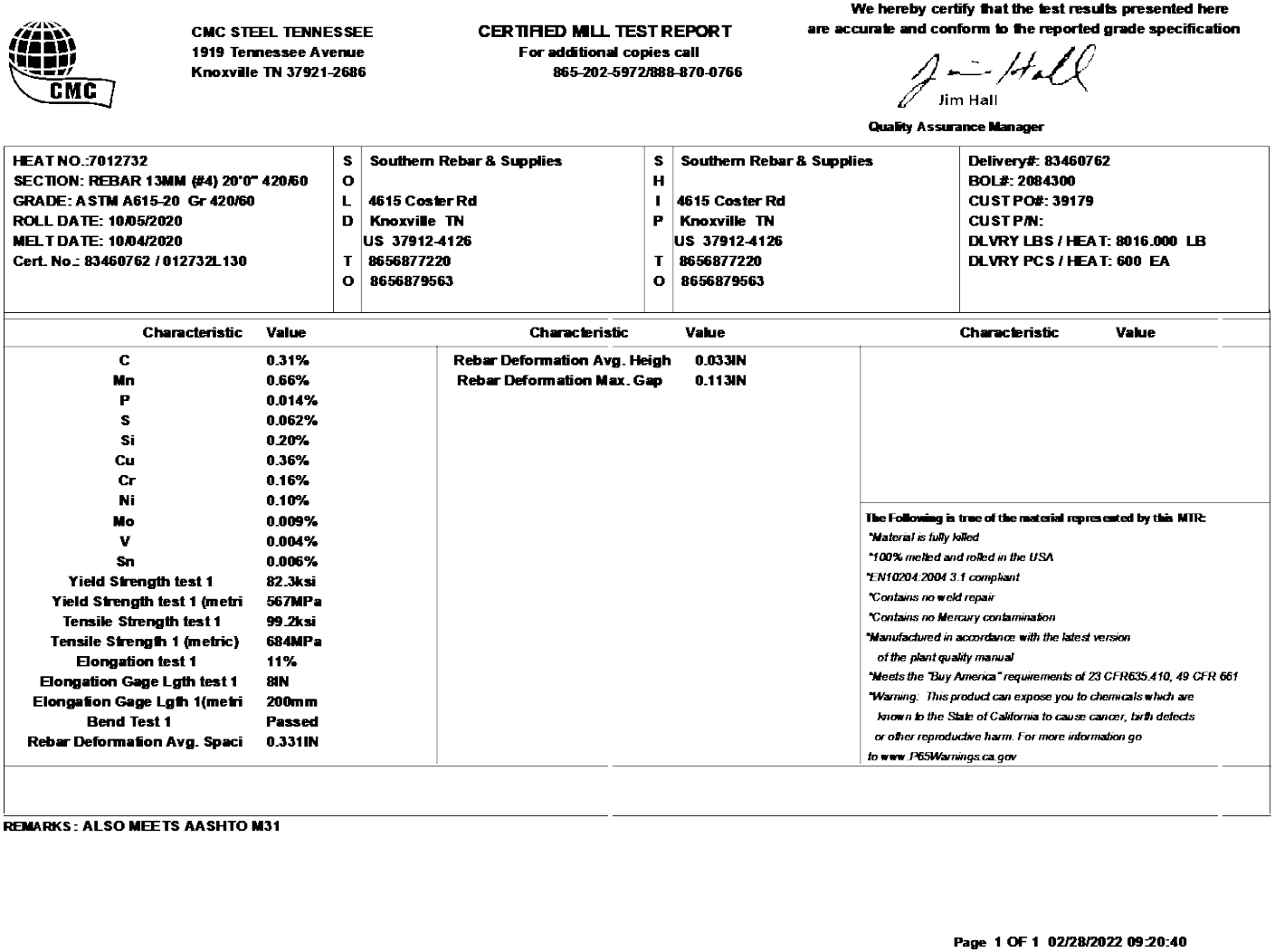

CMC STEEL TENNESSEE
1919 Tennessee Avenue
Knoxville TN 37921-2686

CERTIFIED MILL TEST REPORT
For additional copies call
865-202-5972/888-870-0766

We hereby certify that the test results presented here are accurate and conform to the reported grade specification

Jim Hall
Quality Assurance Manager

HEAT NO.:7012732 SECTION: REBAR 13MM (#4) 20'0" 420/60 GRADE: ASTM A615-20 Gr 420/60 ROLL DATE: 10/05/2020 MELT DATE: 10/04/2020 Cert. No.: 83460762 / 012732L130	SOLD TO	Southern Rebar & Supplies 4615 Coster Rd Knoxville TN US 37912-4126 8656877220 8656879563	SHIP TO	Southern Rebar & Supplies 4615 Coster Rd Knoxville TN US 37912-4126 8656877220 8656879563	Delivery#: 83460762 BOL#: 2084300 CUST PO#: 39179 CUST P/N: DLVRY LBS / HEAT: 8016.000 LB DLVRY PCS / HEAT: 600 EA

Characteristic	Value
C	0.31%
Mn	0.66%
P	0.014%
S	0.062%
Si	0.20%
Cu	0.36%
Cr	0.16%
Ni	0.10%
Mo	0.009%
V	0.004%
Sn	0.006%
Yield Strength test 1	82.3ksi
Yield Strength test 1 (metri	567MPa
Tensile Strength test 1	99.2ksi
Tensile Strength 1 (metric)	684MPa
Elongation test 1	11%
Elongation Gage Lgth test 1	8IN
Elongation Gage Lgth 1(metri	200mm
Bend Test 1	Passed
Rebar Deformation Avg. Spaci	0.331IN

Characteristic	Value
Rebar Deformation Avg. Heigh	0.033IN
Rebar Deformation Max. Gap	0.113IN

The Following is true of the material represented by this MTR:

**Material is fully killed*
**100% melted and rolled in the USA*
**EN10204:2004 3.1 compliant*
**Contains no weld repair*
**Contains no Mercury contamination*
**Manufactured in accordance with the latest version of the plant quality manual*
**Meets the "Buy America" requirements of 23 CFR635.410, 49 CFR 661*
**Warning: This product can expose you to chemicals which are known to the State of California to cause cancer, birth defects or other reproductive harm. For more information go to www.P65Warnings.ca.gov*

REMARKS: ALSO MEETS AASHTO M31

Page 1 OF 1 02/28/2022 09:20:40

Figure C.4 *Mill Certificate for #5 rebar*

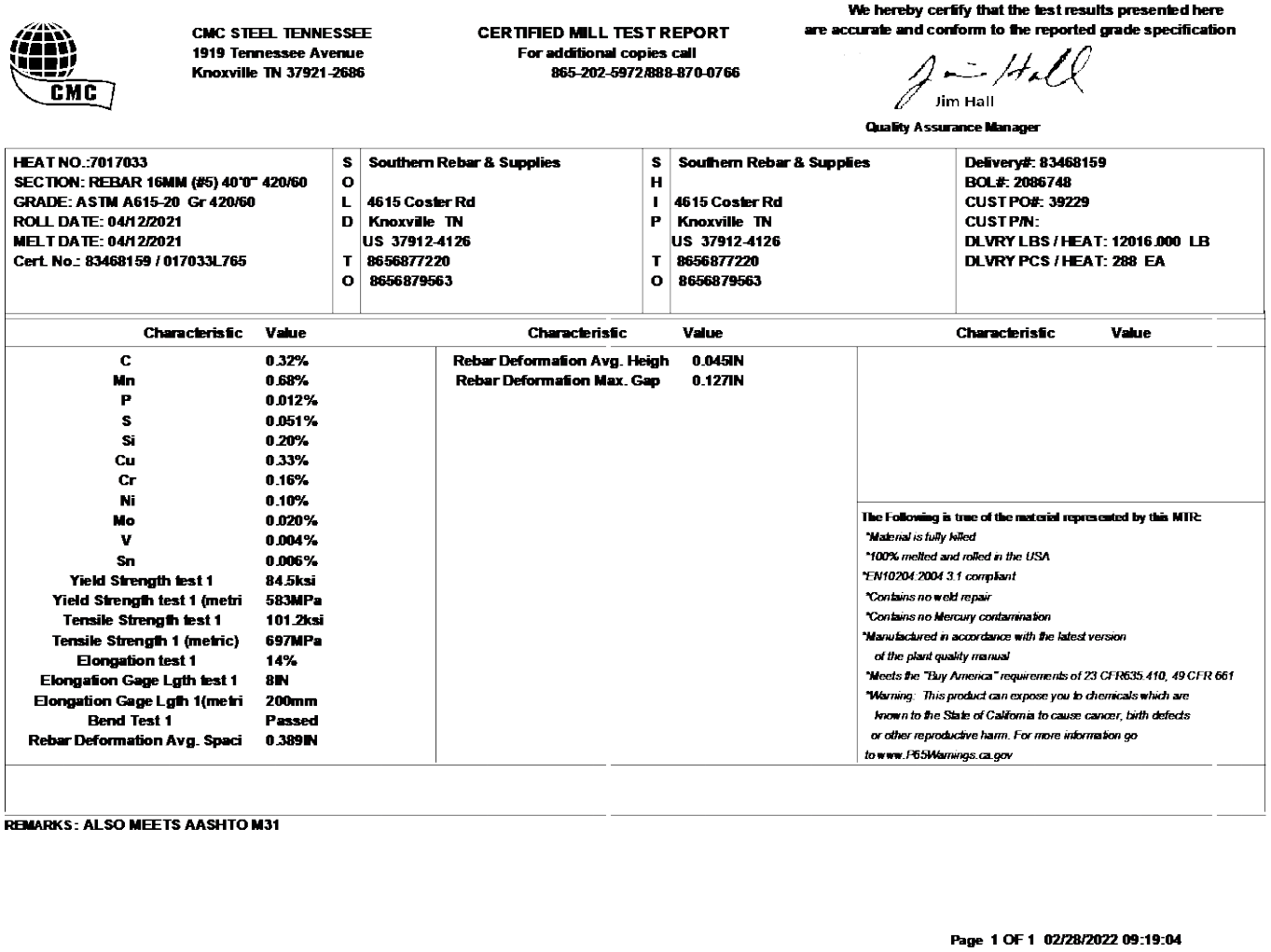

CMC STEEL TENNESSEE
1919 Tennessee Avenue
Knoxville TN 37921-2686

CERTIFIED MILL TEST REPORT
For additional copies call
865-202-5972/888-870-0766

We hereby cerfify that the test results presented here are accurate and conform to the reported grade specification

Jim Hall
Quality Assurance Manager

HEAT NO.:7017033 SECTION: REBAR 16MM (#5) 40'0" 420/60 GRADE: ASTM A615-20 Gr 420/60 ROLL DATE: 04/12/2021 MELT DATE: 04/12/2021 Cert. No.: 83468159 / 017033L765	SOLD TO	Southern Rebar & Supplies 4615 Coster Rd Knoxville TN US 37912-4126 8656877220 8656879563	SHIP TO	Southern Rebar & Supplies 4615 Coster Rd Knoxville TN US 37912-4126 8656877220 8656879563	Delivery#: 83468159 BOL#: 2086748 CUST PO#: 39229 CUST P/N: DLVRY LBS / HEAT: 12016.000 LB DLVRY PCS / HEAT: 288 EA

Characteristic	Value	Characteristic	Value	Characteristic	Value
C	0.32%	Rebar Deformation Avg. Heigh	0.045IN		
Mn	0.68%	Rebar Deformation Max. Gap	0.127IN		
P	0.012%				
S	0.051%				
Si	0.20%				
Cu	0.33%				
Cr	0.16%				
Ni	0.10%				
Mo	0.020%				
V	0.004%				
Sn	0.006%				
Yield Strength test 1	84.5ksi				
Yield Strength test 1 (metri	583MPa				
Tensile Strength test 1	101.2ksi				
Tensile Strength 1 (metric)	697MPa				
Elongation test 1	14%				
Elongation Gage Lgth test 1	8IN				
Elongation Gage Lgth 1(metri	200mm				
Bend Test 1	Passed				
Rebar Deformation Avg. Spaci	0.389IN				

The Following is true of the material represented by this MTR:
**Material is fully killed*
**100% melted and rolled in the USA*
**EN10204:2004 3.1 compliant*
**Contains no weld repair*
**Contains no Mercury contamination*
**Manufactured in accordance with the latest version of the plant quality manual*
**Meets the "Buy America" requirements of 23 CFR635.410, 49 CFR 661*
**Warning: This product can expose you to chemicals which are known to the State of California to cause cancer, birth defects or other reproductive harm. For more information go to www.P65Warnings.ca.gov*

REMARKS: ALSO MEETS AASHTO M31

Page 1 OF 1 02/28/2022 09:19:04

Figure C.5 *Mill Certificate for #6 rebar*

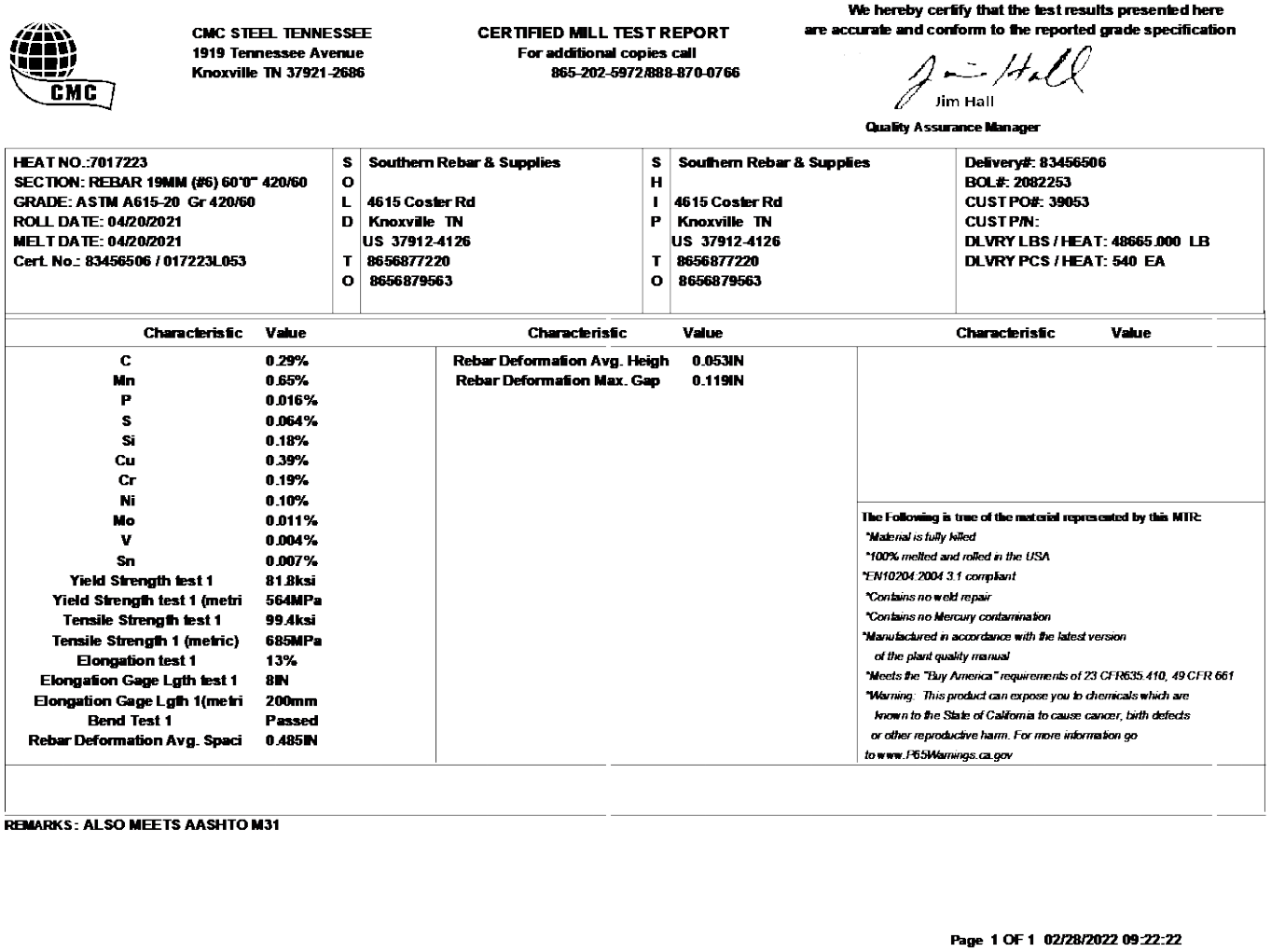

CMC STEEL TENNESSEE
1919 Tennessee Avenue
Knoxville TN 37921-2686

CERTIFIED MILL TEST REPORT
For additional copies call
865-202-5972/888-870-0766

We hereby cerfify that the test results presented here are accurate and conform to the reported grade specification

Jim Hall
Quality Assurance Manager

HEAT NO.:7017223 SECTION: REBAR 19MM (#6) 60'0" 420/60 GRADE: ASTM A615-20 Gr 420/60 ROLL DATE: 04/20/2021 MELT DATE: 04/20/2021 Cert. No.: 83456506 / 017223L053	SOLD TO	Southern Rebar & Supplies 4615 Coster Rd Knoxville TN US 37912-4126 8656877220 8656879563	SHIP TO	Southern Rebar & Supplies 4615 Coster Rd Knoxville TN US 37912-4126 8656877220 8656879563	Delivery#: 83456506 BOL#: 2082253 CUST PO#: 39053 CUST P/N: DLVRY LBS / HEAT: 48665.000 LB DLVRY PCS / HEAT: 540 EA

Characteristic	Value	Characteristic	Value	Characteristic	Value
C	0.29%	Rebar Deformation Avg. Heigh	0.053IN		
Mn	0.65%	Rebar Deformation Max. Gap	0.119IN		
P	0.016%				
S	0.064%				
Si	0.18%				
Cu	0.39%				
Cr	0.19%				
Ni	0.10%				
Mo	0.011%				
V	0.004%				
Sn	0.007%				
Yield Strength test 1	81.8ksi				
Yield Strength test 1 (metri	564MPa				
Tensile Strength test 1	99.4ksi				
Tensile Strength 1 (metric)	685MPa				
Elongation test 1	13%				
Elongation Gage Lgth test 1	8IN				
Elongation Gage Lgth 1(metri	200mm				
Bend Test 1	Passed				
Rebar Deformation Avg. Spaci	0.485IN				

The Following is true of the material represented by this MTR:
**Material is fully killed*
**100% melted and rolled in the USA*
**EN10204:2004 3.1 compliant*
**Contains no weld repair*
**Contains no Mercury contamination*
**Manufactured in accordance with the latest version of the plant quality manual*
**Meets the "Buy America" requirements of 23 CFR635.410, 49 CFR 661*
**Warning: This product can expose you to chemicals which are known to the State of California to cause cancer, birth defects or other reproductive harm. For more information go to www.P65Warnings.ca.gov*

REMARKS: ALSO MEETS AASHTO M31

Page 1 OF 1 02/28/2022 09:22:22

Appendix D: Un-Tensioned Dowel Shear Capacity Design Chart

Instructions for Design Chart Use:

1. Select a dowel size and grade
2. Locate the estimated joint opening size on the horizontal axis
3. From the selected joint opening size, draw a vertical line straight up.
4. The point at which the drawn line crosses the line for your given dowel diameter corresponds to the predicted resisting force for the dowel.
5. In Figure D.1, values for grade 50 dowels are read on the left vertical axis and values for grade 75 dowels are read on the right vertical axis.

Several **technical assumptions** in the research methodology described previously were applied in the construction of this chart:

1. There is no interaction between dowels, the dowel spacing is sufficient that each dowel can mobilize its full capacity.
2. The role of joint friction in the shear resistance is neglected.
3. The un-tensioned dowel method could be applied to wedge failures as well as planar failures. The focus of this investigation was planar geometry.
4. The role of dowel diameter relative to the joint spacing can be investigated with anchor diameters less than typically deployed in practice, since the governing stress and strain relationships are the same.

Notes on inclination angle: The dowel inclination angle with respect to the joint increases the theoretical capacity of a dowel as it increases the subject cross-sectional area. This increase was not observed in the test results used to derive this design chart. Additionally, results in the literature (Spang & Egger, 1990) also failed to see a notable increase in dowel capacity as inclination increased for most cases. As a result, only the case of dowels installed perpendicular to the joint is given for design. This is also the most conservative configuration.

Figure D.1 *Un-tensioned Dowel Design Capacity Chart for Grade 50 and Grade 75 Rebars*

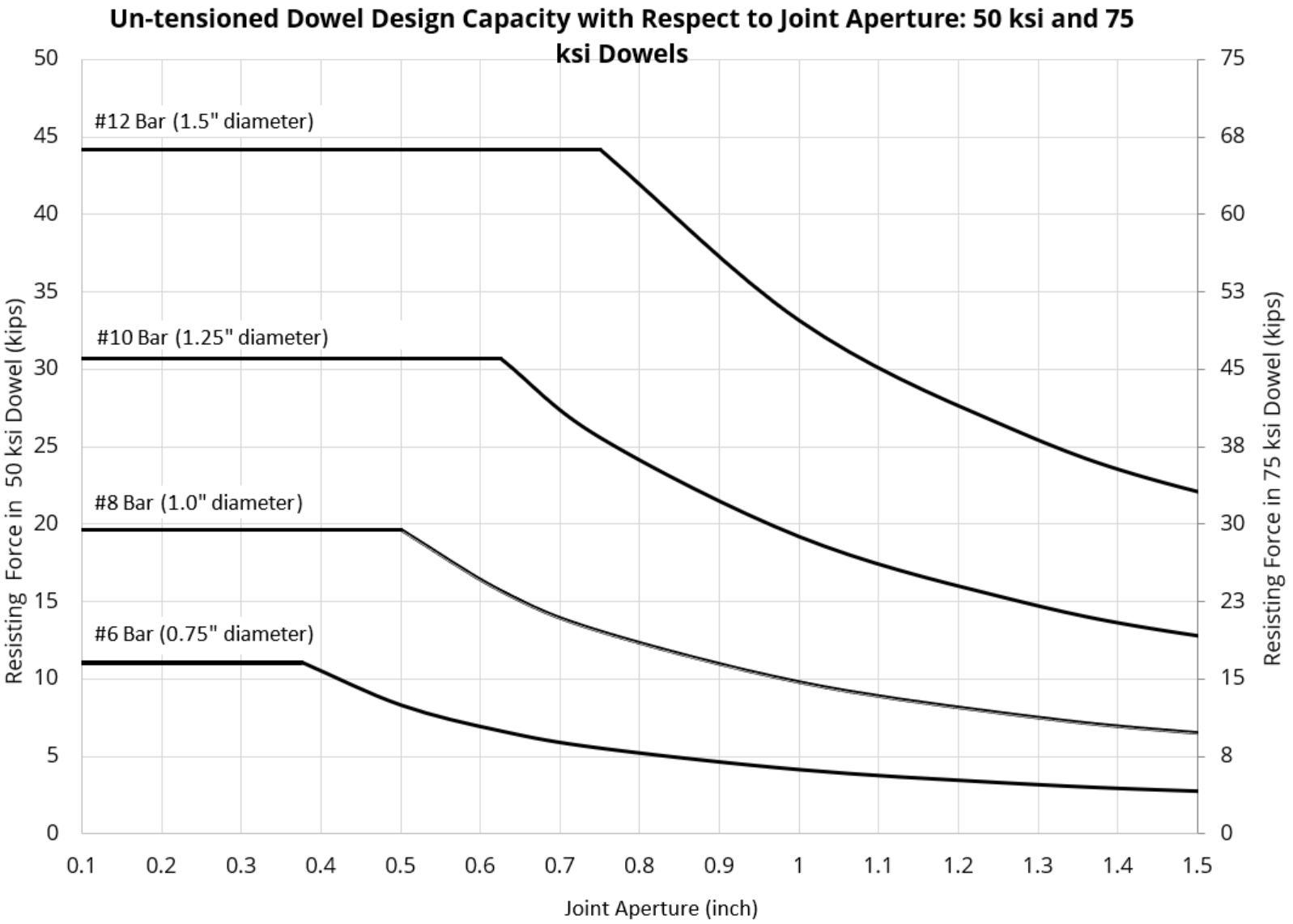

Figure D.2 *Un-tensioned Dowel Design Capacity Chart for Grade 60 and Grade 80 Rebars*

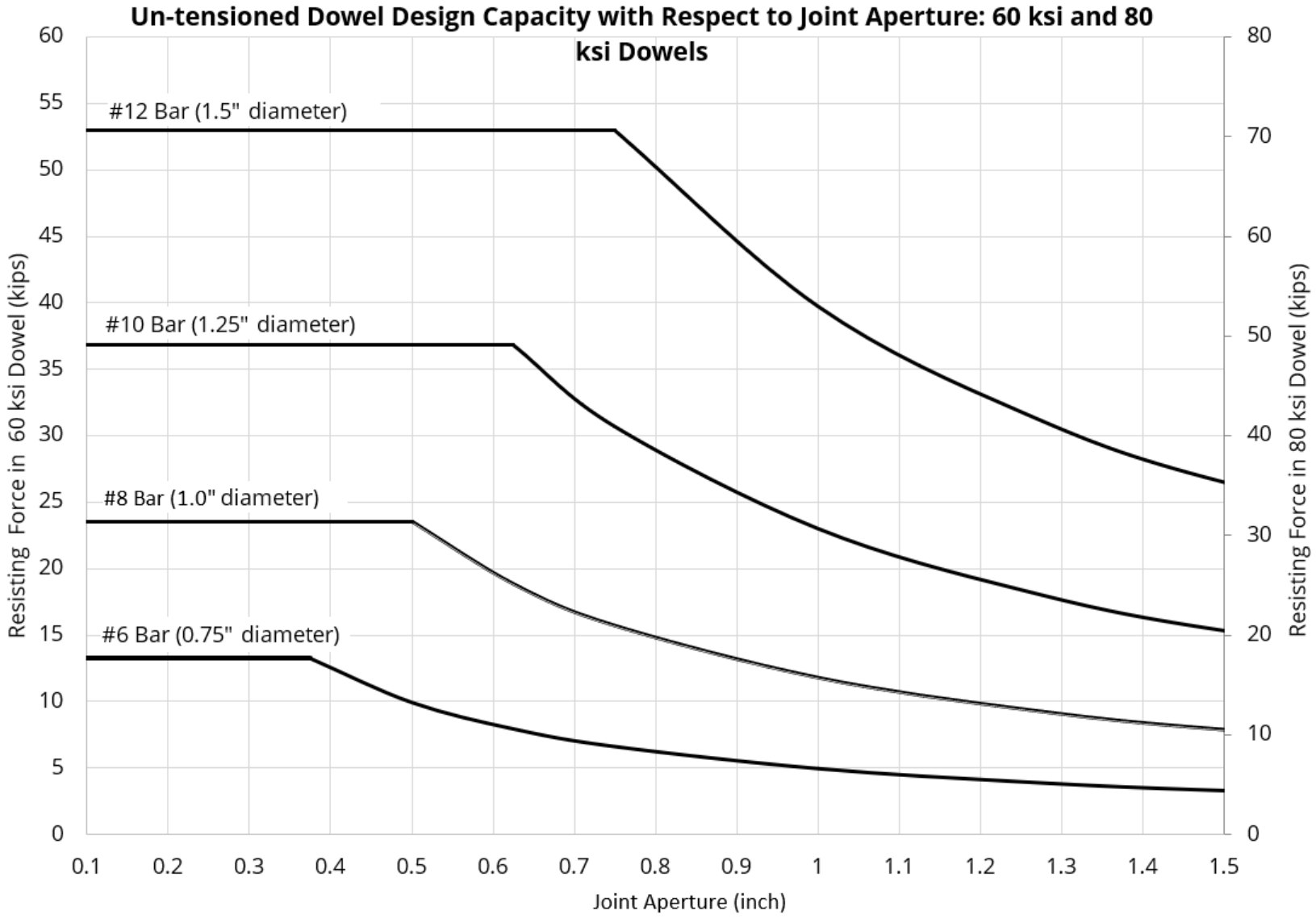

Design Chart Example

Given: Dowel Characteristics: #8, Grade 50

Estimated Joint Aperture: 0.75”

Chart Results: **12.5 kips**

Figure D.3 *Design Chart Example*

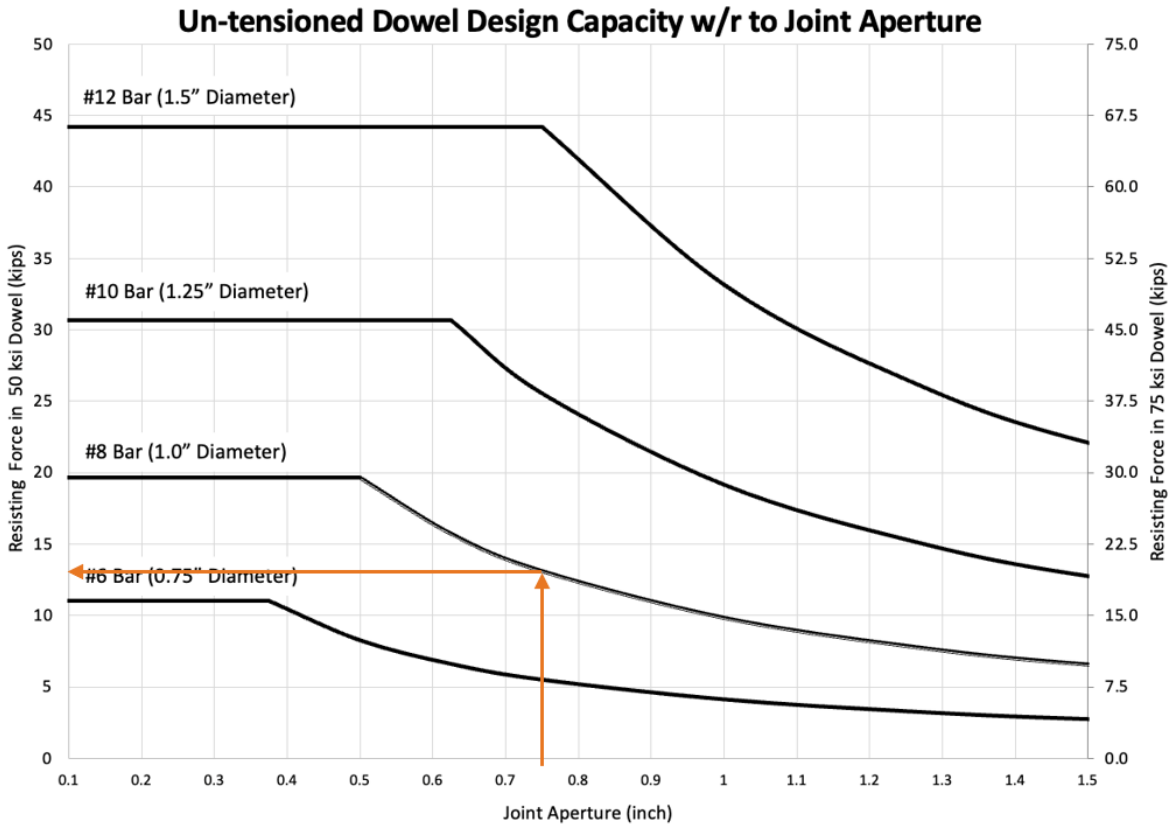

Calculated Shear Capacity:

$$F_{Shear} = 0.5F_yA_b$$

Wherein: F_y = yield strength of the dowel (50ksi)

A_b = Cross sectional area (0.785)

Solution: 19.63 kips

Discussion: The calculated shear value overestimates the capacity of the bolt by 57%. By neglecting the effect of bending at this joint aperture, a designer could be putting systems in place that are unsafe and unsustainable.